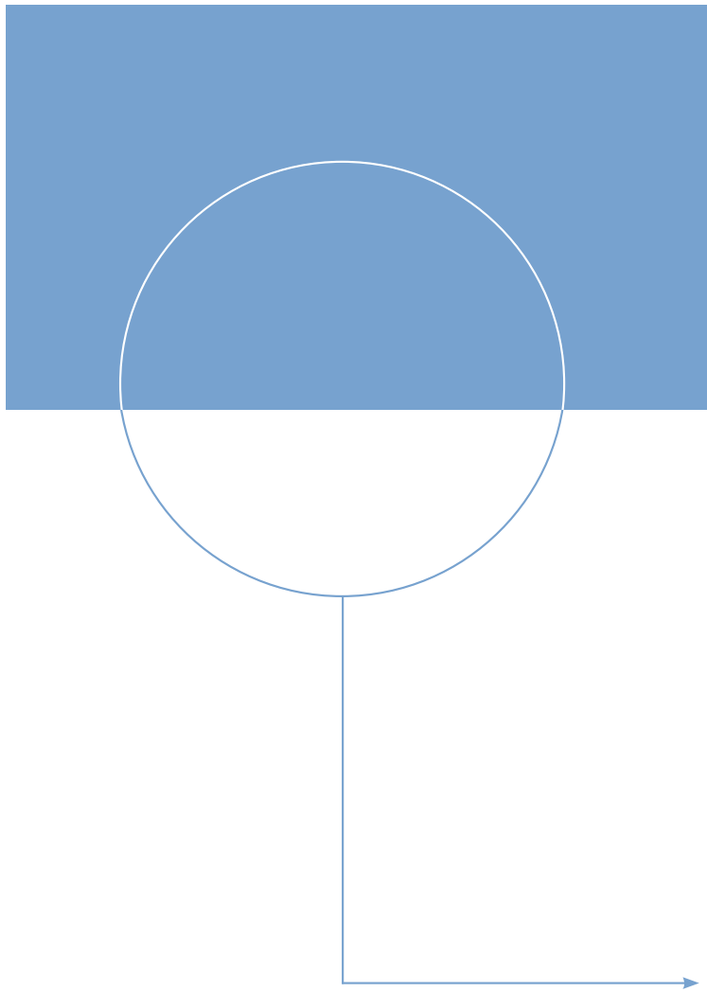

Master's thesis

2019

Marianne Elise Lia

NTNU
Norwegian University of
Science and Technology
Faculty of Natural Sciences
Department of Physics

Marianne Elise Lia

The impact of tumor associated macrophages in delivery of nanoparticles to tumor cells

June 2019

NTNU
Norwegian University of
Science and Technology

NTNU
Norwegian University of
Science and Technology

NTNU
Norwegian University of
Science and Technology

The impact of tumor associated macrophages in delivery of nanoparticles to tumor cells

Marianne Elise Lia

Nanotechnology
Submission date: June 2019
Supervisor: Catharina de Lange Davies

Norwegian University of Science and Technology
Department of Physics

Abstract

Inefficiency in today's cancer treatment is addressed by encapsulating cytotoxic drugs inside engineered nanoparticles in drug delivery systems (DDSs). Tumor associated macrophages (TAMs) may work as a barrier for delivery of nanoparticles due to their phagocytic function. A DDS was characterized for two different xenografts in mice, OHS (osteosarcoma) and PC3 (prostatic adenocarcinoma), with the aim of investigating whether or not TAMs engulf nanoparticles, thus limiting the delivery of nanoparticles to tumor cells. In the DDS, nanoparticles encapsulating a fluorescent drug model were used as a stabilizing shell around microbubbles. Focused ultrasound was applied locally on the tumor, causing cavitations and collapse of the microbubbles. The intention was to increase the delivery of nanoparticles in the tumor tissue, in addition to making the distribution of nanoparticles inside the tissue more even. The uptake of nanoparticles by TAMs in this DDS has not previously been investigated.

Single cell suspensions were made from tumors, and the macrophages were stained with fluorescent antibodies. The samples were analyzed by flow cytometry in order to obtain information regarding the amount of all macrophages, the amount of M1 and M2 macrophages, as well as the uptake of nanoparticles by macrophages. Macrophages in frozen tumor sections were also stained with fluorescent antibodies and imaged by the use of confocal laser scanning microscopy. The captured images were mainly used for distance analysis. Macrophages, nanoparticles, and the uptake of nanoparticles by macrophages at different distances around blood vessels, were studied. The images were also used to calculate the area percentage of nanoparticles within tumor tissue.

Focused ultrasound treatment significantly increased the accumulation of nanoparticles within both OHS tumor tissue and PC3 tumor tissue. From this, an increased percentage of tumor cells containing nanoparticles were also observed for both tumor models by the use of ultrasound, but the increase was only significant for tumor cells in OHS tumor tissue. Large populations of macrophages were found within both OHS tumor tissue and PC3 tumor tissue, where the M2 phenotype was the dominating type of macrophage, absolutely overshadowing the M1 phenotype. Focused ultrasound did not affect the percentage of macrophages in any of the tumor models. In both OHS tumor tissue and PC3 tumor tissue, the macrophages function as barriers for the nanoparticles. The majority of the nanoparticles were engulfed by macrophages, thus limiting the delivery of nanoparticles to tumor cells. For the tumors treated with ultrasound, most of the nanoparticles were also located inside macrophages. The percentage of macrophages and nanoparticles were highest in close proximity to the blood vessel walls, and decreased with increasing distance from the blood vessels. A greater amount of the intratumoral nanoparticles were taken up by macrophages close to the blood vessels in OHS tumor tissue compared to that of PC3 tumor tissue.

This knowledge can prove useful in further studies examining macrophages and how they function as a barrier for delivery of nanoparticles to tumor cells.

Sammendrag

Dagens ineffektive kreftbehandlinger tas hånd om ved innkapsling av cellegift i spesialdesignede nanopartikler som en del av medisinleveringssystemer. Tumorassosierte makrofager (TAMer) kan fungere som en barriere for levering av nanopartikler grunnet deres fagocyttiske funksjon. Et medisinleveringssystem ble karakterisert for to forskjellige xenografter i mus, OHS (osteosarkom) og PC3 (prostata adenokarsinomer), der hensikten var å undersøke hvorvidt TAMer tar opp nanopartikler og dermed begrenser leveringen av nanopartikler til kreftceller. I dette medisinleveringssystemet ble nanopartikler som inneholdt fluorescerende modeller av medisin brukt som et stabiliserende skall rundt mikrobobler. Fokusert ultralyd ble påført lokalt på kreftsvulsten, noe som forårsaket kavitasjoner og kollaps av mikroboblene. Hensikten var å øke leveringen av nanopartikler til kreftvevet, samtidig som man oppnår en jevnere fordeling av nanopartikler inne i vevet. Opptak av nanopartikler ved TAMer i dette medisinleveringssystemet har ikke tidligere blitt undersøkt.

Enkeltcellesuspensjoner ble laget fra kreftsvulster og makrofagene ble farget med fluorescerende antistoffer. Prøvene ble analysert ved flowcytometri for å skaffe informasjon om andelen av alle makrofager, andelen av M1 og M2 makrofager, samt opptak av nanopartikler i makrofager. Makrofager i frosne snitt fra kreftsvulster ble også farget med fluorescerende antistoffer og avbildet ved bruk av konfokalmikroskopi. Bildene ble hovedsakelig brukt til avstandsanalyse. Makrofager, nanopartikler, samt opptaket av nanopartikler i makrofager ved ulike avstander rundt blodårer ble studert nærmere. Bildene ble også brukt til å beregne arealprosenten av nanopartikler inne i kreftvev.

Fokusert ultralyd behandling økte signifikant akkumuleringen av nanopartikler i både OHS og PC3 kreftvev. Dette medførte en økt prosentandel kreftceller som inneholdt nanopartikler. Dette ble observert i begge kreftvevmodellene, men økningen var kun signifikant for kreftceller i OHS kreftvev. Store populasjoner av makrofager ble funnet i både OHS kreftvev og PC3 kreftvev, der M2 makrofager ble observert som den dominerende typen makrofager. Fokusert ultralyd hadde ingen påvirkning på prosentdelen av makrofager i noen av kreftvevmodellene. Makrofagene fungerte som en barriere for nanopartiklene i både OHS kreftvev og PC3 kreftvev. Leveringen av nanopartikler til kreftceller ble kraftig begrenset av det faktum at størsteparten av nanopartiklene var tatt opp i makrofager. Dette var også tilfellet for kreftvev behandlet med fokusert ultralyd. Prosentdelen av makrofager og nanopartikler var høyest i nærheten av blodåreveggene og andelen minket med økende avstand fra blodårene. En større andel av nanopartiklene inne i kreftvevet ble tatt opp av makrofager nærme blodåreveggene i OHS kreftvev sammenlignet med i PC3 kreftvev.

Denne kunnskapen kan være nyttig ved videre studier der man undersøker makrofager og hvordan de fungerer som barrierer for levering av nanopartikler til kreftceller.

Preface

This master thesis concludes five years of education within the Nanotechnology program at the Norwegian University of Science and Technology. For the last three years, my specialization has been in bionanotechnology. After learning about nanomedicine, I wanted to write a master within this subject. I was lucky to get the opportunity to join Catharina de Lange Davies' group at the Department of Physics, where they are working with delivery of drugs to tumors by nanoparticles in combination with ultrasound.

I would like to thank Catharina de Lange Davies and Einar Sulheim for guidance, help and support throughout this project. I am also thankful to Kristin Grendstad for guidance during the optimization process of the flow cytometry experiments, for training on the flow cytometer and for always answering my questions. I would also like to thank Astrid Bjørkøy for training on the confocal laser scanning microscopy and Anne Rein Hatletveit at SINTEF for provisions of nanoparticle-stabilized microbubble complexes. The last I want to thank is Marieke Olsman for giving me tumors left over from her ongoing trials for use in the optimization process.

Marianne Elise Lia
Trondheim, June 2019

Abbreviations

BSA	=	bovine serum albumnin
CLSM	=	confocal laser scanning microscopy
DDS	=	drug delivery system
DMSO	=	dimethyl sulfoxide
DOF	=	depth of field
ECM	=	extra cellular matrix
FBS	=	fetal bovine serum
IFP	=	interstitial fluid pressure
MI	=	mechanical index
MPS	=	monunuclear phagocytic system
NPMB	=	nanoparticle-stabilized microbubble complexe
OHS	=	human osteosarcoma cells
PBS	=	phosphate buffered saline
PC3	=	human prostatic adenocarcinoma cells
PFP	=	perfluoropropane
PRF	=	local pulse repetition frequency
SS	=	solid stress
TAM	=	tumor associated macrophage

Table of Contents

Chapter 1

Introduction

Cancer has become one of medicine's most significant challenges. The number of cases increases every year, and the cancer itself both develops spreads in numerous ways, demanding an assortment of different treatments. The inefficiency of today's treatment methods is directly linked to the disease's fatality. More than 9 million people die each year due to cancer according to the Global Cancer Observatory[1]. The most widely used treatment method today is chemotherapy, but this method of drug injection results in no more than 0.001% to 0.01% of the drug actually reaching the tumor tissue[2, 3]. The vast majority of the drug accumulates in healthy tissue, leading to the death of healthy cells and subsequently a multitude of side effects, both during treatment and afterwards[4, pp.399-405].

Nanotechnology has over the last few decades been paramount as a platform for cancer treatment, working to address the problem of dreadfully inefficient drug delivery to tumors. Today, nanoparticles are tuned to function as drug carriers with the goal of increased efficiency in drug delivery systems (DDSs), but nanoparticles are often poorly distributed within the tumor tissue. *Y. Mørch et al.*[5] presented a DDS designed by SINTEF where nanoparticles and microbubbles are used in combination with focused ultrasound. Nanopaticles encapsulating drugs are used as a stabilizing shell around microbubbles. These complexes are administrated into the blood stream and ultrasound is applied locally on the tumor, causing oscillations and ultimately collapsing the microbubbles. The nanoparticles are shot into the tumor tissue, resulting in an increased deposition and a more even distribution of nanoparticles inside the tumor compared to no use of ultrasound[6].

There are several barriers for the nanoparticles, starting from administration into the blood stream all the way until they reach the cancer cells inside the tumor. One of these barriers may be tumor associated macrophages (TAMs) and their phagocytic function. Macrophages are immune cells with an essential role in apoptotic cell destruction and in development of inflammations[7]. There are two main types of TAMs inside tumor tissue: M1 macrophages and M2 macrophages, where M1 macrophages inhibit tumor growth and M2 macrophages promote tumor growth[8]. TAMs may engulf nanoparticles by fagocytosis when the nanoparticles passes through the tumor tissue, thus limiting the delivery of drugs to tumor cells. At the time of writing, there is no published literature that describes the uptake of nanoparticles by TAMs in a DDS based on nanoparticle-stabilized microbubbles in combination with focused ultrasound.

The aim of this thesis was to investigate whether or not TAMs would hinder the delivery of nanoparticles to tumor cells. This was done by studying the uptake of nanoparticles by macrophages and tumor cells in OHS (osteosarcoma) and PC3 (prostate adenocarcinoma) xenografts. The total amount of all macrophages, M1 macrophages and M2 macrophages, and nanoparticles, was also examined for the different tumor models. In addition to this, distance analysis was performed with the aim of gaining information on how macrophages and nanoparticles were distributed around blood vessels. The distance analysis also included a study on the amount of nanoparticles engulfed by macrophages at different distances from the vasculature. All of the analysis were performed for both a control group and a treated group. The animals in the control group were only injected with nanoparticle-stabilized microbubbles, while the animals in the treated group were injected with nanoparticle-stabilized microbubbles in combination with focused ultrasound treatment on the tumor. OHS and PC3 xenografts were chosen based on their different morphology and properties. *E. Sulheim et al.*[9] characterized these tumor models and found that OHS tumors were better perfused and had a much higher density of blood vessels compared to PC3 tumors.

Single cell suspensions were made from tumors, followed by staining of macrophages with fluorescent antibodies. These samples were analyzed by flow cytometry in order to obtain information regarding the amount of macrophages and uptake of nanoparticles by macrophages. Macrophages in frozen tumor sections were stained and imaged by the use of confocal laser scanning microscopy. The captured images were mainly used for distance analysis, but the area percentage of nanoparticles within the tumor tissue were also analyzed from these images.

Information regarding the uptake of nanoparticles by macrophages contribute to new knowledge on how macrophages limit the delivery of drugs to tumor cells. This is important in further improvements of DDS and in designing of more efficient and safer treatment method for cancer patients.

This master project is a continuation of the specialization project carried out by the author during the autumn 2018 [10]. Due to this, there is some overlap between the two thesis, notably in the chapters dedicated to theory and methods.

Chapter 2

Theory

This master thesis is a continuation of the specialization project carried out by the author during the autumn 2018 [10]. Since the two works are in the same topic, there will be overlap between the theory sections in these works. Therefore, some of the following sections are similar to the theory sections in the specialization project.

2.1 Cancer

Cancer arise from uncontrolled proliferation of cells. This usually occurs due to mutations and results in tumor growth. It may take several years between the first mutation in a single cell to a tumor appears.

2.1.1 The biology of cancer

For healthy tissues and organs, the growth is strictly regulated by a balance between stimulating and inhibitory factors. Tissue growth occurs by either hypertrophy or hyperplasia. Hypertrophy is an increase in the size of individual cells. This is seen for muscle cells as a result of physical exercise. Hyperplasia is an increase in the number of cells due to cell proliferation. This occurs during the cell cycle where the DNA in one cell is duplicated and the product is two daughter cells. In normally healthy tissue, this process stops when the tissue is healed. If any of the steps through the cell cycle goes wrong, this may results in mutated cells with unlimited proliferation and tumor growth[4, p.4].

Telomeres are structures at the end of chromosomes and these become shorter for each cell division. In normal tissue, this causes the cells to divide for a limited number before the telomere is too short and the cells die. Telomeres are synthesized by the telomerase enzyme, a highly active enzyme in tumor cells. The length of the telomeres are maintained, resulting in the cells being able to divide indefinitely and cause tumor growth[4, p.173].

Tumors are divided into three main groups[4, pp.4-16]:

- *Benign tumors:* These tumors arise in most tissues. They are unable to spread throughout the body, but they may cause local pressure and damage to surrounding tissues and organs.

- *In situ tumors:* These are small tumors located in the epithelium. Normally, these tumors do not spread to surrounding basement membrane and mesenchyme.
- *Malignant tumors:* Cancer cells from these tumors invade different parts of the body by following the blood stream to lymph nodes and organs. This process is called metastasis.

To maintain the high proliferation rate of cells within tumors, a continuous supply of oxygen and nutrients from the blood is necessary. Due to this, new blood vessels are rapidly formed from existing vessels. This is called angiogenesis, and the new blood vessels are formed in the direction of growth factors released from cancer cells[4, pp.309]. This rapid formation results in leaky blood vessels. In healthy vasculature, the endothelial cells are lined up without any gaps between them. Comparatively, there are gaps between the endothelial cells in tumor vasculature, making these blood vessels highly permeable. The fast growing nature inside tumors results in non-functional lymphatics and occurrence of a high interstitial fluid pressure (IFP) inside the tumor. The leaky blood vessels and non-functional lymphatics lead to an enhanced permeability and retention effect (EPR), a phenomenon described by *Maeda et al*[11]. An illustration of the EPR effect is shown in Figure 2.1.

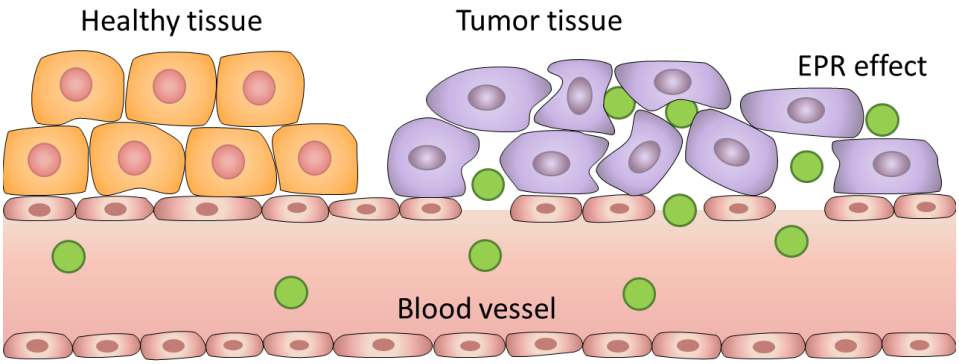

Figure 2.1: Illustration of the enhanced permeability and retention effect (EPR) inside tumor tissue. In healthy vasculature, the endothelial cells are lined up without any gaps between them. In tumor tissue, the fast growing nature results in leaky blood vessels and non-functional lymphatics. Gaps between the endothelial cells make the blood vessels highly permeable.

2.1.2 Today's treatment methods

Today's most common cancer treatments consists mostly of chemotherapy, radiation, surgeries or a combination of the methods. These treatments may cause side effects, sometimes to such an extent that the treatment must be interrupted.

For chemotherapy, the treatment lasts for several months or even years to make sure every single cancer cell is dealt with. The action site for the injected drugs is usually the DNA. However, this treatment method attacks healthy tissue as well as tumor tissue. Tissues that contain cells with rapid turnovers are severely affected. This includes the bone

marrow, hair follicle, skin and gastrointestinal mucosa[4, pp.399-405]. Only a fraction, between 0.001% and 0.01%, of the injected drug reaches the tumor cells[2, 3]. The accumulation of drugs in healthy tissue causes a range of side effect for the patients, both during and after the treatment period. Examples of early side effects are fatigue, nausea, hair loss and diarrhoea, myelosuppression (decreased activity of the bone marrow), mucositis (inflammation of mucous membranes), peripheral neutotoxicity (toxicity in the pheripheral nerve system) and nephrotoxicity (toxicity in the kidneys). Early side effects are mostly temporary and heals in the intervals between each treatment period. This is due to healthy tissue having more efficient mechanisms to repair DNA damage compared to tumor tissue. Late side effects may occur several years after the end of the treatment. These side effects includes cardiotoxicity (weakened of muscles and dysfunctions of the electrical signals in the heart), acute leukemia, premature menopause, infertility and pulmonary fibrosis (lung disease)[4, pp.399-405].

Radiation therapy ionizes the DNA of cells, slowing their growth and ultimately terminating them. This local treatment is focused on the tumor, but surrounding healthy tissue is unfortunately also damaged in the process, ultimately causing side effects[4, pp.414-416].

A tumor that is solid and conveniently located can in some cases be surgically removed. The surgery do however pose a huge risk for the patient, and will lead to pains and a statistically higher rate of infections following the surgery[4, p.309].

2.2 Macrophages in tumor tissue

Macrophages are immune cells located in tissues throughout the body. These cells are derived from the bone marrow and a part of the mononuclear phagocytic system (MPS). Macrophages perform an essential role in development of inflammations and recruitment of additional macrophages from transmission of inflammatory signals. They also have a phagocytic function and are important in apoptotic cell destruction of dead cells and debris, sick cells, bacteria, viruses and foreign substances inside the body. Nanoparticles in drug delivery systems may be recognized as foreign substances and engulfed by macrophages. Due to this, macrophages works as a barrier for delivering of nanoparticles to tumor tissue[7].

The macrophages inside tumor tissue are called tumor associated macrophages (TAMs), and they are divided into two main groups: M1 macrophages and M2 macrophages. Their functions depend on signals in the local tumor microenvironment. This is illustrated in Figure 2.2. Small pro-inflammatory proteins called CC chemokines (CCL2, CCL3, CCL5, CCL7, CCL8) and vascular endothelial growth factor (VEGF) recruit monocytes from the peripheral blood stream into the tumor tissue[8, 12]. The presence of Th1 cytokines and the exogenous tumor necrosis factor alpha (TNF-α) inside the tumor microenvironment convert the monocytes into M1 macrophages[8]. M1 macrophages are polarized into M2 macrophages inside the tumor tissue. This polarization occurs in the presence of certain exogenous factors in the tumor microenvironment. This includes a high level of lactic acid, hypoxia (lack of oxygen), cytokines (IL-4, IL-13), the transforming growth factor beta (TGF-β) and vitamin D3[8, 13, 14].

The two types of macrophages perform different functions inside the tumor tissue. M1 is classical activated macrophages and they inhibit tumor growth by production of pro-inflammatory cytokines (IL-6, IL-8, IL-12, IL-23) and TNF-α[8, 14]. These macrophages also produce a high level of both nitric oxide and reactive oxygen species. This makes M1 macrophages efficient at killing tumor cells[15]. Differently from M1 macrophages, the alternatively activated M2 macrophages promote tumor growth and metastasis, as well as suppressing the immune response by inactivation of T-cells. This occurs due to production of anti-inflammatory cytokines (IL-4, IL-10, IL-13), TGF-β, angiogenesis factors and matrix-degrading enzymes [8, 14, 16].

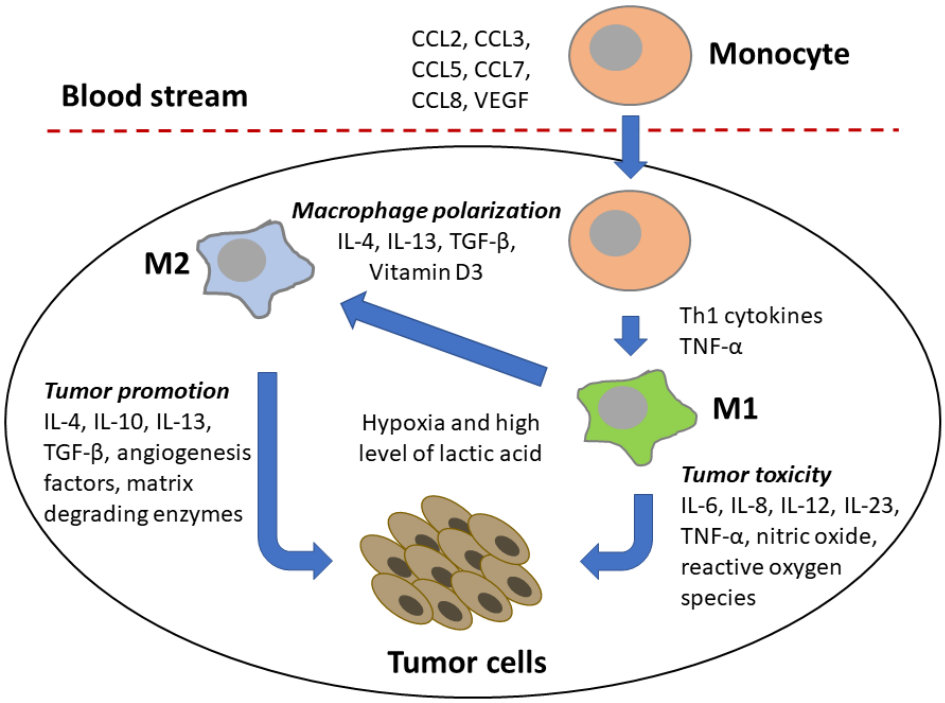

Figure 2.2: Illustration of signals and macrophages inside the tumor microenvironment. CC chemokines (CCL2, CCL3, CCL5, CCL7, CCL8) and VEGF recruit monocytes from the blood stream into the tumor tissue. Monocytes are converted to M1 macrophages in the presence of Th1 cytokines and TGF-α. Polarization of M1 macrophages into M2 macrophages are promoted by high levels of lactic acid, hypoxia, cytokines (IL-4, IL-13), TGF-β and vitamin D3. M1 macrophages inhibit tumor growth by production of cytokines (IL-6, IL-8, IL-12, IL-23), TNF-α, nitric oxide and reactive oxygen species. M2 macrophages produce cytokies (IL-4, IL-10, IL-13), TGF-β, angiogenesis factors and matrix-degrading enzymes, resulting in promotion of tumor growth.

According to *Jung KY et.al*[17], a high level of M2 macrophages is related to poor survival rate. They have conducted a study where they looked at the relationship between the level of M2 macrophages and survival rate in 14 different types of human cancer.

2.2.1 Specific surface receptors for tumor associated macrophages

The classical activated M1 macrophages have no characteristic surface receptors that make it possible to label these cells. However, they do have an overexpression of certain receptors: cluster of differentiation 16 (CD16), CD86. CD80, interleukin-1 receptor (IL-1R), major histocompatibility complex class II (MHC II), toll-like receptor 2 (TLR2) and TLR4[15, 18]. Due to the lack of specific surface receptors, M1 macrophages are often identified based on their expression of certain cytokines[15].

The alternatively activated M2 macrophages express several specific surface receptors that are used to label these cells. Examples of specific M2 receptor are: IL-1R type II, CD204 macrophage scavenger receptor I, CD206 mannose receptor and CD163 hemoglobin scavenger receptor[15, 18].

2.3 Nanoparticles in drug delivery

A range of different nanoparticles have been developed for use in biomedical applications such as drug delivery systems (DDS). The aim is to functionalize these nanoparticles to reach specific targets inside the body[19]. There are strict requirements that must be fulfilled in order to obtain useful nanoparticles. The particles must be biocompatible and biodegradable to avoid toxic or immunological responses from the body. After release of the drugs, the particles must be degraded to avoid accumulation in healthy tissue[19, 20]. Special engineered nanoparticles can be utilized as carriers for drugs in DDS, where the aim is to achieve a more efficient delivery of drugs to the target site. There are several advantages by encapsulation of drugs inside nanocarriers. Some of them are listed below[19]:

- The EPR effect is utilized in the delivery of nanoparticles. Drugs are small molecules that accumulate in both healthy tissue and tumor tissue. Nanoparticles are small enough to penetrate through leaky blood vessel walls inside tumor tissue, but they are too big to penetrate through healthy vasculature. This leads to less toxic effects in the body by the use of nanoparticles, due to less accumulation of cytotoxic drugs in healthy tissue.
- Most types of cytotoxic drugs used to treat cancer are poorly soluble in water. Nanocarriers can be used to transport hydrophobic drugs inside the blood stream.
- The half-life of the drugs is increased by encapsulation due to protection from the environment in the blood stream.
- Nanoparticles can be functionalized to reach specific targets where the drug is released. This increases the efficacy of the treatment and decreases side effects for the patient, due to less accumulation of drugs in healthy tissue.
- It is possible to obtain time specific controlled release of the encapsulated drug.
- Nanoparticles can be used in combination with diagnostic agents in order to perform combination therapy.

Some examples of nanoparticles used as nanocarriers in DDS are micelles, liposomes and polymeric nanoparticles. Illustrations of these are shown in Figure 2.3. A micelle is formed by self-assembling of amphiphiles, which are molecules with both hydrophilic and hydrophobic properties. Hydrophobic agents can be carried inside the core. A liposome is a spherical vesicle that consists of a lipid bilayer. These vesicles can carry both hydrophobic agents (inside the bilayer) and hydrophilic agents (inside the aqueous core). The polymeric nanoparticle is a solid particle. Depending on the polymer matrix, these nanoparticles have the ability to carry different types of agents inside the core[19].

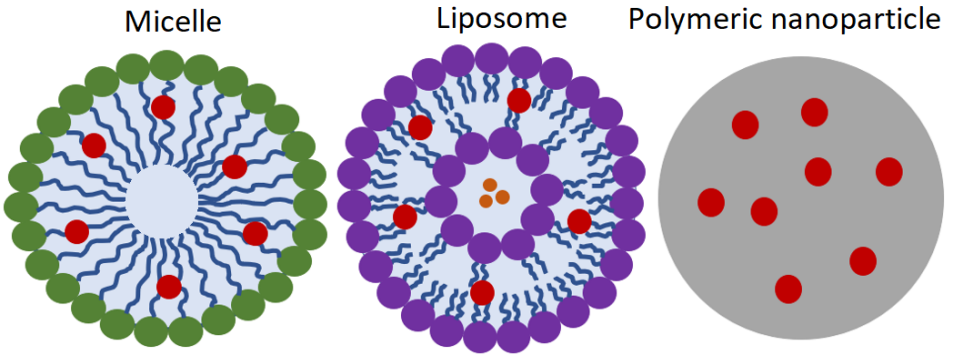

Figure 2.3: Illustration of different types of nanocarriers used in drug delivery systems. From left: micelle, liposome and polymeric nanoparticle. The red particles illustrate hydrophobic drugs, while the organge particles illustrate hydrophilic drugs. Micelles can carry hydrophobic drugs inside the core. Liposomes can carry hydrophobic drugs inside the bilayer and hydrophilic drigs in the aqueous core. Polymeric nanoparticles can carry different agents, depending on the polymer matrix.

2.3.1 Nanoparticles and tumor targeting strategies

There are three main strategies to deliver nanoparticles to the tumor cells: passive targeting, active targeting and triggered drug release.

Passive targeting: This target strategy utilized the EPR effect. Nanoparticles are not able to pass through healthy endothelial cells in the vasculature. They will circulate in blood stream until they are removed by the mononuclear phagocyte system. Due to the EPR effect, the vasculature inside tumors are leaky. This allows nanoparticles to pass through the gaps between the endothelial cells and enter the tumor tissue. This targeting strategy is inefficient and requires a long circulation time of the nanoparticles[19, 21, 22].

Active targeting: The nanoparticles are surface functionalized before administration into the blood stream. Specific ligands, like antibodies and peptides, are attached to the surfaces of the nanoparticles. These ligands bind to specific receptors that are overexpressed at the target site[19, 21].

Triggered drug release: An external stimuli is applied to direct the nanoparticles to the target site. External stimuli is also used to release the encapsulated drug from the particles due to changes in the tumor environment. Examples of external stimuli are heat, magnetism, light, ultrasound and pH value[19, 21].

2.3.2 Barriers to nanoparticles

The nanoparticles must pass through several barriers from the blood stream to the tumor cells. These barriers are illustrated in Figure 2.4 and explained in the following sections.

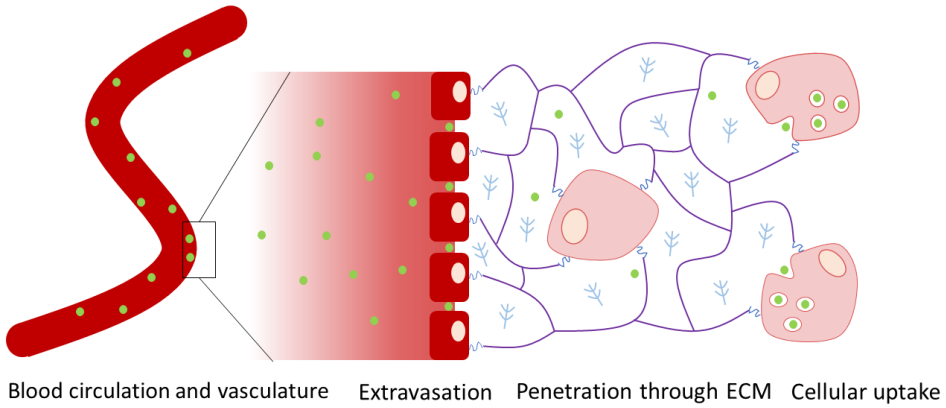

Figure 2.4: Illustration of barriers for the nanoparticles from the blood stream to uptake in tumor cells. The nanoparticles are green. From left: Blood circulation and vasculature, extravasation, penetration through the extracellular matrix and cellular uptake.

Blood circulation: The first barrier after administration of the nanoparticles into the body is the blood circulation. A long circulation time of the nanoparticles in the blood stream is desirable in order to obtain a therapeutic effect. The nanoparticles must stay in the circulation for a long enough time period to achieve an accumulation of nanoparticles at the target site. The circulation time is limited by opsonization, which is one of the most important biological barriers[23]. Opsonins are specific proteins present in the blood serum. These proteins bind easily to foreign substances, including nanoparticles, if they are brought in contact. Contact between opsonins and nanoparticles occur due to brownian motions. This results in the nanoparticles' surfaces being covered by opsonins, which make the nanoparticles visible for the monunuclear phagocytic system (MPS). Macrophages from the MPS recognise the opsonins on the nanoparticle surfaces, and registers them as foreign substances. The nanoparticles are then taken up by phagocytosis and degrades inside the macrophages by enzymes and oxidative-reactive chemical factors[23, 24].

Several methods are developed to hide the nanoparticles from the MPS and overcome the opsonization problem. The most preferred method is PEGylation of the nanoparticles before they are administrated into the blood stream[23]. PEG (poly ethylene glycol) is a hydrophilic molecule, which is adsorbed at the surfaces of the nanoparticles. The PEG chains create a steric corona around the nanoparticles, which works as a barrier and pre-

vents binding of opsonins to the particle surfaces. PEGylation results in longer circulation time for the nanoparticles in the blood stream, since the macrophages do not recognize the particles without opsonins on their surfaces[25].

Vasculature: An irregular morphology of the vasculature within the tumor tissue makes it difficult for the nanoparticles to be distributed throughout the tumor. In healthy vasculature, the endothelial cells double over a period of approximately 1000 days, while in tumor tissue this process occurs within 10 days[26]. This is an evidence for the need of rapid formation of new blood vessels in tumors. To maintain tumor growth, the cancer cells need a continuous supply of nutrients and oxygen from the blood vessels. The result of this fast growing vasculature is irregular structures and uneven leakiness of the new blood vessels. Some areas along the blood vessels will be highly permeable, while other areas are not leaky at all. The irregular vasculature also reduces the blood flow within the tumor due to high blood flow resistance. This uneven leakiness of the blood vessels and reduced blood flow limit the transport of nanoparticles to cancer cells throughout the tumor[22].

Extravasation: The high interstitial fluid (IFP) pressure[27] and the solid stress (SS) inside a tumor work as barriers to distribution of nanoparticles. In healthy tissue, the drainage of excess fluid from the tissue is maintained by the lymphatic network. This results in a fluid balance and a stable interstitial fluid pressure inside the tissue. In tumors, the proliferation of the cancer cells results in collapse of lymphatic vessels, especially in the center of the tumor. Due to the non-functional lymphatics, there is no drainage of excess fluid. This causes a high IFP, which decreases towards the periphery of the tumor. SS on the blood vessel walls occurs due to the continuous proliferation of cancer cells within the tumor. The combination of a high IFP and SS leads to collapse of blood vessels and thus limit the transport of nanoparticles throughout the tumor[22]. On the other hand, the collapse of blood vessels also causes cell death due to necrosis.

The transport of nanoparticles across the blood vessel wall is called extravasation and it is driven by convection and diffusion, as described in the following Equation 2.1[22]:

$$J = PA(C_v - C_i) + L_pA(1-\sigma)(P_v - P_i) - C_v\sigma(\pi_v - \pi_i) \tag{2.1}$$

where J is the flow of nanoparticles across the blood vessel wall, A is the blood vessel surface area, $C_v - C_i$ is the difference in concentration between the vascular and interstitial solute, L_p is the hydraulic conductivity (the ease of fluid movement through a pore), σ is the osmotic reflection coefficient due to fluid flow, $P_v - P_i$ is the difference between vascular hydrostatic pressure and interstitial hydrostatic pressure and $\pi_v - \pi_i$ is the difference in osmotic pressure across the blood vessel wall.

Convection is limited due to the high IFP in the center of a tumor, and this causes diffusion to be the main mechanism for transport of nanoparticles from the vasculature to the tumor tissue[22].

Penetration through extra cellular matrix: The extravasation of the nanoparticles from the blood vessels are followed by penetration through the extra cellular matrix (ECM). The ECM is a dense network of non-cellular component, like collagen fibers, elastin, fibronectin, proteoglycans and glycosaminoglycans. This network is presented in all tis-

sues, including tumor tissue[22, 28]. The penetration of nanoparticles through the ECM is limited by a high IFP in the center of the tumor and is driven by diffusion[22]. This is described by Fick's first law in Equation 2.2[29, pp.79-82]:

$$\mathbf{J} = -D\nabla c \tag{2.2}$$

where **J** is the number of nanoparticles that flows through a unit area during a certain time interval, ∇c is the concentration gradient of the nanoparticles in three dimensions, and D is the diffusion coefficient. D is valid for small spherical particles in solutions, and is given by Equation 2.3:

$$D = \frac{k_B T}{6\pi\eta R_s} \tag{2.3}$$

where k_B is the Boltzmann constant, T is the temperature, η is the viscosity of the fluid (ECM) and R_s is the radius of the particles.

The diffusion of particles through the ECM is dependent on size, charge and conformation of the particles, in addition to their ability to interact with the matrix. The main barrier for the nanoparticles inside the ECM is the collagen content. Collagen fibers work as a steric hindrance and limit the penetration of nanoparticles inside the interstitial matrix. Due to this, there is less movement of the nanoparticles inside tumors with a high content of collagen compared to tumors with low collagen content[30]. Nanoparticles for use in DDS usually have a diameter up to a few hundred nanometers. The penetration of nanoparticles and the dependency of particle size has been studied for several tumors. It has been shown that nanoparticles with a diameter larger than 60 nm, not penetrates with a sufficient rate within the ECM to achieve a desirable drug delivery throughout the tumor.[22].

Cellular uptake: Most of the cytotoxic drugs works intracellularly, which means that the nanoparticles must be taken up by the cells before the drug is released[31]. Once a nanoparticle has reached its target cell, it is taken up by the cell through endocytosis. There are four main pathways[19] and these are shown in Figure 2.5.

- *Phagocytosis:* This is mainly performed by professional phagocytic cells: macrophages, monocytes, neutrophils and dendritic cells. Phagocytes engulf substances of sizes up to tens of micrometers like e.g. cellular debris, damaged cells and microorganisms. Phagocytosis occurs after opzonization of the substance[32]. The uptake mechanism includes folding of the cell membrane around the substance before ingestion into the intracellular space[33, pp.371-372].

- *Clathrin-mediated endocytosis:* A receptor mediated endocytosis mechanism for internalization of substances by eukaryotic cells, including cancer cells. This is the main internalization mechanism used by eukaryotic cell. When a substance binds to surface receptors on the cell, an inward budding of the cell membrane occurs. Adapter proteins and clathrin from inside the cytosol cover the substance on the cytosolic side of the membrane. A vesicle is formed inside the cell and cut of from the cell membrane by a complex of dyanamin proteins[33, pp.371-372].

- *Caveolae-mediated endocytosis:* This is the main internalization mechanism by eukaryotic cells after clathrin-mediated endocytosis, and it is used by cancer cells. The mechanism involves small bulb-shaped vesicles in the plasma membrane formed by caveolins (integral membrane proteins) and cavins (adapter proteins). These vesicles are called caveolae and they are used to trap extracellular substances. This leads to recruitment of dynamin proteins that cut the vesicle from the membrane and into the cytosol[19, 34, 35].

- *Pinocytosis:* Substances and fluid from the extracellular space are transported into the cytosol by invagination of the cell membrane. The method is non-specific since no receptors are used to determine which substances that are brought into the cell. This is called fluid endocytosis or cell drinking, and it is performed by eukaryotic cells like cancer cells[19].

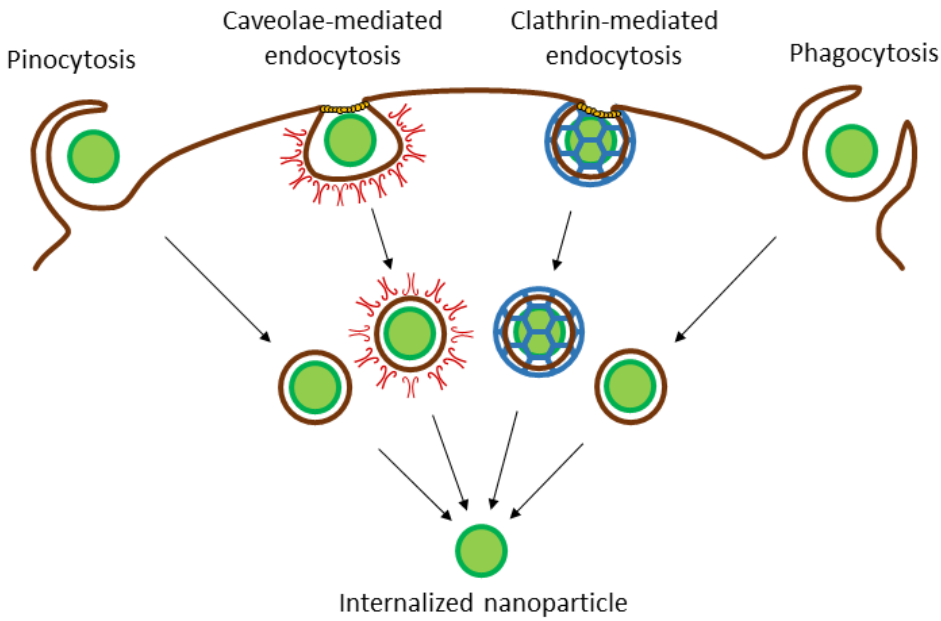

Figure 2.5: Illustration of the four main endocytic pathways for internalization of nanoparticles. From left: pinocytosis, caveolae-mediated endocytosis, clathrin-mediated endocytosis and phagocytosis.

The working site for the drugs encapsulated inside the nanoparticles are normally the cytosol. After internalization of the nanoparticles into the cytosol, the nanoparticles have to escape from the endolysosomal network in order to avoid degradation by lysosomes. Lysosomes have a low pH environment and contain a high level of enzymes, which is used to degrade foreign substances that enter the cell[19].

2.4 Ultrasound

Ultrasound is sound waves with frequencies higher than 20kHz. These frequencies are above the upper limit of the audibility range for the human ear. Sound waves are transmission of energy through a medium by collisions of adjacent particles. The particles oscillate around their equilibrium and there is no net displacement of the particles. Sound waves occur as two types, transverse and longitudinal waves. The type of wave is dependent on the direction of particle oscillations, relative to the direction of the transmitted energy. The wave is defined as transverse if the individual particles inside the medium oscillate in a direction perpendicular to the direction of the propagating energy. If the particles oscillate in the same direction as the propagating energy, the sound wave is defined as longitudinal[36]. These two types of sound waves are illustrated in Figure 2.6. Transverse waves require solid material to be able to transfer energy through the material, where as longitudinal waves can propagate through all kinds of materials, including soft tissues. Due to this, ultrasound is usually transmitted through the body by longitudinal waves. One exception is transmission of sound waves through bones. Solid bones inside the body can also experience transverse waves[36, 37].

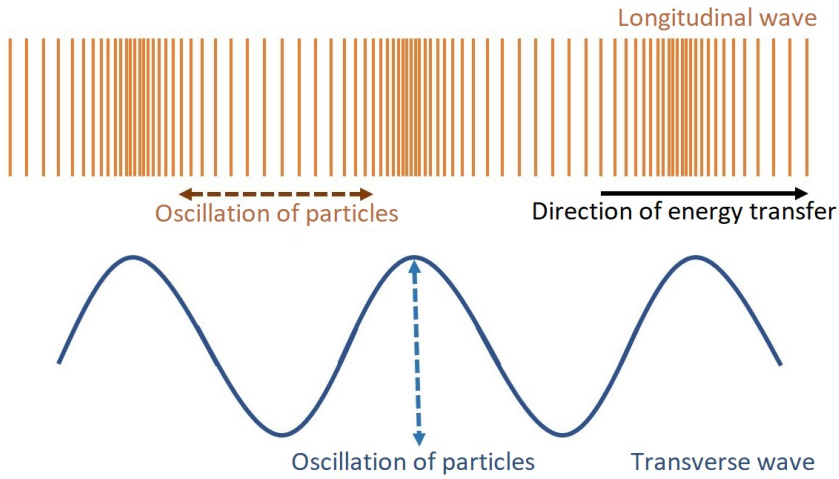

Figure 2.6: Illustration of longitudinal and transverse waves. In longitudinal waves the particles inside the medium oscillate in the same direction as the energy transfer. In transverse waves the particles oscillate perpendicular to the direction of the energy transfer.

Ultrasound is generated by piezoelectric transducers, where an applied voltage waveform is converted into mechanical pressure waves or sound waves[38]. These waves are described by wave parameters, like amplitude, wavelength, frequency and period. The amplitude is the difference between maximum compression and rarefaction of the wave. The wavelength is the distance between two point where the shape of the wave repeats. The frequency is the number of wave cycles per second, while the period is the time needed to complete one wave cycle. The relationship between the velocity, wavelength, frequency

and period of the wave is given in Equation 2.4[39]:

$$c = \lambda f = \frac{\lambda}{T} \tag{2.4}$$

where c is the velocity of the propagating wave through the medium, λ is the wavelength, f is the frequency and T is the period. The velocity is dependent on the elasticity and density of the medium, according to Equation 2.5[39, 40]:

$$c = \sqrt{\frac{E}{\rho}} \tag{2.5}$$

where c is the velocity, E is the elasticity and ρ is the density of the medium. Elasticity is the material's ability to regain its original form after deformation, like compression due to a sound wave. The density is mass per unit volume. The average velocity for propagating sound waves through body tissue is found be 1540 m/s[39].

Generation mode of an ultrasonic wave is a temporal characteristic of the waveform. There are two main generation modes for use in medical ultrasound, namely continuous wave mode and pulsed wave mode. In continuous generation mode, the transducer is continuously excited with an electric sine wave. This results in an ultrasonic wave with constant amplitude. For the pulsed wave, the transducer is excited by a very short electric signal, followed by a break. This is repeated and the ultrasonic wave is produced as pulses. The pulse duration (τ) is given is given by Equation 2.6[39]:

$$\tau = NT = \frac{N}{f} \tag{2.6}$$

where N is the number of cycles per pulse, T is the period and f is the frequency. The pulse is activated a fractional amount of time, given by the duty factor (DF) presented in Equation 2.7[39]:

$$DF = \frac{\tau}{PRP} = \tau PRF \tag{2.7}$$

where τ is the duration of the pulse, PRP is the pulse repetition period (the time from the start of one pulse to the start of the next) and PRF is the pulse repetition frequency (the number of pulses during a time unit)[39].

The mechanical index (MI) is an important value in therapeutic ultrasound, which is discussed in section 2.4.1. MI is a measure of mechanical effects on biological tissue due to ultrasound and is described by Equation 2.8[39]:

$$MI = \frac{p_{neg}}{\sqrt{f}} \tag{2.8}$$

where p_{neg} is the peak negative pressure in MPa, and f is the frequency of the sound wave in MHz.

Both diagnostic and therapeutic ultrasound are used within medicine. Diagnostic ultrasound is used regularly in clinical imaging. The method is safe for the patients and does not lead to biological effects inside the body due to the low deposition of energy[41]. Therapeutic ultrasound is used to achieve a certain biological effect inside the body by deposition of energy[42, p.1].

2.4.1 Therapautic ultrasound in nanoparticle drug delivery

Ultrasound has great potential in therapeutic drug delivery systems (DDS). It can be focused and used as local treatment on a target without effecting the surrounding tissue. The deposition of energy in tissues is used to produce both a thermal and a mechanical effect, depending on the aim of the treatment[43].

When the tissue absorbs energy from ultrasound waves, a local heating of the tissue occurs. If the intensity of the sound waves is high enough, this may lead to local hyperthermia. This results in an increased permeability of the blood vessels and increased blood flow to the heated area. This is utilized in drug delivery since an increased blood flow increases the flux and uptake of therapeutic agents[42–44]. Thermal effects from US can also be used in DDS as external stimuli for release of drugs from heat sensitive nanocarriers[42, 44].

Mechanical effects from ultrasound treatment are utilized in the DDS which is characterized in this thesis. The DDS is described by *Y. Mørch et al*[5]. PEGylated polymeric nanoparticles are used as a stabilizing shell around microbubbles. These complexes were administrated intravenously into the blood stream and focused ultrasound was applied locally on the tumor.

Several reviews [38, 42–44] describe the mechanical effects of ultrasound in combination with microbubbles. Microbubbles have a smaller size than the wavelenght of the ultrasound. This leads to volume oscillations of the microbubbles when they are located in a pressure field from sound waves. The bubbles expand at low pressure and contract at higher pressure. Volume oscillations around an equilibrium radius are called stable cavitation and occur at low values of the MI, described in Equation 2.8. Microstreaming (circulating fluid flow) occurs as a result of the volume oscillations. Also, an increased permeability of the vasculature is observed due to the formation of pores from expansion of microbubbles close to blood vessel walls. If sound waves with a high MI are applied, this may lead to inertial cavitation. Due to a high pressure, the radius of the microbubbles increase during the oscillations until a point where they collapse. The results from the collapse of microbubbles are shock waves and jet streams which increase the permeability of the vasculature even more[38, 42–44]. Both stable cavitation and inertial cavitation are illustrated in Figure 2.7.

If the microbubbles consist of a stabilizing shell of nanoparticles (encapsulating drugs), the nanoparticles are shot into the surrounding tissue during inertial cavitation. This increase the delivery of drugs to the tumor compared to tumors not treated with local focused ultrasound. The ultrasound treatment is usually applied as pulsed waves instead of a continuous waveform. This avoids heating of surrounding tissues, in addition to making it possible for new microbubbles to enter the pressure field in the break between the pulses[43].

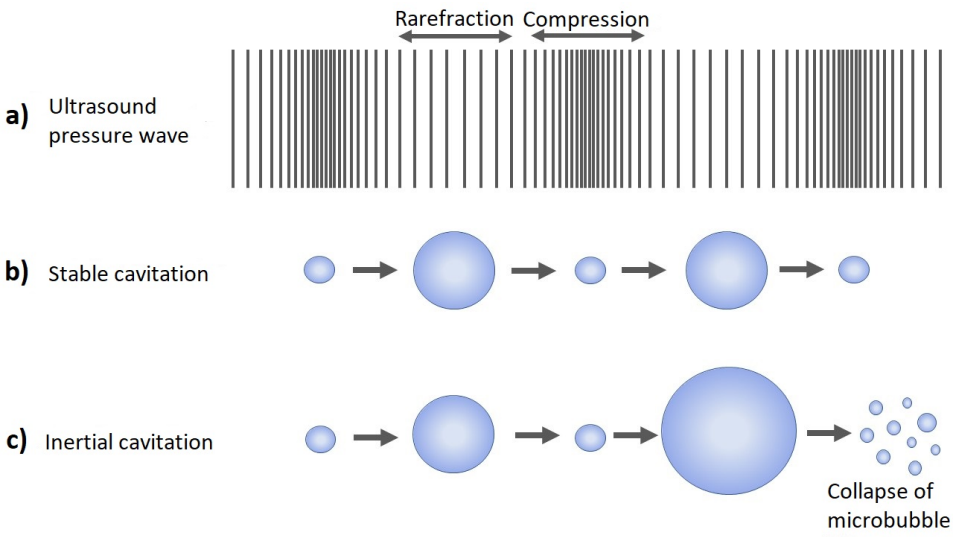

Figure 2.7: a) An ultrasound pressure wave. **b)** Stable cavitation where the microbubble oscillate in volume around an equilibrium radius. **c)** Inertial cavitation where the microbubble collapse due to a high acoustic pressure.

2.5 Experimental techniques

In this thesis, flow cytometry is used to analyse the tumors from trial 3 and 4, while confocal laser scanning microscopy (CLSM) is used to image the tumor sections from trial 1 and 2, Table 3.1, section 3.3. Both of these experimental techniques utilize fluorescence from fluorescent dyes.

2.5.1 The principle of fluorescence

Fluorescence techniques are based on fluorescent dyes, which are specific molecules or parts of molecules. These fluorescent dyes absorb and emit light. The absorbed light has specific wavelengths and energies. The light emitted from the fluorescent dyes has less energy and longer wavelengths compared to the absorbed light. The emitted light is therefore red shifted in the electromagnetic spectrum[45, pp.86-87]. Figure 2.8 illustrates the different energy states of a fluorescent dye. Photons with energies $h\nu_{ex}$ from an external source are supplied to the sample. These incoming photons excite the fluorescent dye from the ground state to an electronic singlet state S_1. The fluorescent dye stays in this excited state for a very short time period, normally between 1 to 10 ns. During this period, the fluorescent dye loses energy through conformational changes and non-radiative transitions between vibrational states, until it reaches a relaxed singlet state S_2. From this state, the fluorescence occurs when a photon with energy $h\nu_{em}$ is emitted and the fluorescent dye returns back to its original ground state S_0. From this ground state, the process could be repeated[46, p.3].

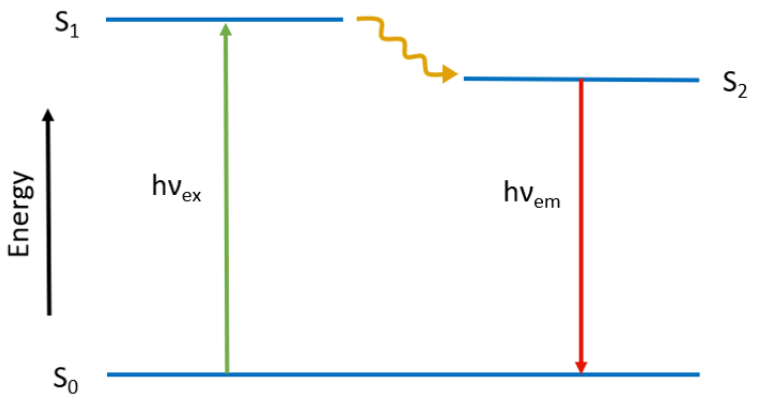

Figure 2.8: A Jablonski diagram showing the different energy states of a fluorescent dye. Incoming light excites the fluorescent dye from the ground state S_0 to a higher energy level S_1. The fluorescent dye stays in this excited state for a very short time period. During this period, the fluorescent dye loses energy through conformational changes and non-radiative transitions between vibrational states, until it reaches S_2. From S_2 and back to the ground state S_0, fluorescence occurs. The emitted light has lower energies and longer wavelengths than the exciting light.

2.5.2 Staining of biological components with fluorescent antibodies

Antibodies with fluorescent dyes are widely used in staining of biological components. In this thesis, the macrophages are stained with fluorescent antibodies. Both primary and secondary antibodies are used for staining, and they are produced in host animals. Primary antibodies are produced with the aim of binding to specific surface receptors on the cells. Secondary antibodies binds to primary antibodies from specific host animals[47, p.148].

There are two staining methods, direct or indirect immunostaining. Fluorescent dyes are labelled directly to the primary antibodies in direct immunostaining. In indirect immunostaining, both primary and secondary antibodies are used. Fluorescent dyes are labelled to the secondary antibodies. This method consists of two steps. First, the primary antibody binds to specific surface receptors. This is followed by binding of secondary antibodies to the primary antibodies. Indirect immunostaining has higher sensitivity compared to direct immunostaining. This is due to possibilities for signal amplifications, where several secondary antibodies bind to one primary antibody[47, pp.31-34]. An illustration of this is shown in Figure 2.9.

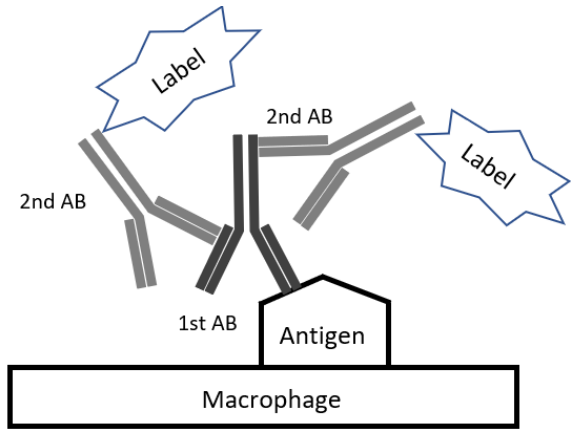

Figure 2.9: Illustration of indirect immunostaining. A primary antibody binds to a specific receptor on the surface of a macrophage. Several secondary antibodies with fluorescent dyes bind to the primary antibody to visualize the macrophage.

2.5.3 Flow cytometry

Flow cytometry is a quantitative method used to measure optical and fluorescence characteristics of single cells[48]. Based on this, flow cytometry can be used to distinguish between different types of cells in a single cell suspension. The general setup of a flow cytometer is illustrated in Figure 2.10.

The analysis requires a suspension of single cells. The cells in the suspension are stained with different fluorescent dyes that label the cell populations of interest. The fluorescent dyes are selected based on the available wavelengths of the lasers presented in the flow cytometer. The stained cell suspension is introduced into the flow cytometer together with a sheath fluid solution[49]. The sheath fluid solution is a cell-free buffer solution used for hydrodynamic focusing of the single cell suspension. A laminar flow occurs when two solutions with different flow rates are running side by side inside a small channel. In a flow cytometer, the single cell suspension is focused by the surrounding sheath fluid. The single cell suspension have a higher flow rate compared to the sheath fluid. This results in a focused stream of the cell sample where there is only room for one cell at the time[49, 50]. This is called hydrodynamic focusing, and the principle is illustrated as a part of Figure 2.10.

The streams of single cells are directed orthogonal through a laser beam, where the cells are illuminated. The fluorescent dyes are excited and release light with a specific wavelength. The optical system is designed to allow detection of multiple surface markers at the same time. This is done through the use of dichroic mirrors and several fluorescent detectors. The emission spectra of the fluorescent dyes are often wide and the signal from one dye is detected by several detectors. Thus, a single detector will detect emission from various fluorescent markers in varying degrees. The spillover fluorescence is removed by the use of a mathematical algorithm. The aim is that one detector only reports signals from one fluorescent dye. This is called compensation[49].

Flow cytometry presents relative data. A control sample, a sample not stained with the specific fluorescent dyes, has to be included in each analysis. These control samples are used to measure autofluorescence, and they are compared to the samples stained with the desired fluorescent dyes[49].

Optical information, like the forward scatter signal and side scatter signal, is also obtained when a cell sample is run through the flow cytometer. The scattered light from a cell is detected in the front of the cell with a forward scatter detector. Light that scatters at an angel orthogonal to the incoming laser beam is detected by a side scatter detector. The forward scatter signal provides information about the size of the cell, while the side scatter signal gives information about the granularity[49].

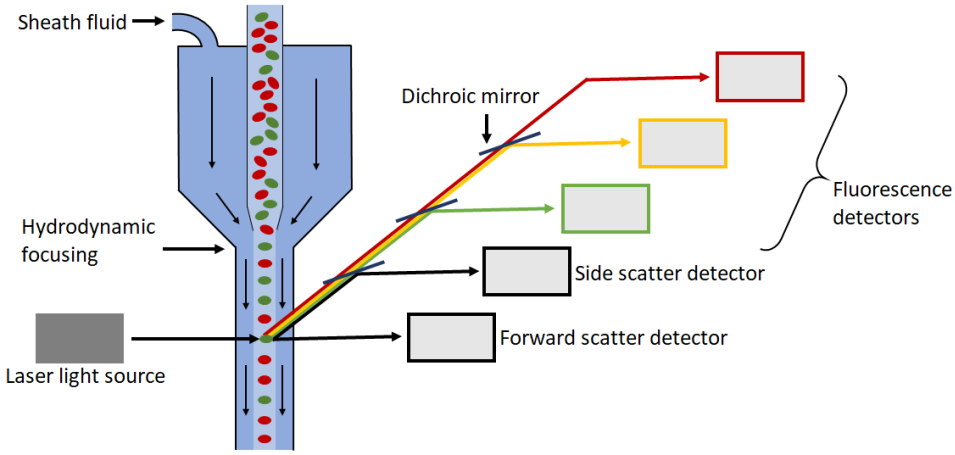

Figure 2.10: Illustration of the general setup of a flow cytometer. The cells are illuminated by a laser and the emitted fluorescent light is detected by several detectors. Light scattered from a cell is detected in the front of the cell by a forward scatter detector, while light that scatters at an angel orthogonal to the incoming light is detected by a side scatter detector. The principle of hydrodynamic focusing is also presented in the figure.

2.5.4 Confocal laser scanning microscopy

Confocal laser scanning microscopy (CLSM) is based on fluorescence, and the technique is popular within biological imaging[51, p.265-267]. The use of CLSM makes it possible to obtain images with high resolution, contrast, sensitivity, specificity and selectivity, all necessary in characterization of biological samples[45, p.86]. In CLSM, light with a certain wavelength is focused onto a sample where different components are stained with fluorescent dyes. The fluorescent dyes are excited and the emitted light is detected, resulting in an image of the stained components in the sample[51, p.267-272].

In traditional wide field microscopy, the entire sample is illuminated at once and an image of the whole illuminated region is created. The created image is based on light from both the focus-region inside the sample and light emitted from out-of-focus regions. This causes a blurry result. If the magnification and numerical aperture of the lens are low,

there will be a large dept of field (DOF). This is the distance between the lower and upper planes that define the focus-region. The light from the out-of-focus regions will not be a noticeable problem in the image if the DOF is large. On the other hand, if an objective with high magnification and numerical aperture is used, this produce a small DOF and the out-of-focus light becomes problematic[52, pp.221-223].

This problem is solved in confocal fluorescence microscopy by the use of a pinhole aperture. The pinhole is placed in the image plane in the front of the detector and it works as filter. The emitted light from the out-of-focus regions in the sample is stopped and do not contribute to the created image. The light emitted from the focal plane will converge on the pinhole and reach the detector. This is illustrated in Figure 2.11, where the light path through a confocal laser scanning microscopy is shown. When the out-of-focus light is filtered out, an optical section of the focus plane is created. The thickness of the optical section is dependent on several factors, including the wavelength of the laser and the size of the pinhole[52, pp.221-223].

The size of the pinhole depends on airy units. A small value of the airy unit gives a small diameter of the pinhole, resulting in a thin optical section. A decrease in the size of the pinhole improves the horizontal resolution in the image and gives a higher contrast. On the other hand, a small size of the pinhole limits the number of photons that reaches the detector. To obtain good images by the use of small pinhole sizes, the power of the excitation lasers have to be higher and the exposure time longer compared to the use of larger pinhole sizes. This increases the risk of photobleaching and light-induced damage to the sample[51, p.277].

The laser beam is scanned over the sample surface to obtain an image of the entire sample, hence the name confocal laser scanning microscopy. Two methods are used to scan the surface. The laser beam is either scanned systematically over the surface, or the laser beam is stationary and the sample stage is moved horizontally. The stationary laser beam is located at the optical axis to reduce aberration from the lenses[52, pp.221-223]. Aberration occurs when light that passes through a lens is not focused in the same point. For an ideal lens, the light is focused at the same point, but no lens is ideal in the reality. This may cause a blurred and distorted image[53]. Aberration is reduced by the use of a stationary laser beam, but movement of biological samples may cause distortions of the tissue. Due to this, the laser beam is usually scanned over the surface while the sample stage is stationary[52, pp.221-223].

By the use of CLSM, it is possible to obtain images of a sample in both 2D and 3D. If the optical section within the sample is moved in the z-direction, the data obtained from each point along the z-axis can be reconstructed as a 3D model of the sample[52, pp.221-223].

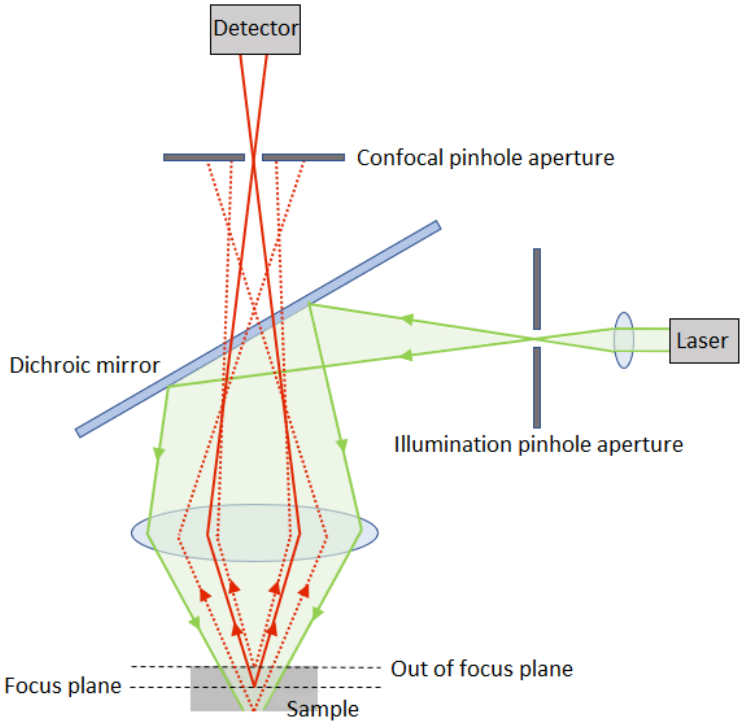

Figure 2.11: Illustration showing the light path through a confocal laser scanning microscopy. The confocal pinhole aperture works as a filter, and the emitted light from out-of-focus regions in the sample is stopped and do not contribute to the created image. The emitted light from the focal plane will converge on the pinhole aperture and reaches the detector.

Challenges of confocal laser scanning microscopy imaging

There are some important factors to be aware of during imaging of fluorescent dyes, and the most relevant ones are listed below:

- *Photobleaching:* This refers to photochemical destruction of fluorescent dyes, resulting in gradual loss of the emitted fluorescence intensity. When fluorescent dyes are exposed to light, photobleaching may occur due to oxidation or thermal decomposition of the chemical structure. This process is irreversible and a common problem during imaging of organic fluorescent dyes. The problem can be reduced by the use of reactive oxygen scavengers, reduced intensity of the excitation light and shorter exposure time of the sample[45, pp.124-125].

- *Bleed-through:* During subsequent imaging of fluorescent dyes in different color channels, bleed-through may be a challenge. If there is an overlap in the emission spectra from different fluorescent dyes, the same channel detects fluorescence from more than one dye. This makes it hard to distinguish between the different dyes.

It is possible to overcome this problem by the use of fluorescent dyes with proper distances between their emission spectra. In addition to this, suitable emission filters have to be chosen to separate the different signals[45, p.123].

- *Light-induced damage in tissues:* When tissues are exposed to light, several tissue-light reactions can arise and damage the sample. This includes photodisruption (mechanical forces disrupt tissue due to the occurrence of shock waves) and thermal interactions (the absorbed light is converted into heat that damage structures in the tissue)[52, p.173].
- *Autofluorescence:* Cellular components and the extracellular matrix have photophysical properties that leads to emission of fluorescence when they are exposed to light with certain wavelengths. This is called autofluorescence, and it may occur even though the components are not stained with fluorescent dyes. Sometimes, this makes it difficult to separate the background in the sample from the components stained with fluorescent dyes. The problem can be addressed by the use of suitable emission filters[52, p.163].

Chapter 3

Materials and methods

This master's thesis is a continuation of the specialization project carried out by the author in the autumn 2018[10]. Therefore, there will be some overlap between the method sections in these two works.

3.1 Cell cultivation

In this master thesis, human prostatic adenocarcinoma cells (PC3, American Type Culture Collection) and human osteosarcoma cells (OHS, Department of tumor biology at the Radium Hospital Oslo) were cultured with the aim of further implantation into mice. RAW cell line macrophages (St.Olavs, Trondheim University Hospital) were cultured for use in optimization of the protocol for flow cytometry analysis. PC3 and RAW cells were cultured in Dulbecco's Modified Eagle Medium (DMEM) with 10% fetal bovine serum (FBS) and 1% penicillin streptomycin. OHS cells were cultured in Roswell Park Memorial Institute (RPMI) 1640 Medium with 10% FBS, 0.5% L-glutamine and 1% penicillin streptomycin.

OHS and PC3 cells were first cultured in 75 cm^2 cell culturing flasks (VWR) containing 15ml growth medium and then transferred to 300 cm^2 flasks containing 60ml growth medium. This was done in order to grow the necessary amount of cells for implantation. RAW cells were only cultured in 75 cm^2 flasks. All cells were incubated at 37 °C with 5% CO_2 and kept at exponential growth. The growth medium was changed twice a week and cell splitting was done once a week.

The cells were split by removing the growth medium before they were washed in either 5ml (75 cm^2 flasks) or 20ml (300 cm^2 flasks) phosphate buffered saline (PBS). PBS was then removed and replaced by 3ml (75 cm^2) or 12ml (300 cm^2) 0.25% trypsin and 0.2% EDTA in order to detach the cells from the culturing flask. This solution was allowed to work for 3 minutes at 37 °C before adding of 8ml (75 cm^2) or 20ml (300 cm^2) growth medium to stop the trypsination. A light microscope (Leica DMIL) was used to confirm the detachment of the cells. One droplet of the solution was transferred to a Bürker chamber and the cells were counted under the light microscope. The remaining solution was transferred to a 14ml (75 cm^2) or 50 ml (300 cm^2) centrifuge tube (Corning Centristar)

and centrifuged at 1500 rpm for 5 minutes (Heraeus Megafuge 1.0). The supernatant was removed and the cells were resuspended in growth medium to obtain an concentration of either 1x10^6 cells/ml. 1.5 million cells (75 cm^2) or 6 million cells (300 cm^2) were transferred to a new flask.

The remaining non-discarded cells were used for implantation or experiments. Harvesting cells for implantation was done during a cell splitting process. After the centrifugation step, the supernatant was removed and cell medium was added to make a cell concentration of 3x10^6 cells/μl. The cell suspension was kept on ice in 2 ml tubes (VWR) until implantation.

3.2 Nanoparticle - stabilized microbubble complexes

The nanoparticles used in this master thesis were PEBCA (poly ethyl-butyl cyanoacrylate) polymeric nanoparticles loaded with nile red 688 fluorescent dye. The nanoparticles were coated with two different types of PEG (Brij and Kolliphor) and their diameter were between 100-200 nm. The nanoparticle-stabilized microbubble complexes were fabricated by self-assembly including 2 minutes mixing of 0.1 wt% nanoparticles and 0.5% casein in phosphate buffered saline (PBS) saturated with perfluoropropane (PFP). The diameter of the nanoparticle-stabilized microbubble complexes were approximately 2-4 µm. Both the nanoparticles and the microbubbles were synthesized at SINTEF Trondheim[5], by Anne Rein Hatletveit. Figure 3.1 shows a scanning electron microscopy image of a microbubble stabilized with nanoparticles.

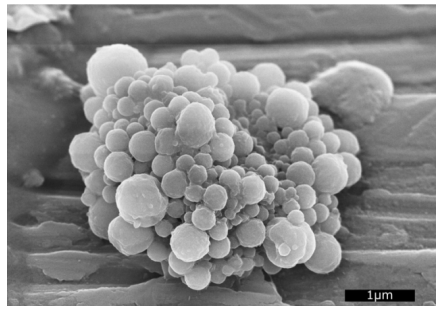

Figure 3.1: Scanning electron microscopy image of a nanoparticle-stabilized microbubble. The image is taken by Einar Sulheim, SINTEF/NTNU. Scale bar is 1 µm.

3.3 Animal trials

The tumor sections characterized in this master thesis are from two animal trials (trial 1 and trial 2) carried out during the spring of 2018. The tumors used for flow cytometry analysis are from two animal trials (trial 3 and trial 4) executed during the spring of 2019. All trials were performed by Einar Sulheim in accordance with strict regulations set by Norwegian Animal Research Authorities. The author assisted in the third and forth trial, but did not handle the animals.

Athymic Balb/c nude mice were used as an animal model. All of the animals were kept in ventilated cages with pathogen free conditions at 22-23°C and 50-60% relative humidity. There was free access to sterile water and food during the whole experiment period.

3.3.1 Tumor implantation

In all trials, the animals were anesthetized by a subcutaneous injection of fentanyl, medetomidine, midazolam and water in a concentration of 2:1:2:5. The given dose was 0.1 mL per 10 g. The animals were under anaesthesia during the implantation of cells, treatment and euthanasia, which was done by cervical dislocation. During this time period, their body temperature was kept stable by the use of a heat blanket.

Both human osteosarcoma cells (OHS) and human prostatic adenocarcinoma cells (PC3) were implanted under the skin on the left hind leg of the animals. In trial 1 and trial 2 the animals were randomly divided into groups of four, while in trial 3 and trial 4 the animals were divided into groups of five. One group in each trial was used as a control group while animals from the other groups were treated with ultrasound on the tumor. Table 3.1 gives a overview over the number of animals in the different trials and groups.

Table 3.1: The number of animals in the different animal trials. Tumors from trial 1 and trial 2 were analyzed by using CLSM, while tumors from trial 3 and trial 4 were analyzed by flow cytometry. The control groups were injected with nanoparticle-stabilized bubbles, while the treated groups were injected with nanoparticle-stabilized micobubbles in combination with ultrasound treatment.

Group	Trial 1 (OHS)	Trial 2 (PC3)	Trial 3 (OHS)	Trial 4 (PC3)
Control	4	4	5	5
Treated with US	4	4	5	5

3.3.2 Tumor treatment

The tumors were treated when they had reached a size of about 10 mm along the longest axis, a growing process taking typically 3-5 weeks after implantation of the cancer cells. An injection of nanoparticle-stabilized microbubble complexes (NPMBs) was given to all the animals in both the control group and the treated group. For the animals in the treated group the injection of NPMBs was combined with local ultrasound treatment on the tumor. Ultrasound treatment was not used on the animals in the control group.

The ultrasound setup is shown in Figure 3.2. A single-element focused transducer with a center frequency of 1MHz was used. The signal was generated by using a waveform generator combined with a 50-dB power amplifier. The transducer was placed at the bottom of a water bath. The animal was placed on top of an absorber coated lid over the water bath. The left hind leg with the tumor was placed into the water bath in focus of the transducer by the use of a 10 mm hole in the cover. The distance between the tumor and the transducer was 190 mm throughout the whole ultrasound exposure period. The water bath had a temperature of 34°C to maintain a stable body temperature in the animals and to avoid hypothermia. An external heat lamp was also used for this purpose.

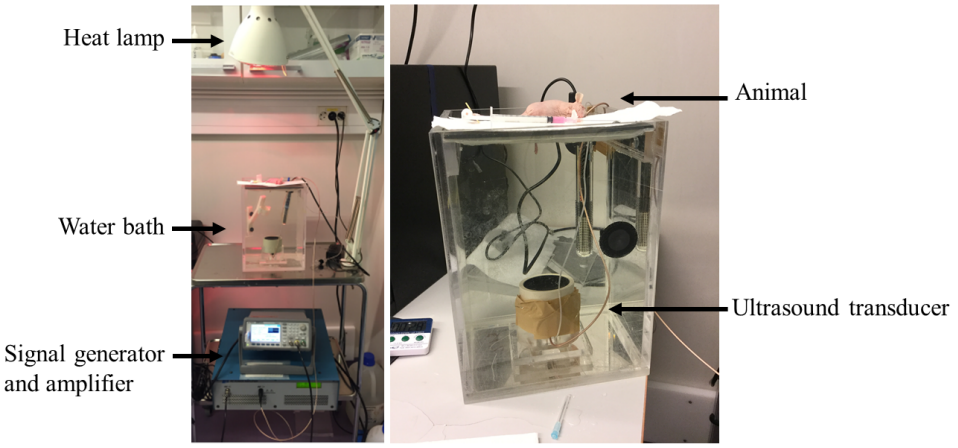

Figure 3.2: Images of the ultrasound setup used to treat the animals included in the treated groups in all trials. The image to the left is an overview of the entire setup which includes a signal generator, amplifier, ultrasound transducer, water bath, animal and heat lamp. To the right is a close up image of the US transducer, water bath and the animal placed on the top of the lid with its left hind leg inside the water bath.

100 µL NPMBs with a concentration of 10 mg/mL were injected into the animals during a period of 10-15 sec. For the treated group inn all trials, US treatment was started at the same time as the beginning of the injections. The US treatment was the same as previously used by *Snipstad et al.*[6]. For all treated animals, the US exposure lasted for 2 minutes. The treatment expected a total destruction of all microbubbles and consists of bursts of 10 000 cycles every 100 ms for 0.5 sec. This was followed by a break of 1.5 sec. The local pulse repetition frequency (PRF) was 10 Hz, while the global PRF was 0.5 Hz and the total duty cycle was 2.5%. The mechanical index (MI) of the US treatment was 0.5. The animals in the control groups were also placed with their left hind legs inside the water bath in 2 minutes from the beginning of the injection of NPMBs, although they where not treated with US. This was done to make sure that the US treatment was the only different factor between the control groups and the treated groups.

In trial 1 and trial 2, an injection dose of 100 µL fluorescent labeled lectin-FITC was given to the animals 5 minutes before euthanasia. This was done to stain vascular endothelial cells inside the tumor, making it possible for further imaging of the blood vessels inside the tumors. The animals in all trials were euthanized 30 minutes after the US treatment, followed by immediate removal of the tumors from the hind legs of the animals. The tumors from trial 1 and trial 2 were then flash frozen in liquid nitrogen before each tumor was sectioned into evenly distributed 25 µm sections. The sectioning was performed by Ingunn Nervik at CMIC NTNU. The sections were then mounted on glass slides and stored in a freezer at -80°C before further staining and imaging. The tumors from trial 2 and trial 3 were stored in growth medium at 4°C over the night before they were used for flow cytometry analysis the following day.

3.4 Flow cytometry analysis

Tumors from animal trial 3 and trial 4 were used for flow cytometry analysis. To make it possible to analyse a tumor by the use of flow cytometry, a single cell suspension was made and the macrophages in the cell suspension was stained with fluorescent antibodies.

The following sections describe the method from a tumor to digital results. This method is a result of an optimization process where the starting point was a project work by Unni Cecilie Nygaard written in the spring 1996[54]. Each of the sections below contain a subsection which describes the optimization process and the tested parameters. The tumors used in this optimization process and the development of the method were left over from other ongoing trials in Catharina de Lange Davies' research group.

3.4.1 Single cell suspension

There are two methods used to make single cell suspension from a tumor, mechanical disintegration or enzymatic disintegration. Both methods were tested in this thesis and mechanical disintegration was chosen to be used for the tumors in trial 3 and trial 4.

Mechanical disintegration

During disintegration a Stomacher Lab-Blender 80 (Seward Medical, London. Model No. BA 6020, 50Hz) was used. The centrifuge used, was a Heraeus Megafuge 1.0.

1. The tumor was weighed and placed in a special Stomacher plastic bag. A mortar and a pestle was used to crush the tumor into small pieces inside the plastic bag.
2. The crushed tumor was transferred to a new Stomacher plastic bag and 25 ml growth medium was added. The growth medium was dependent on the type of tumor, PC3 or OHS. Growth medium for the different tumors are described in section 3.1.
3. For OHS tumors the plastic bag was placed in the Stomacher for 3 minutes, while for PC3 tumors the time in the Stomacher was 7 minutes.
4. The cell suspension was filtered through a cell strainer (Falcon) with pore size $70\,\mu\mathrm{m}$, followed by filtration though a cell strainer (Falcon) with pore size $40\,\mu\mathrm{m}$. The strainers were moisturized with PBS before the filtration of the cell suspension.
5. The cell suspension was transferred to a centrifuge tube (Corning Centristar) and centifuged at 1500 rpm for 5 minutes.
6. The supernatant was removed and the cells were resuspended in 50 ml PBS.

Enzymatic disintegration

A Heraeus Megafuge 1.0 was used for centrifugation of the samples. The enzymatic solution consist of 0.14% (0.014g/10ml) Collagenase type I (SIGMA), collagenase activity 246 unit/mg solid. The second substance was 0.1% (0.01g/10ml) DNase (SIGMA) with activity 2840 unit/mg solid. These chemicals were solved in PBS with 1% bovine serum albumin (BSA).

1. The tumor was weighed and placed in a special Stomacher plastic bag. A mortar and a pestle was used to crush the tumor into small pieces inside the plastic bag.
2. The crushed tumor was transferred to a centrifuge tube (Corning Centristar) and incubated with the enzymatic solution at 37°C for 40-60 minutes. The suspension was mixed with a vortex mixer every 5 minutes.
3. To stop the enzymatic disintegration, 10 ml PBS was added to the suspension.
4. The cell suspension was filtered through a cell strainer (Falcon) with pore size $70\,\mu\mathrm{m}$, followed by filtration though a cell strainer (Falcon) with pore size $40\,\mu\mathrm{m}$. The strainers were moisturized with PBS before the filtration of the cell suspension.
5. The cell suspension was transferred to a new centrifuge tube and centifuged at 1500 rpm for 5 minutes.
6. The supernatant was removed and the cells were resuspended in 50 ml PBS.

Optimization of the method to make single cell suspension

To find the best way to make a single cell suspension from a tumor, both mechanical and enzymatic disintegration were tested. Both methods were tested with different time parameters to find the best parameters to obtain a high number of viable cells per gram tumor. One million viable cells were used for one sample (this means that the number of viable cells from one tumor had to be higher than one million). The two methods were tested for both OHS and PC3 tumors. Several experimental series, consisting of 2 tumors) were performed where tumors with approximately the same weight were compared. Mechanical disintegration was used to make a single cell suspension of one tumor, whereas enzymatic disintegration was used on the other tumor. Mechanical and enzymatic disintegration were performed as described in previous sections, but the time in the Stomacher and the enzymatic incubation time varied in the different series.

For OHS tumors, two series were performed and the results are shown in Table 4.1, section 4.1.1. For mechanical disintegration the Stomacher time was 3 minutes and for enzymatic disintegration the incubation time was 40 minutes. The OHS tumors have a soft consistency and they were easy to crush. These times parameters gave a large number of viable cells per gram tumor for both mechanical and enzymatic disintegration and were therefore used again in series 2.

Three PC3 series were performed and the results are shown in Table 4.2, section 4.1.1. In series 1, the Stomacher time was 3 minutes for mechanical disintegration and the enzymatic incubation time was 40 minutes. This was the same parameters as used for OHS tumors, but the PC3 tumors have a hard consistency and were difficult to crush. These times gave a very small number of viable cells per gram for both of the disintegration methods. Two more series where therefore performed. For mechanical disintegration, the Stomacher time was increased by two minutes for each series and for enzymatic disintegration the incubation time was increased by ten minutes. The Stomacher time was 5 minutes for series 2 and 7 minutes for series 3. The enzymatic incubation time was 50 minutes for series 2 and 60 minutes for series 3.

Mechanical disintegration gave the highest number of viable cells per gram tumor and was therefore chosen to be the best option to make single cell suspensions from both OHS and PC3 tumors. The Stomacher times was chosen to be 3 minutes for OHS tumors and 7 minutes for PC3 tumors.

3.4.2 Counting of viable cells

The cells in the single cell suspension were counted to find the number of viable cells in the sample. A Countess automated cell counter (Invitrogen) was used. Cell suspension and trypan blue were added to a counting chamber slide (Invitrogen) in ratio 1:1 (10 µL cell suspension and 10 µL trypan blue). Trypan blue gives the dead cells a blue color. The counting chamber slide was placed inside the cell counter, and the instrument gave the number of viable and dead cells in the cell suspension.

3.4.3 Staining of macrophages

Indirect immunostaining with primary and secondary antibodies was used to stain the M1 and M2 macrophages in the cell suspensions. Two primary antibodies were used. One binds to F4/80 receptors on the surface of all macrophages (M1 + M2), while the other primary antibody binds to CD206 mannose receptors on the surface of only M2 macrophages. M1 macrophages have no characteristic surface receptors which make it possible to label them with specific antibodies. M2 macrophages, on the other hand, are possible to stain with antibodies due to characteristic surface receptors[15]. This is the reason why one primary antibody was selected to bind to all macrophages (M1 + M2) and the other primary antibody was chosen to only bind M2 macrophages.

The F4/80 antibody was purchased from Bio-Rad[55] and was raised in rats as host animals. The antibody was delivered as a liquid in a concentration of 1.0 mg/mL. CD206 was purchased from Thermo Fisher Scientific[56] with goats as host animals. This antibody came as powder and was reconstituted in sterile PBS to obtain a concentration of 0.2 mg/mL, as given in the datasheet.

An anti-goat antibody with AlexaFluor488 as fluorescent marker was selected as secondary antibody to stain M2 macrophages. The secondary antibody used to stain all macrophages (M1 + M2) was an anti-rat antibody with DyLight405 as fluorescent dye. Both these secondary antibodies were purchased from Dianova[57] and delivered as powder. The powder was reconstituted in 1:1 dH_2O and glycerol to obtain a concentration of 1.5 mg/mL for the AlexaFluor488 antibody and a concentration of 1.0 mg/mL for the DyLight405 antibody. The information about the reconstitution was given in their datasheets.

Preparation of antibodies before staining

A volume of 100 µL primary and secondary antibodies in correct concentration (diluted in PBS with 1% BSA) were used to stain 10^6 cells. The antibody concentrations are given in Table 3.2.

Table 3.2: The concentrations of the primary and secondary antibodies used to stain macrophages in the single cell suspension.

Antibody	Concentration per million cells
F4/80	4 µg
CD206	5 µg
AlexaFluor488	0.5 µg
DyLight405	0.5 µg

The staining procedure

The staining procedure was performed at 4°C to prevent capping of the antibodies.

1. The cells in the single cell suspension were counted and 10^6 viable cells were placed within a centrifuge tube (Corning Centristar). The sample was centrifuged at 1500 rpm for 5 minutes followed by removal of the supernatant.

2. *Incubation with primary antibodies:* 100 µL F4/80 antibody in correct concentration (diluted in PBS with 1% BSA) was added to the sample. This was immediately followed by adding of 100 µL CD206 antibody in correct concentration (diluted in PBS with 1% BSA). The sample was resuspended and incubated with the antibodies at 4°C for 45 minutes.

3. *Washing step to remove unbounded primary antibodies:* 3 ml PBS with 1% BSA was added to the sample. The sample was resuspended and centrifuged at 1500 rpm for 5 minutes. The supernatant was removed and the same washing procedure was repeated.

4. *Incubation with secondary antibodies:* 100 µL DyLight405 antibody in correct concentration (diluted in PBS with 1% BSA) was added to the sample. This was immediately followed by adding 100 µL AlexaFLuor488 antibody in correct concentration (diluted in PBS with 1% BSA). The sample was resuspended and incubated with the antibodies in the dark at 4°C for 30 minutes.

5. *Washing step to remove unbounded secondary antibodies:* 3 ml PBS with 1% BSA was added to the sample. The sample was resuspended and centrifuged at 1500 rpm for 5 minutes. The supernatant was removed and the same washing procedure was repeated.

Optimization of the antibody concentration for staining of macrophages

The recommended concentrations for the primary and secondary antibodies for use in flow cytometry were given in their respective datasheets. These concentrations were tested for both OHS and PC3 single cell suspensions, but no staining was seen during the flow cytometry. A concentration study was therefore performed to find the most suitable concentrations of antibodies.

The concentration of secondary antibodies was constantly kept at $0.5\,\mu g/10^6$ cells. This was the highest recommended concentration of the secondary antibodies according to their datasheets. For the primary antibodies, different concentrations were tested. The starting point was the concentrations from the datasheets. These concentrations were increased 5, 10 and 20 times, as shown in Table 3.3.

Table 3.3: Concentrations of primary antibodies tested to find the most suitable concentration for use in this flow cytometry analysis.

Concentration	F4/80 antibody	CD206 antibody
Concentration from datasheet	$0.2\,\mu g/10^6$ cells	$0.25\,\mu g/10^6$ cells
5 X	$1\,\mu g/10^6$ cells	$1.25\,\mu g/10^6$ cells
10 X	$2\,\mu g/10^6$ cells	$2.5\,\mu g/10^6$ cells
20 X	$4\,\mu g/10^6$ cells	$5\,\mu g/10^6$ cells

OHS samples were stained by either DyLight405 and varying concentrations of the F4/80 antibody, or AlexaFluor488 and varying concentrations of the CD206 antibody. The concentration of the antibodies were either 5, 10 or 20 times higher than the datasheet concentration. One control sample not stained with antibodies was also included. Overlay plots of the histograms from these samples are shown in Figure 4.1, section 4.1.2. These staining procedures were repeated for the PC3 samples. Overlay plots of the histograms from these samples are shown in Figure 4.2, section 4.1.2.

All samples in these four series were also stained with a live/dead dye to separate the dead cells from the live cells, as explained in section 3.4.4. From the results in Figure 4.1 and 4.2, section 4.1.2, it was decided to use a concentration of 20 times the datasheet concentration for both the F4/80 and CD206 primary antibodies. The concentration of secondary antbodies was kept as the highest recommended concentrations from their respective datasheets. These concentrations of antibodies were used for both OHS and PC3 samples in trial 3 and 4.

3.4.4 Live/dead staining

Dead cells will have a lot of unspecific binding of secondary antibodies which will give false positive results. These dead cells have to be separated from the live cells before the results can be analyzed. A live/dead staining kit purchased from Thermo Fisher Scientific [58] was used for this purpose.

The live/dead kit consist of five separate vials, where each of them contain 0.3 mg powder of a near-IR reactive dye with 633 nm as excitation length. The dye had to be reconstituted before use. 50 µL dimethyl sulfoxide (DMSO) was added to one viral with 0.3 mg powder and the solution was mixed well. The reconstituted DMSO solution with reactive dye was somewhat unstable and had to be used within a few hour.

The incubation with this live/dead dye was done immediately after incubation with secondary antibodies. After the centrifugation in the last washing step used to remove unbounded secondary antibodies, the supernatant was removed and the sample was resuspended in 1 ml PBS. 1 µL of the DMSO solution with dye was added and the sample was mixed properly. This was followed by incubation in the dark on ice for 30 minutes.

The fluorescent dye will react with the live cells and bind to their surface, resulting in a weak fluorescent signal. Dead cells with permeable membranes will react with this dye throughout their whole volume, resulting in a high fluorescent signal. This will appear as two peaks in the live/dead histogram from the flow cytometry analysis. An example of a histogram is shown in Figure 3.3, section 3.4.6.

3.4.5 Flow cytometry

The cell samples were analyzed by the use of a Gallios Beckman Coulter Flow Cytometer. This flow cytometer had four lasers and ten detectors. Before running the flow cytometry, the cells from each sample were transferred to flow cytometry tubes. The cell samples contained four dyes, which all were excited by the use of different lasers. The used excitation lasers and detectors are listed below:

- The AlexaFluor488 dye, which stained M2 macrophages, was excited by a blue laser at wavelength λ = 488nm. The dye was detected at λ = 525nm using detector FL1 with a 40nm band-pass filter.
- The dye in the nanoparticles was nile red (NR688). This dye was excited at λ = 561nm by a green laser. The particles were detected at λ = 620nm using detector FL3 with 30nm band-pass filter.
- The near-IR dye from the live/dead kit was exited by a red laser at wavelength λ = 633nm. The dye was detected at wavelength λ = 755nm using FL8 with a low-pass filter.
- The DyLight405 dye which stained all macrophages (M1 + M2) was excited by a violet laser at wavelength λ = 405nm. The dye was detected at λ = 450nm using detector FL9 with a 50nm band-pass filter.

The voltage was set to place the unlabeled cell population in the interval from 0-1 on a log scale that shows the fluorescence intensity. 100 000 cells from each sample were counted, but if this was not achievable the flow cytometer stopped counting the cells after 3 minutes.

Development of a protocol in the flow cytometer software

A protocol in the flow cytometer software was made before trial 3 and 4 were executed, and the samples from these trials were run through the flow cytometer. Calibration of this protocol relied primarily on two factors of errors, namely non-specific binding of secondary antibodies and spillover of fluorescence between the different detectors. These factors were determined through test runs of several stained samples.

Both OHS and PC3 samples, stained only with either the DyLight405 secondary antibody or the AlexaFluor488 antibody, were made. These samples were stained with secondary antibodies in a concentration of $0.5\,\mu g/10^6$ cells which was the concentration used in trial 3 and 4. Live/dead staining was also included in these samples. OHS and PC3 control samples stained only with live/dead were also run though the flow cytometer. Overlay histograms with fluorescence intensity versus number of cells, for both the samples stained with secondary antibodies and the samples only stained with live/dead, are shown in Appendix A. These histograms were used to determine if there were any non-specific bindings of secondary antibodies.

To check for spillover of fluorescence between the different detectors, several samples of both OHS and PC3 cells were made and run through the flow cytometer. This includes the samples listed below. All of these samples were also stained with the near-IR live/dead dye to gate out the dead cells.

- Control samples with only cells.
- Samples stained with the primary F4/80 antibody ($4\,\mu g/10^6$ cells) followed by the secondary DyLight405 antibody ($0.5\,\mu g/10^6$ cells).
- Samples stained with the primary CD206 antibody ($5\,\mu g/10^6$ cells) followed by the secondary AlexaFluor488 antibody ($0.5\,\mu g/10^6$ cells).
- Samples stained with the F4/80 antibody ($4\,\mu g/10^6$ cells) followed by the DyLight405 antibody ($0.5\,\mu g/10^6$ cells), in addition to the CD206 antibody ($5\,\mu g/10^6$ cells) followed by the AlexaFluor488 antibody ($0.5\,\mu g/10^6$ cells).
- Samples containing nanoparticles with Nile Red 688 fluorescent dye.
- Samples stained with the primary F4/80 antibody ($4\,\mu g/10^6$ cells) followed by the secondary DyLight405 antibody ($0.5\,\mu g/10^6$ cells). These samples also contained nanoparticles with Nile Red 688 fluorescent dye.
- Samples stained with the primary CD206 antibody ($5\,\mu g/10^6$ cells) followed by the secondary AlexaFluor488 antibody ($0.5\,\mu g/10^6$ cells). These samples also contained nanoparticles with Nile Red 688 fluorescent dye.
- Samples stained with the F4/80 antibody ($4\,\mu g/10^6$ cells) followed by the DyLight405 antibody ($0.5\,\mu g/10^6$ cells), in addition to the CD206 antibody ($5\,\mu g/10^6$ cells) followed by the AlexaFluor488 antibody ($0.5\,\mu g/10^6$ cells). These samples also contained nanoparticles with Nile Red 688 fluorescent dye.

The information from these test runs and from the samples only stained with secondary antibodies, was used to make a compensation for the spillover of fluorescence between the different detectors. The compensation was saved as a protocol in the flow cytometer software and used for all samples in trial 3 and 4. The compensation file is shown in Appendix B.

Testing of the flow cytometry protocol with RAW cells cultivated in the cell lab

When the compensation was completed, the flow cytometer protocol was run with cells cultivated in the cell lab. Two samples was made. One sample consisted of OHS cells mixed with 10% RAW macrophages, while the other sample consisted of PC3 cells mixed with 10% RAW macrophages. These samples were used to test the protocol, in addition to control if all macrophages were stained by the use of the current antibodies, since the percentage of macrophages in the samples was know. All antibodies were used in the concentrations listed in Table 3.2, section 3.4.3. This is the same concentration as used for the tumors in trial 3 and 4. The results are shown in Figure 4.3 and 4.4, section 4.1.3. They are gated and analyzed like explained in section 3.4.6.

3.4.6 Data analysis in Kaluza

The flow cytometry data was analyzed using the Kaluza Analysis 1.3 software[59]. A detailed description of the analysis is given in Figure 3.3 - 3.6.

Histogram A in Figure 3.3 shows the near-IR live/dead dye fluorescence intensity (log) on the x-axis versus number of cells on the y-axis. The viable cells have a weak fluorescent signal and are placed to the left in the histogram, while the dead cells have a strong fluorescent signal and are placed to the right. These two peaks are possible to distinguish as two populations as shown in B, Figure 3.3. The forward scatter signal (linear) versus the live/dead fluorescence intensity (log) are shown as a density plot. This plot was used to create a gate containing the viable cells and the dead cells were separated out from further analysis. Histogram C, D and E in Figure 3.3 show the fluorescence intensity (log) of DyLight405 (M1 + M2 macrophages), AlexaFluor488 (M2 macrophages) and Nile Red 688 (nanoparticles) versus the number of cells. The histograms were gated for viable cells and their positive fluorescent peak indicates successful staining.

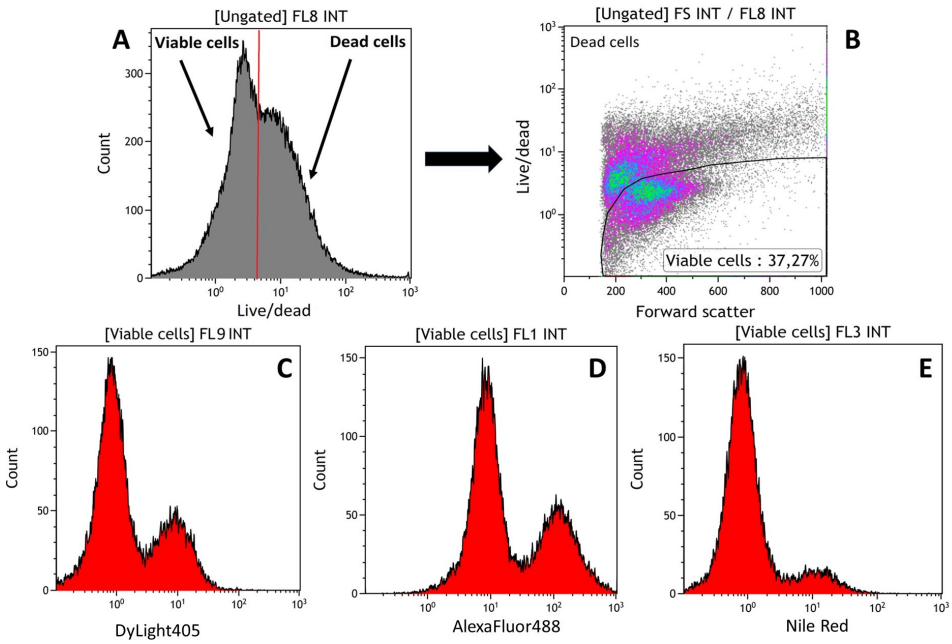

Figure 3.3: A shows a histogram with live/dead dye fluorescence intensity (log) on the x-axis versus number of cells on the y-axis. The two peaks in the histogram indicate the viable and dead cell populations. The density plot in B shows the forward scatter signal (linear) versus the live/dead fluorescence intensity (log). This plot was used to gate for the viable cells. Histogram C, D and E show the fluorescence intensity (log) of DyLight405 (M1 + M2 macrophages), AlexaFluor488 (M2 macrophages) and Nile Red 688 (nanoparticles) versus the number of cells. The histograms are gated for viable cells and their positive fluorescent peak indicates successful staining.

The further gating strategy used in Figure 3.4 and 3.5 is previously described by *Qin Dai et.al* [60] in the supporting information.

Plot F in Figure 3.4 is a density plot and shows the DyLight405 fluorescence intensity (log) versus the side scatter signal (log). The plot is gated for viable cells and shows two cell populations. The population to the right is positive for DyLight405 and gated as M1+M2 macrophages. The population to the left is negative for DyLight405 and gated as tumor cells. The gate was put in the middle of the two populations. This provided information about the percentage of macrophages in the sample.

The density plot G in Figure 3.4 shows the DyLight405 fluorescence intensity (log) versus the Nile Red fluorescence intensity (log). This plot is gated for M1+M2 macrophages, and it was used to decide the percentage of macrophages containing nanoparticles in the sample. The population placed towards the upper right corner of this plot is M1 + M2 macrophages positive for Nile Red, and it is gated as M1 + M2 macrophages containing nanoparticles. A drift of cells is seen from this populations towards the bottom line of the plot. These cells are negative for Nile Red and defined as M1 + M2 macrophages without nanoparticles.

H in Figure 3.4 also shows a density plot with the DyLight405 fluorescence intensity (log) versus the Nile Red fluorescence intensity (log), but this plot is gated for tumor cells. The information from this plot was used to decide the percentage of tumor cells containing nanoparticles in the sample. The population placed towards the bottom left corner of the plot is tumor cells negative for Nile Red, and it is defined as tumor cells without nanoparticles. A small drift of cells is seen towards the upper line of the diagram and these cells are gated as tumor cells with nanoparticles.

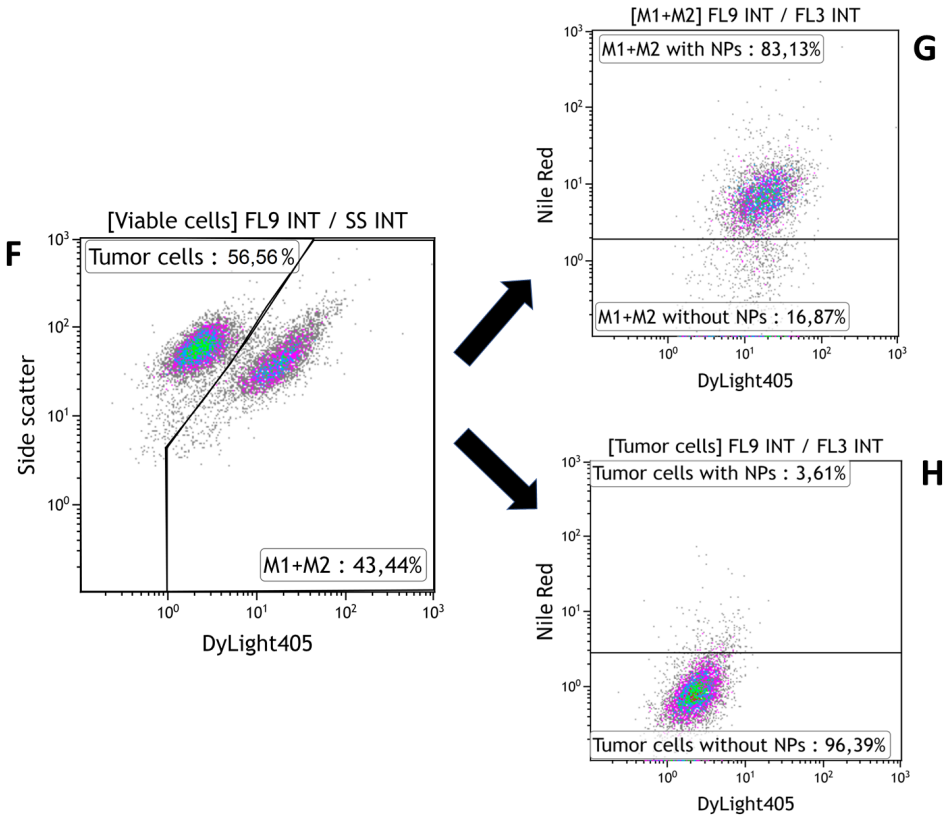

Figure 3.4: Density plot F shows the DyLight405 fluorescence intensity (log) versus the side scatter signal (log). The plot is gated for viable cells and shows two cell populations. The population to the right is positive for DyLight405 and gated as M1+M2 macrophages. The population to the left is negative for DyLight405 and gated as tumor cells. This provides information about the percentage of macrophages in the sample. The density plots G and H show the DyLight405 fluorescence intensity (log) versus the Nile Red fluorescence intensity (log). Plot G and H is gated for M1+M2 macrophages and tumor cells respectively, and gives information about the percentage of cells containing nanoparticles.

The density plot I in Figure 3.5 shows the AlexaFluor488 fluorescence intensity (log) versus the side scatter signal (log). The plot is gated for viable cells and shows two cell populations. The population to the right is positive for AlexaFluor488 and gated as M2 macrophages. The population to the left is negative for AlexaFluor488 and gated as tumor cells + M1 macrophages. The gate was put in the middle of the two populations. This provided information about the percentage of M2 macrophages in the sample.

Plot J in Figure 3.4 is a density plot and shows the AlexaFluor488 fluorescence intensity (log) versus the Nile Red fluorescence intensity (log). This plot is gated for M2 macrophages, and it was used to decide the percentage of M2 macrophages containing nanoparticles in the sample. The population placed towards the upper right corner of this plot is M2 macrophages positive for Nile Red, and it is gated as M2 macrophages containing nanoparticles. A drift of cells is seen from this populations towards the bottom line of the plot. These cells are negative for Nile Red and defined as M2 macrophages without nanoparticles.

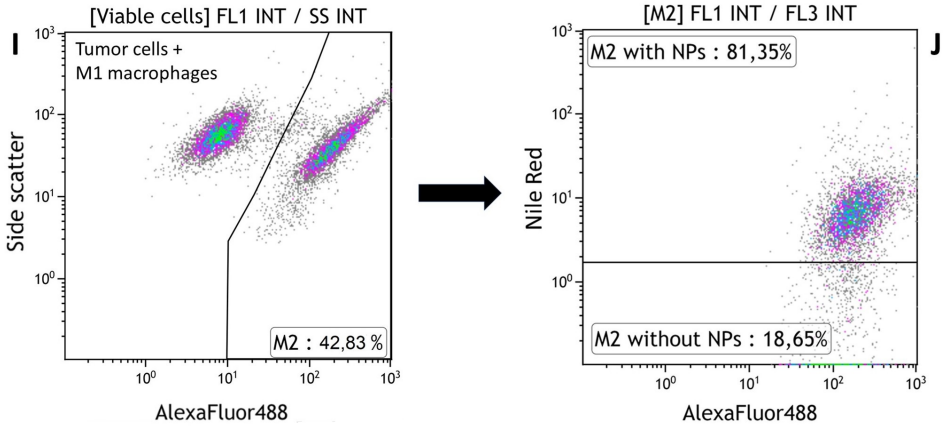

Figure 3.5: Density plot I shows the AlexaFluor488 fluorescence intensity (log) versus the side scatter signal (log). The plot is gated for viable cells and shows two cell populations. The population to the right is positive for AlexaFluor488 and gated as M2 macrophages. The population to the left is negative for AlexaFluor488 and gated as tumor cells + M1 macrophages. This provides information about the percentage of M2 macrophages in the sample. The density plot J shows the AlexaFluor488 fluorescence intensity (log) versus the Nile Red fluorescence intensity (log). Plot J is gated for M2 macrophages and it is used to decide the percentage of M2 macrophages containing nanoparticles in the sample.

Figure 3.6 show two histograms where the Nile Red fluorescence intensity (log) is plotted against the number of cells. Histogram K is gated for M1+M2 macrophages containing nanoparticles, while histogram L is gated for tumor cells with nanoparticles. The fluorescence values from the cells in the histograms were used to calculate the percentage of nanoparticles that accumulated in both macrophages and in tumor cells.

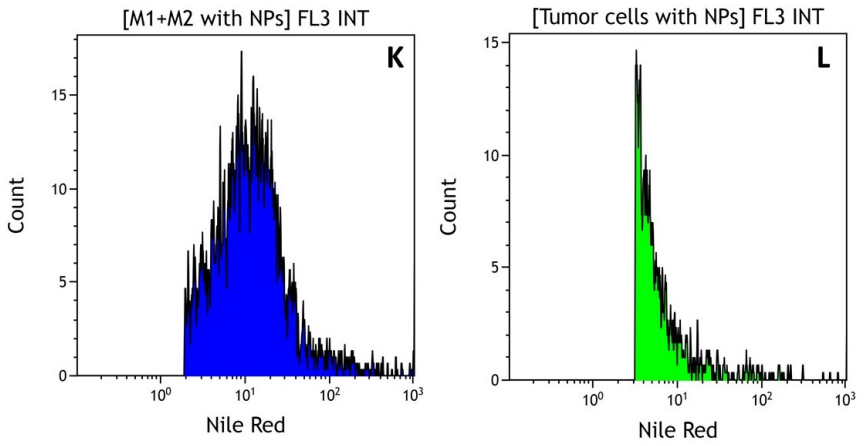

Figure 3.6: Two histograms where the Nile Red fluorescence intensity (log) is plotted against the number of cells. Histogram K is gated for M1+M2 macrophages containing nanoparticles, while histogram L is gated for tumor cells with nanoparticles. The information from these histograms were used to calculate the accumulation of nanoparticles in macrophages and tumor cells.

3.4.7 Statistical analysis

The data achieved from the analysis in Kaluza were exported to Microsoft Excel and all statistical analysis for this part of the project was executed using this program. Student t-test were used to determine significance of the results. P-values ≤ 0.05 were considered as significant.

3.5 Confocal laser scanning microscopy analysis

The tumor sections from animal trial 1 and 2 were analyzed using confocal laser scanning microscopy. The following sections describe the method from tumor sections to digital results.

3.5.1 Staining of macrophages and mounting of tumor sections

This procedure for staining of macrophages was made in the specialization project carried out by the author in the autumn 2018[10]. All macrophages (M1 + M2) were stained by the use of indirect immunostaining. One primary and one secondary antibody were used. The primary antibody binds to F4/80 receptors on the surface of all macrophages and was the same as one of the primary antibodies used for flow cytometry analysis. The F4/80 antibody has rat as host animal and it was purchased from Bio-Rad [55]. The antibody was delivered as liquid in a concentration of 1.0 mg/mL. An anti-rat antibody with Cy3 as fluorescent marker was used as secondary antibody, and this was purchased from Dianova[57] as powder. The powder was reconstituted in 1:1 dH_2O and glycerol to obtain a concentration of 1.0 mg/mL. The information about the reconstitution was given in the datasheet.

The staining procedure

1. *Fixation:* The sections were washed in room tempered PBS for 2 minutes. This was followed by fixation in room tempered 80% methanol for 5 minutes and 100% acetone at temperature -20°C for 2 minutes.

2. *Pap pen barrier:* A pap pen was used to draw a hydrophobic barrier around the tumor sections. This was done to make sure that the following chemicals and antibodies stayed on the tumor sections throughout their incubation times.

3. *Permeabilization:* The tumor sections were incubated with the nonionic surfactant Triton X-100 0.1% for 10 minutes.

4. *Washing step to remove Triton X-100:* The sections were washed in room tempered PBS for 5 minutes.

5. *Incubation with primary antibodies:* The F4/80 primary antibody was diluted in dH_2O with 12% BSA and used in a final concentration of 20 µg/mL. The sections were incubated with the antibody for 60 minutes.

6. *Washing step to remove unbounded primary antibodies:* The sections were washed in room tempered PBS for 3x5 minutes.

7. *Incubation with secondary antibodies:* After reconstitution of the secondary antibody with Cy3 as fluorescent dye, the antibody was diluted in dH_2O with 12% BSA to a final concentration of 2 µg/mL. The tumor sections were incubated with the antibody in the dark for 45 minutes.

8. *Washing step to remove unbounded secondary antibodies:* The sections were washed in room tempered PBS for 3x5 minutes.

Mounting of tumor sections

The tumor sections were mounted by the use of VECTASHIELD mounting medium for fluorescence H-1000 (Vector Laboratories). One drop of the mounting medium was added to the tumor section before it was covered with a cover glass (VWR). After mounting, the sections were stored at 4°C before further imaging.

3.5.2 Imaging with confocal laser scanning microscopy

A CLSM Zeiss LM800 was used to image the tumor sections from trial 1 and 2, shown in Table 3.1. As the tumor sections were washed during the staining process, which is a necessary step to highlight macrophages, the nanoparticles were removed from the sections. To obtain information regarding the amount of nanoparticles inside and outside of the macrophages, the sections were imaged before and after staining. Before staining, the sections were imaged without mounting medium and cover glass. Imaging by the use of this would have provided better images, but it was not possible to remove the cover glass without changing the structures in the tumor sections. For one tumor section, 8 images were captured at the periphery, while 4 images were captured in the center. Each tumor

section was imaged on the exact same areas before and after staining. The staining procedure was performed immediately after the first imaging of the tumor section in order to prevent damage to the section caused by drying.

For both OHS and PC3 tumors, one section from each tumor in the control group and one section from each tumor in the treated group was imaged. Some of the tumor sections were difficult to image without mounting medium and cover glass due to a lot of autofluorescence and weak signals from the blood vessels. As a result of this problem, not all sections were possible to image. The number of imaged sections and the number of images captured before and after staining of macrophages are shown in Table 3.4.

Table 3.4: A table showing the number of imaged sections and the number of captured images from each section before and after staining of macrophages. The control group is injected with nanoparticle-stabilized bubbles. The treated group is injected with nanoparticle-stabilized micobubbles in combination with ultrasound treatment.

Groups	Nr. of sections	Nr. of images before and after staining
OHS control group	3	36 (before) + 36 (after)
OHS treated	4	48 (before) + 48 (after)
PC3 control group	4	48 (before) + 48 (after)
PC3 treated	3	36 (before) + 36 (after)

A 20X plan apochromat objective with numerical aperture NA 0.8 was used. All images were obtained with a frame size of $319.5\,\mu m$ x $319.5\,\mu m$ which consist of 1024x1024 pixels, using bidirectional scanning with a scan speed of 52 429 pixels/s and a line average of 4. Each image was captured in two channels. During the imaging before staining of macrophages, channel 1 imaged vascular endothelial cells stained with lectin-FITC, and channel 2 imaged nanoparticles with Nile Red 688 fluorescent dye. The image settings used to capture these images are shown in Table 3.5. After staining of macrophages the images were also achieved in two channels, where channel 1 imaged vascular endothelial cells stained with lectin-FITC and channel 2 imaged macrophages (M1 + M2) stained with Cy3 fluorescent dye. The image settings used to capture the images after staining are shown in Table 3.6.

Table 3.5: The CLSM image settings used for imaging of nanoparticles before staining of macrophages in PC3 and OHS xenograft models. Channel 1 imaged vascular endothelial cells stained with lectin-FITC, and channel 2 imaged nanoparticles with Nile Red 688 fluorescent dye. The pinhole size was determined to obtain an optical section of $3\,\mu m$.

Channel	1	2
Fluorophore	FITC	Nile Red
Laser wavelength	488nm	561nm
Laser intensity	5%	5%
Detector range	490nm-540nm	570nm-700nm
Detector gain	750V	750V
Pinhole size	1,70AU	1,60AU

Table 3.6: The image settings used for imaging of macrophages in PC3 and OHS xenograft models with CLSM. Channel 1 imaged vascular endothelial cells stained with lectin-FITC, and channel 2 imaged both types of macrophages (M1 + M2) stained with Cy3. The pinhole size was determined to obtain an optical section of $3\,\mu m$.

Channel	**1**	**2**
Fluorophore	FITC	Cy3
Laser wavelength	488nm	561nm
Laser intensity	0,4%	2,5%
Detector range	490nm-540nm	565nm-615nm
Detector gain	640V	560V
Pinhole size	1,65AU	1,45AU

The image settings were determined after testing on a selection of images using the range indicator available in the microscope software. The pinhole size was adjusted to obtain an optical section with a thickness of $3\,\mu m$. The images of the different channels were captured in sequence to prevent bleed-through between the channels.

To be able to image the exact same area on the tumor sections before and after staining of macrophages, a list of coordinates in the microscopy software was created for each section. During the first imaging of the tumor sections, the ocular was used to find a characteristic and recognizable blood vessel. This blood vessel was given (0, 0) as coordinate and defined to be a zero point. The ocular was further used to find areas with blood vessels located throughout the section. Each of these areas were given new coordinates relative to the zero point. All coordinates were saved as a list and used for the second imaging of the tumor sections. During the second imaging the ocular was used to find the characteristic blood vessel and the fixed zero point. This area was set to (0, 0) and the list of coordinates was used to find the same areas as previously imaged. The result of this process gave one pair of images for each area on the tumor sections. This pair consists of one image taken before staining of macrophages and one image taken after staining.

For the PC3 sections, the blood vessels were placed in the center of the images. This was done to make it easier to study the distribution of nanoparticles and macrophages around the blood vessels in further image analysis. For OHS tumor sections, the high density of blood vessels made it impossible to capture images with the blood vessels placed in the center.

3.5.3 Image analysis with FIJI

Image analysis was used to study the amount and distribution of nanoparticles and macrophages around blood vessels. In addition to this, the percentage of nanoparticles inside macrophages at different distances around the blood vessels was evaluated. The total amount of macrophages, nanoparticles and nanoparticles inside macrophages were also determined for the different experimental groups. The image analysis was performed using the ImageJ software, delivered as a part of the software package FIJI [61].

The distribution of macrophages around blood vessels

One of the uses for the images captured after staining of macrophages, was to decide the distribution of all macrophages (M1 + M2) at different distances from the nearest blood vessel. Both the blood vessel channel and the macrophage channel were used in this analysis. A detailed description of this image analysis is given in Figure 3.7, where G1 and M1 are the original fluorescent images of the blood vessel channel and macrophage channel. The blood vessel image was converted to a binary image by using a threshold value from the Otsu algorithm, while the image with macrophages was converted to a binary image by the use of the Triangle algorithm. These algorithms are included in FIJI and gave all pixels with an intensity above a certain limit a new value of 255, while all pixels below this value were set to 0. This means that the backgrounds in the images were set to 0 and the fluorescent objects (blood vessel and macrophages) were given a value of 255. The two algorithms were selected after testing of several algorithms on a range of images, from both OHS and PC3 tumors. These algorithms gave binary images that included the blood vessels and macrophages without including too much noise. A Despeckle filter was used to reduce the amount of noise even further before analysis. G2 and M2 in Figure 3.7 show the resulting binary imaging of the blood vessel channel and the macrophage channel.

The binary image of the blood vessel channel was used to create a distance map around the blood vessel. The distance map is a feature included in FIJI. The binary image was inverted to make this possible. This means that the blood vessel was defined to be the background in the image and its pixel value were set to 0. The distance map was created based on the inverted binary image. Each pixel in this image were given a new gray value to represent the distance in pixels from the nearest background pixel (blood vessel). Image G3 in Figure 3.7 shows a distance map created from an inverted version of the binary image G2 in the same Figure.

The binary image of the macrophage channel consists of regions of interests, which are the macrophages. A mask around the macrophages was formed using a function in FIJI called Analyze Particles. The mask was defined to only include particles with an area larger than $40\,\mu m^2$. This value was chosen after testing of different values between $10\,\mu m^2$ and $100\,\mu m^2$ on a range of images. A value of $40\,\mu m^2$ seems to include the macrophages without including unwanted noise. The mask created around the macrophages are shown in image M3, Figure 3.7. This mask was put on top of the distance map, illustrated in image G4, Figure 3.7. The pixel values inside the mask were counted and the result was a histogram, shown in H, Figure 3.7. This represent the number of pixels defined as macrophages at different distances around the blood vessel. The number of bins was chosen to be 32 for all histograms and the number of pixels counted at bin 0 was defined to be macrophages inside the blood vessels.

To make the analysis efficient, a macro/script which contains all steps in FIJI was created. The program was applied to each image and the result was one text file per image. The text files contained the information from the histograms. Each file was checked for errors during the process. These files were used in further statistical analysis. This macro/script is shown in Appendix C.

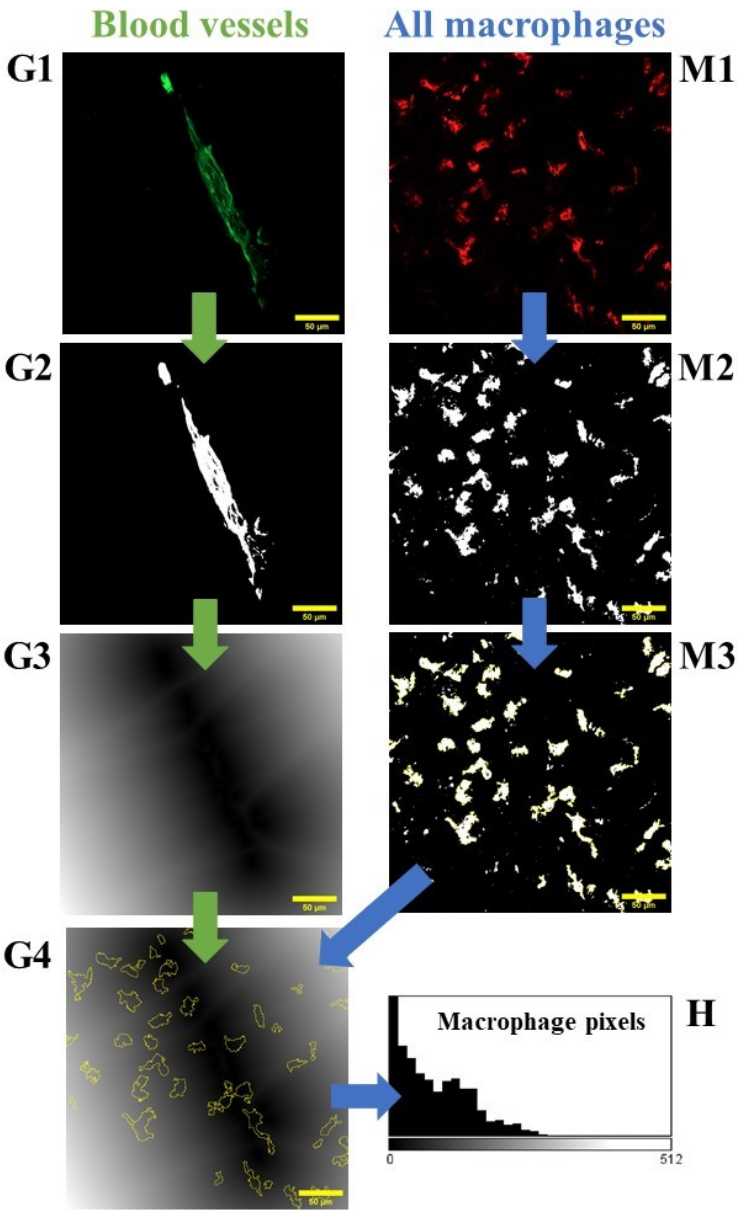

Figure 3.7: A description of the image analysis used to decide the distribution of macrophages at different distances from the nearest blood vessel. G1 and M1: Original fluorescent images of the blood vessel channel and the macrophages channel. G2 and M2: Binary images of the blood vessel channel and macrophage channel resulting from applying a pixel threshold. G3: A distance map around the blood vessel in G2. M3: A mask defined as macrophages. G4: The mask from M3 placed on the top of the distance map from G3. H: Histogram which represents the number of pixels defined as macrophages at different distances from the nearest blood vessel. The scale bars in the images are $50\,\mu\mathrm{m}$.

The uptake of nanoparticles in macrophages around blood vessels

The images were analyzed with the aim of deciding the amount of nanoparticles inside and outside of macrophages at different distances from the nearest blood vessel. A detailed description of this image analysis is shown in Figure 3.8. The starting point was the nanoparticle channel captured before staining of macrophages, in addition to the blood vessel channel and the macrophage channel from the imaging after staining. Image G1, N1 and M2 in Figure 3.8 are the original fluorescent images. Image G2, N2 and M2 are binary images resulting from applying a pixel threshold. The Otsu algorithm was used for the blood vessel channel, the Moments algorithm for the nanoparticle channel and the Triangle algorithm was applied on the macrophage channel. These algorithms are all included in FIJI, and they were chosen after testing of several algorithms on a selection of images from both OHS and PC3 xenografts. The algorithms worked as explained for image 3.7. The backgrounds in the images were set to 0 and the fluorescent objects (blood vessels, nanoparticles and macrophages) were given a new value of 255. Although the algorithms removed a lot of noise, a Despeckle filter was used to further reduce the noise.

The binary image of the blood vessel was used to create a distance map around the blood vessel. This was done in the same way as explained for Figure 3.7. Each pixel in the distance map got a gray value which represented a distance in pixels from the nearest background pixel (blood vessel). Image G3 in Figure 3.8 show the distance map created from an inverted version of the binary image G2 in the same Figure.

The binary image of the macrophage channel was used to create a mask around the macrophages, shown in image M3, Figure 3.8. This was performed in the same way as explained previously for Figure 3.7. The mask was put on the top of the binary image of the nanoparticle channel, illustrated in image N3, Figure 3.8. The nanoparticles inside and outside the macrophage mask were separated and a new masks was created around the nanoparticles by using the FIJI function Analyze Particles. No area limit was set on these masks to make sure all nanoparticles were included. The mask including the nanoparticles inside the macrophages was put on the top of the distance map, illustrated in image G4, Figure 3.8. Also the mask around the nanoparticles outside the macrophages was placed over the distance map, shown in image G5, Figure 3.8. The pixel values inside the nanoparticle mask were counted and presented as histograms. Histogram H1 in Figure 3.8 show the pixel values for nanoparticles inside macrophages, while histogram H2 in the same figure show the pixel values of nanoparticles outside macrophages. The number of bins was chosen to be 32 for all histograms and the number of pixels counted at bin 0 was defined to be inside the blood vessels.

In order to make the analysis efficient two macros/scripts which included all steps in FIJI were written. One script contained the analysis of nanoparticle pixels inside macrophages, and the other included the analysis of the nanoparticle pixels outside macrophages. The programs were applied to each set of images. One set of images consist of images taken before and after staining of macrophages. In Figure 3.8, image G1, N1 and M1 represent one of these sets. The result for each set of images was two text files. One of the files contains the information from the histogram created by counting of nanoparticle pixels inside macrophages. The other file contains information about the histogram including nanoparticle pixels outside macrophages. Each file was checked for errors before they were used in further statistical analysis. The two macros/scrips are shown in Appendix C.

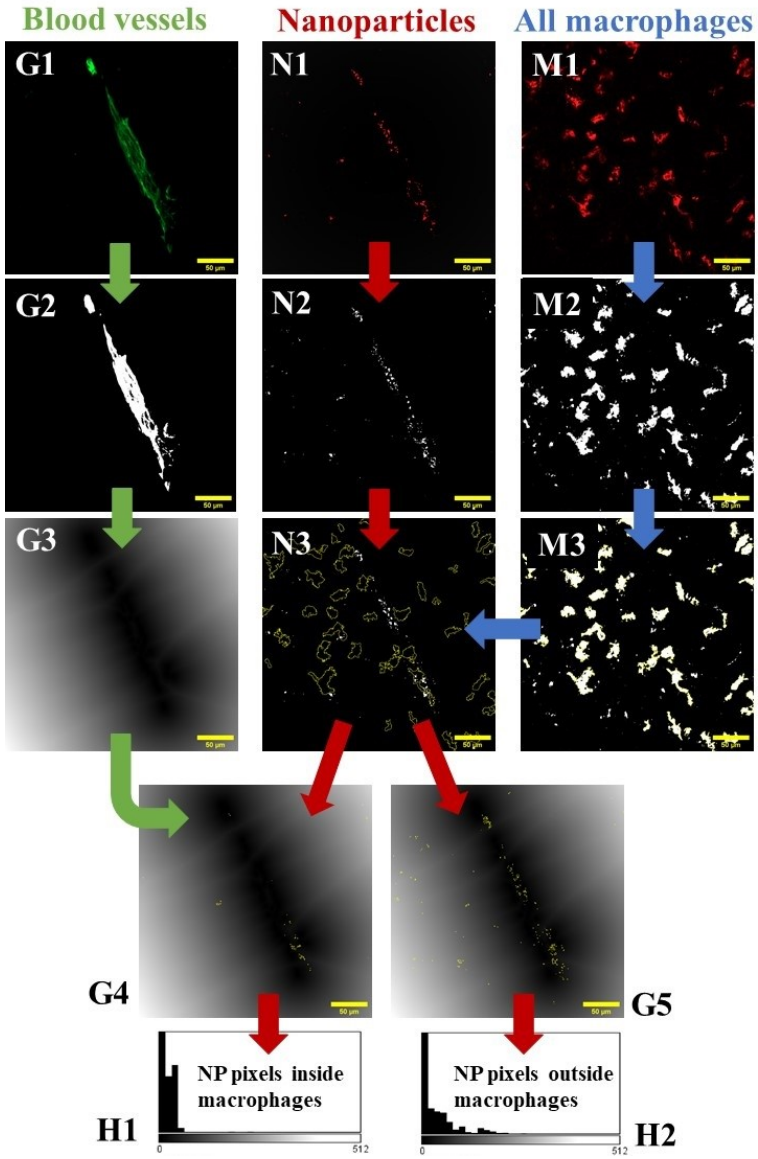

Figure 3.8: A description of the image analysis used to study the uptake of nanoparticles in macrophages at different distances from the nearest blood vessel. G1, N1 and M1: Original fluorescent images of the blood vessel channel, nanoparticle channel and macrophages channel. G1, N2 and M2: Binary images of the blood vessel channel, nanoparticle channel and macrophage channel. G3: A distance map around the blood vessel in G2. M3: A mask defined as macrophages. N3: The mask from M3 placed on the top of the binary image of nanoparticles. G4 and G5: A mask defined as nanoparticles inside and outside macrophages are put on top of the distance map from G3. H1 and H2: Histograms which represent the number of pixels defined as nanoparticles inside and outside macrophages at different distances from the nearest blood vessel. The scale bars in the images are $50\,\mu\mathrm{m}$.

3.5.4 Statistical analysis

Python and Microsoft Excel were used for the statistical analysis of the data resulting from the image analysis in ImageJ, FIJI. Python was used to sort the text files from the image analysis and to calculate the desired information from these text files. Microsoft Excel was used to perform student t-test and to make plots of the data achieved from python.

Macrophages around blood vessels

For each image, the image analysis created a text file containing information about the number of pixels defined as macrophages and their distances to the nearest blood vessel. The total distance was divided into 32 bins, where a number of pixels was registered for each bin. A self-made python script was written to sort the text files from the image analysis into the four experimental groups: OHS control, OHS treated, PC3 control and PC3 treated. The script was further modified to merge the 32 bins into 9 distance groups (5-15 µm, 15-25 µm, 25-35 µm, 35-45 µm, 45-55 µm, 55-65 µm, 65-75 µm, 75-85 µm and >85 µm) and to separate bin 0 from the rest of the bins. The pixels counted at bin 0 were defined to be inside the blood vessels. This corresponds to the interval between 0-5 µm, where the pixels at distance 0 are included. The script calculated the fraction of macrophage pixels at the different distances for each image. The total number of macrophage pixels at each distance was divided by the total number of macrophage pixels for all distances. An average fraction of macrophage pixels at different distances around the nearest blood vessel was calculated for each experimental group. The result was presented in a new text file. The standard deviations were also given in this file.

The same script was also used to calculate the total fraction of macrophages in the images. This was done by summing up the pixels defined as macrophages over all distances. This number was divided by the total number of pixels in the image. An average fraction of macrophages in the images was calculated for each experimental group. The results were presented in a text file which also included the standard deviations.

Nanoparticles around blood vessels

The image analysis of the nanoparticles created two text files for each image. These files contained information about the number of pixels defined as nanoparticles around blood vessels. One of the files contained the number of pixels defined as nanoparticles inside macrophages at different distances from the nearest blood vessel. The other file contained the number of nanoparticle pixels outside the macrophages at different distances from the nearest blood vessel. For both files, the total distance was divided into 32 bins and a number of pixels was registered for each bin. A self-made python script was written to sort the text files from the image analysis into the four experimental groups (OHS control, OHS treated, PC3 control and PC3 treated) and to add the two text files from each image into one new file. This text file contained information about the total number of pixels defined as nanoparticles at different distances from the nearest blood vessel. The script was further modified to merge the 32 bins into 9 distance groups (5-15 µm, 15-25 µm, 25-35 µm, 35-45 µm, 45-55 µm, 55-65 µm, 65-75 µm, 75-85 µm and >85 µm) and to separate bin 0 from the rest of the bins. The pixels counted at bin 0 were defined to be nanoparticles

inside the blood vessels. This corresponds to the interval between 0-5 µm, where the pixels at distance 0 are included. The script calculated the fraction of nanoparticle pixels at the different distances for each image. The total number of nanoparticle pixels at each distance were divided by the total number of nanoparticle pixels for all distances. An average fraction of nanoparticle pixels at different distances from the nearest blood vessel was calculated for each experimental group. The result was presented in a new text file, where the standard deviations also were included.

The total fraction of nanoparticles in the images was calculated by the same script. This was done by summing up the pixels defined as nanoparticles over all distances. This number was divided by the total number of pixels in the image. An average fraction of nanoparticles in the images was calculated for each experimental group. The results were presented in a text file which also included the standard deviations.

The uptake of nanoparticles in macrophages around blood vessels

Two text files were used to calculate the fractions of nanoparticle pixels inside macrophages. One text file contained the total number of pixels defined as nanoparticles at different distances. This text file was created as described in the previous section and it presented the number of pixels in the 9 distance groups. The other file consisted of the number of pixels defined as nanoparticles inside macrophages at different distances from the nearest blood vessel. In this file the total distance was divided into 32 bins and a number of pixels was counted for each bin. A self-made python script was written to sort the text files into four experimental groups (OHS control, OHS treated, PC3 control, PC3 treated). The script was also used to merge the 32 bins into 9 distance groups (5-15 µm, 15-25 µm, 25-35 µm, 35-45 µm, 45-55 µm, 55-65 µm, 65-75 µm, 75-85 µm and >85 µm) and to separate bin 0 from the rest of the bins. The pixels counted at bin 0 were defined to be nanoparticles inside the blood vessels. This corresponds to the interval between 0-5 µm, where the pixels at distance 0 are included. The script calculated the fraction of nanoparticles inside macrophages at different distances for each image. The number of nanoparticle pixels defined to be inside macrophages at each was divided by the the total number of nanoparticle pixel at the same distance. An average fraction of nanoparticles inside macrophages at different distances from the nearest blood vessel was calculated for each experimental groups. The results was presented in a new text file. The standard deviations were also included in this file.

The same script was used to calculate the total fraction of nanoparticles inside macrophages in the images. The text files which contained the number of pixels defined as nanoparticles inside macrophages at different distances from the blood vessels were used. The pixels defined as nanoparticles inside macrophages were summed over all distances. This number was divided by the total number of pixels in the image. An average fraction of nanoparticles inside macrophages in the images was calculated for each experimental group. The results were presented in a text file which also included the standard deviations.

Chapter 4

Results

4.1 Optimization - flow cytometry analysis

The method described in section 3.4 is a product of an optimization process. The following sections describe the results after testing of different parameters during this process.

4.1.1 Single cell suspension

Mechanical disintegration and enzymatic disintegration were tested to find the best method to make a single cell suspension from a tumor. The methods were tested for both OHS and PC3 tumors, and the results are shown in Table 4.1 and 4.2.

Table 4.1 shows the number of viable cell per gram tumor for two series of OHS tumors. The same parameters were used for both series. For mechanical disintegration, the Stomacher time was 3 minutes and for enzymatic disintegration the incubation time was 40 minutes. The OHS tumors had a soft consistency and they were easy to crush. This resulted in a high number of viable cells per gram tumor by the use of either methods. Nevertheless, mechanical disintegration was timesaving compared to enzymatic disintegration, and it also gave the largest number of viable cells. Mechanical disintegration was therefore chosen to be the best method to make single cell suspensions from OHS tumors.

Table 4.1: Overview over the number of viable cells per gram of tumor after mechanical or enzymatic disintegration. These results are from OHS tumors. For mechanical disintegration, the Stomacher was used for 3 minutes and for enzymatic disintegration the incubation time was 40 minutes. These parameters were used for both series 1 and 2.

Series	Weight tumors	Mechanical disintegration	Enzymatic disintegration
1	1.17g and 1.23g	51.3x10^6 viable cells/g	33.4x10^6 viable cells/g
2	0.79g and 0.85g	28.7x10^6 viable cells/g	20.9x10^6 viable cells/g

Table 4.2 gives the number of viable cells per gram of tumor for three series of PC3 tumors. The PC3 tumors had very different consistency compared to the OHS tumors. They were hard and difficult to crush. For series 1, the Stomacher time was 3 minutes for mechanical disintegration, and the incubation time was 40 minutes for enzymatic disintegration. This was the same parameters as used for OHS tumors, but the results for PC3 tumors were not good. The number of viable cells per gram tumor was very low for both of the methods. For the two tumors in this series, the total number of viable cells was less than one million, which is the amount of cells needed for one sample. For series 2, the Stomacher time was 5 minutes, while the enzymatic incubation lasted for 50 minutes. The number of viable cells per gram of tumor was higher than obtained in series 1, but still low compared to the OHS tumors. This was the result for both of the disintegration methods. For series 3, the Stomacher time was 7 minutes, while the incubation time was 60 minutes. For mechanical disintegration the number of viable cells per gram tumor was high and similar to the results for the OHS tumors. For enzymatic disintegration the number of viable cells per gram of tumor was higher than the previous series, but still quite low. Based on these result, mechanical disintegration with stomacher time 7 minutes was chosen to be the best method to make single cell suspensions from PC3 tumors.

Table 4.2: Overview over the number of viable cells per gram of tumor after mechanical or enzymatic disintegration. These results are from PC3 tumors. For series 1, the time in the Stomacher was 3 minutes and the enzymatic incubation lasted for 40 minutes. For series 2, the Stomacher time was 5 minutes and the enzymatic incubation time was 50 minutes. For series 3, the Stomacher was used for 7 minutes and the enzymatic incubation lasted for 60 minutes.

Series	Weight tumors	Mechanical disintegration	Enzymatic disintegration
1	0.50g and 0.56g	$1.9\text{x}10^6$ viable cells/g	$1.2\text{x}10^6$ viable cells/g
2	0.94g and 1.04g	$10.3\text{x}10^6$ viable cells/g	$7.7\text{x}10^6$ viable cells/g
3	0.83g and 0.87g	$36.1\text{x}10^6$ viable cells/g	$12.7\text{x}10^6$ viable cells/g

4.1.2 Staining of macrophages - concentration study

A concentration study was performed to find the most suitable concentrations of the F4/80 and the CD206 primary antibodies for staining of macrophages in the single cell suspensions. This was done for both OHS and PC3 samples, and the results are shown in Figure 4.1 and 4.2. Table 3.3 in section 3.4.3 presents the tested concentrations of primary antibodies. The concentrations of the secondary DyLight405 antibody (binds to the F4/80 antibody) and the secondary AlexaFluor488 antibody (binds to the CD206 antibody) were kept constant at $0.5\,\mu g/10^6$ cells.

To the left in Figure 4.1 is an overlay plot of histograms from staining of macrophages (M1 + M2) in OHS samples. The macrophages were stained with DyLight405, with different concentrations of the primary antibody F4/80 being used. This overlay plot shows the fluorescence intensity (log) of DyLight405 versus the number of cells. One sample was not stained with antibodies and the histogram for this sample is located to the left in the plot. This indicate that the sample was negative for DyLight405 and the sample had an x-median of 0.3. The x-medians were 0.57, 0.64 and 0.93 for the samples stained with

Dylight405 by the use of 5, 10 and 20 times the datasheet concentrations of the F4/80 antibody. This was a slight increase in x-median and fluorescence intensity signal compared to the sample which was not stained with antibodies.

The M2 macrophages were stained with AlexaFluor488 by the use of different concentration of the CD206 primary antibody. The achieved histograms from staining of M2 macrophages in OHS samples are shown to the right in Figure 4.1. This plot shows the fluorescence intensity (log) of AlexaFluor488 versus the number of cells. The histogram from the unstained sample was negative for AlexaFluor488 and located to the left in the plot with an x-median of 0.82. The samples stained with AlexaFluor488 and primary antibodies in concentrations of 5, 10 and 20 times the datasheet concentrations had x-medians of 1.16, 1.27 and 1.37. This indicated a weak increase in the fluorescence intensity signal compared to the signal from the sample not stained with antibodies.

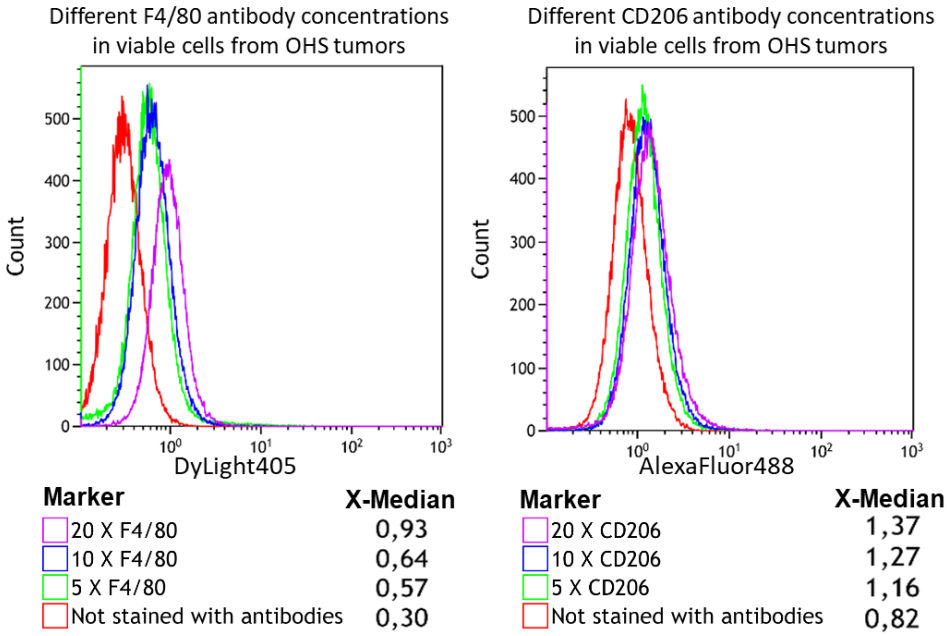

Figure 4.1: Two overlay plots showing histograms from staining of macrophages in OHS single cell suspensions. The overlay plot to the left shows the fluorescence intensity (log) of DyLight405 versus the number of cells. The macrophages (M1 + M2) were stained with DyLight405 in a concentration of $0.5\,\mu g/10^6$ cells by the use of different concentration of the primary antibody F4/80. The concentrations of F4/80 primary antibody were 5, 10 and 20 timed the original datasheet concentration. The overlay plot to the right shows the fluorescence intensity (log) of AlexaFluor488 versus the number of cells. The M2 macrophages were stained with AlexaFluor488 in a concentration of $0.5\,\mu g/10^6$ cells. 5, 10 or 20 times the original datasheet concentrations of the CD206 primary antibody were used. The x-medians for the fluorescence intensity signal from the different samples are presented for both of the overlay plots.

The overlay plot to the left in the Figure 4.2 shows fluorescence intensity (log) of DyLight405 versus the number of cells for PC3 samples. The histograms in this plot are obtained from samples where all macrophages (M1 + M2) are stained with DyLight405, using different concentration of the F4/80 primary antibody. One sample was not stained with antibodies. The resulting histogram from this sample are located to the left in the plot and have an x-median of 1.49. This sample was negative for DyLight405. The other three histograms were achieved from samples where 5, 10 and 20 times the datasheet concentration of the primary F4/80 antibody were used. These samples had x-medians of 1.76, 2.15 and 2.51. This was a slight increase in the fluorescence intensity signal compared to the sample not stained with antibodies.

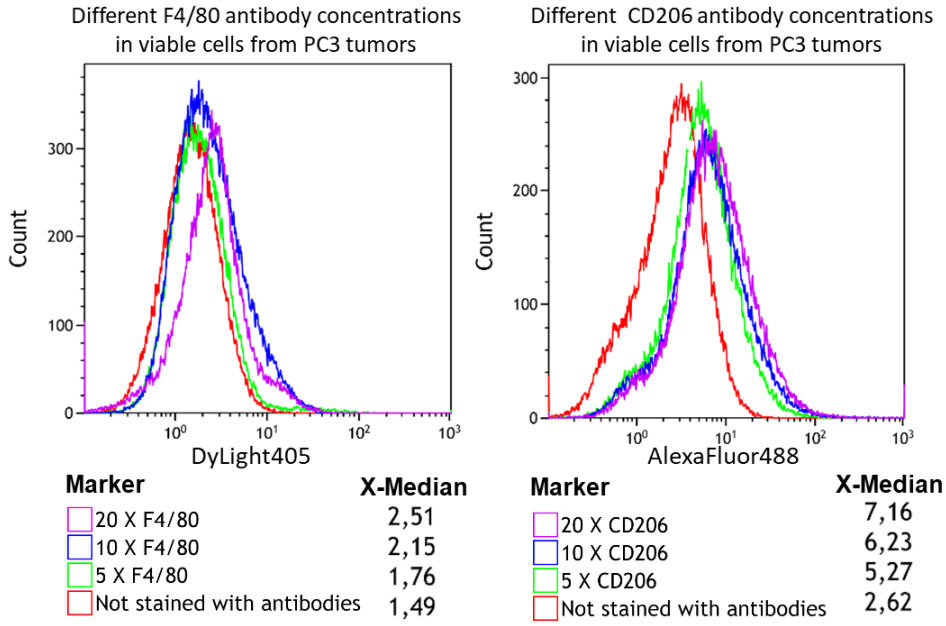

Figure 4.2: Two overlay plots showing histograms from staining of macrophages in PC3 single cell suspensions. The overlay plot to the left shows the fluorescence intensity (log) of DyLight405 versus the number of cells. The macrophages (M1 + M2) were stained with DyLight405 in a concentration of $0.5\,\mu g/10^6$ cells by the use of different concentration of the primary antibody F4/80. The concentrations of F4/80 primary antibody were 5, 10 and 20 timed the original datasheet concentration. The overlay plot to the right shows the fluorescence intensity (log) of AlexaFluor488 versus the number of cells. The M2 macrophages were stained with AlexaFluor488 in a concentration of $0.5\,\mu g/10^6$ cells. 5, 10 or 20 times the original datasheet concentrations of the CD206 primary antibody were used. The x-medians for the fluorescence intensity signal from the different samples are presented for both of the overlay plots.

To the right in Figure 4.2, there is an overlay plot of histograms which present the fluorescence intensity (log) of AlexaFluor488 versus the number of cells. In these samples, the M2 macrophages were stained with AlexaFluor488 and different concentration of the CD206 antibody. One sample was not stained with antibodies. This sample was negative

for AlexaFluor488 and located to the left in the plot with an x-median of 2.62. The samples stained with AlexaFluor488 and primary antibodies in concentrations of 5, 10 and 20 times the datasheet concentrations had x-medians of 5.27, 6.23 and 7.16. This indicated a small increase in the fluorescence intensity signal compared to the signal from the sample not stained with antibodies.

For PC3 and OHS samples, an increase in the x-median values was observed when a larger amount of both primary antibodies was used for staining of the macrophages. This occurred for an increase in the amount of both the F4/80 antibody and the CD206 antibody. An increase in the x-median value indicate a higher fluorescence intensity signal and some positive results for staining of the macrophages. However, the increase in x-median was very small for all four concentration studies when the amount of primary antibodies was increased. No apparent positive fluorescence peaks of macrophages were observed in any of the studies. To be able to separate the macrophages from the rest of the cells, a concentration of 20 times the datasheet concentration was used for both the F4/80 and CD206 primary antibodies. This is a high concentration of antibodies, but this was the best option due to the weak increase in x-medians when a larger amount of antibodies was added. These concentrations of primary antibodies were used for both OHS and PC3 samples.

4.1.3 Flow cytometry of RAW cells cultivated in the cell lab

Two samples that consisted of tumor cells mixed with RAW macrophages were run through the flow cytometer to test the flow cytometer protocol. Figure 4.3 and 4.4 show the achieved results. The fluorescence of DyLight405 was studied because this dye stained all macrophages (M1 + M2). Since the amount of macrophages in the samples was known, it was desirable to study whether all the macrophages were stained or not.

One sample consisted of OHS cells mixed with 10% RAW macrophages. The result for this sample is shown in Figure 4.3. The obtained histogram, which presents the fluorescence intensity (log) of DyLight405 versus the number of cells, is shown to the left in the figure. Two peaks are shown in this histogram. The peak to the left was cells negative for DyLight405, while the small peak placed to the right was cells positive for Dylight405. Macrophages were defined as the cells positive for DyLight405. To the right in the same figure is a density plot where the DyLight405 fluorescence intensity (log) is plotted against the side scatter signal (log). This plot shows two population of cells. The small population to the right was more positive for DyLight405 compared to the large population. According to the plot, there were also cells in the large population which was positive for DyLight405. This was indicated by the fact that cells in both populations had the same fluorescence intensity. However, it was possible to distinguish the macrophages from the tumor cells by looking at the fluorescence intensity in combination with the granularity (side scatter signal). In this sample 8.4% of the cells were defined as macrophages. This is a bit lower than 10% which is the added percentage of macrophages in the sample.

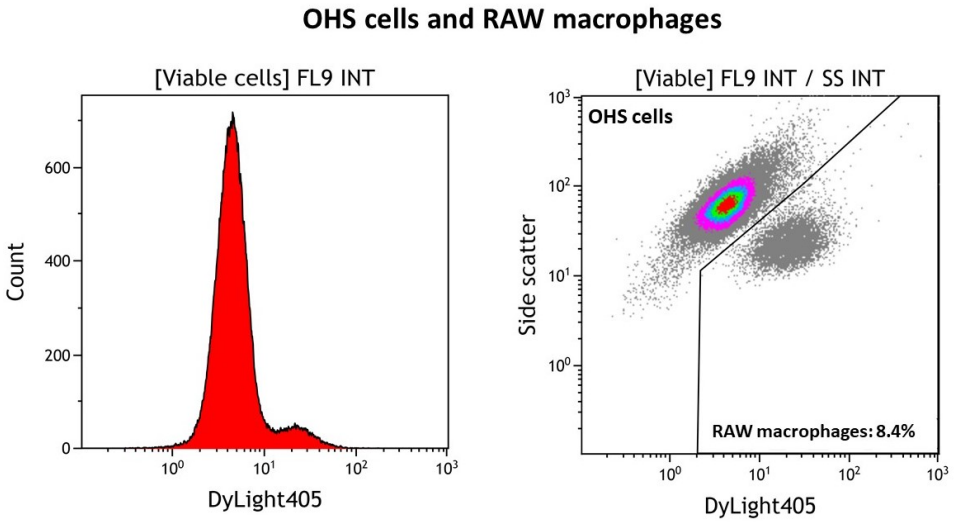

Figure 4.3: Two plots showing flow cytometry results from a sample which consisted of OHS cells mixed with 10% RAW macrophages. All of the cells were cultivated in the cell lab. The macrophages (M1 + M2) were stained with the DyLight405 secondary antibody in a concentration of $0.5\,\mu g/10^6$ cells by the use of the F4/80 primary antibody in a concentration of $4\,\mu g/10^6$ cells. To the left is the obtained histogram with the fluorescence intensity of DyLight405 versus the number of cells. The plot to the right is a density plot which shows the DyLight405 fluorescence intensity (log) versus the side scatter signal (log).

Figure 4.4 shows the result for the sample, which consisted of PC3 cells mixed with 10% RAW macrophages. The histogram to the left in the figure shows the fluorescence intensity (log) of DyLight405 versus the number of cells. No distinct positive fluorescence peak was observed in this histogram. To the right in the same figure is a density plot with the DyLight405 fluorescence intensity (log) versus the side scatter signal. Two populations of cells are shown in this plot. These populations are placed above each other, which means that they have the same fluorescence intensity. This made it difficult to distinguish between the macrophages and tumor cells based on the fluorescence intensity. Nevertheless, it was possible to separate the macrophages from the tumor cells by the use of fluorescence intensity in combination with granularity (side scatter signal). In this sample 10.1% of the cells were defined as macrophages. This was similar to the actual percentage of macrophages in the sample.

These results show that there were difficulties in distinguishing between the macrophages and the tumor cells by the use of only the fluorescence intensity. However, it was possible to observe two populations of cells when the fluorescence intensity signal was plotted against the granularity (side scatter signal). These two populations were tumor cells and macrophages. The flow cytometry results gave an amount of macrophages in the samples which was very similar to known percentage of macrophages. This method was able to separated the macrophages from the tumor cells and was used in trial 3 and 4.

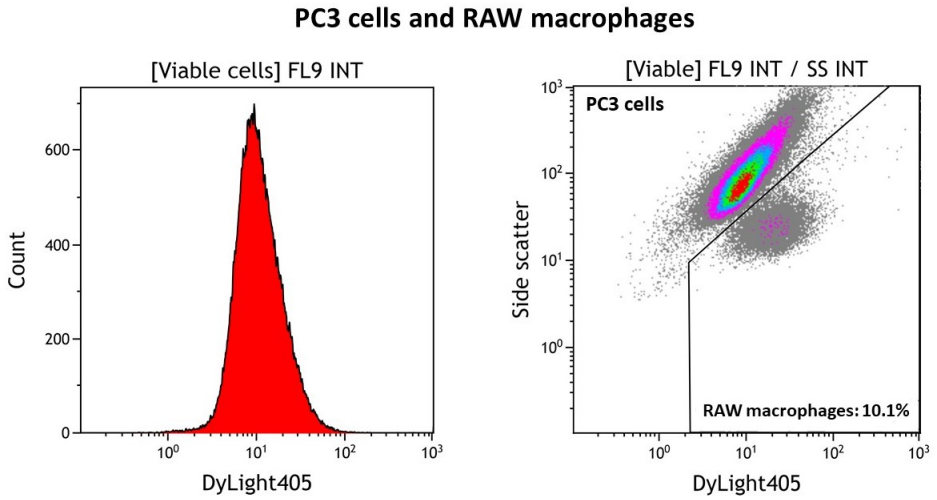

Figure 4.4: Two plots showing flow cytometry results from a sample which consisted of PC3 cells mixed with 10% RAW macrophages. All of the cells were cultivated in the cell lab. The macrophages (M1 + M2) were stained with the DyLight405 secondary antibody in a concentration of $0.5\,\mu g/10^6$ cells by the use of the F4/80 primary antibody in a concentration of $4\,\mu g/10^6$ cells. To the left is the obtained histogram with the fluorescence intensity of DyLight405 versus the number of cells. The plot to the right is a density plot which shows the DyLight405 fluorescence intensity (log) versus the side scatter signal (log).

4.2 Flow cytometry analysis

Flow cytometry was used to study macrophages and nanoparticles in OHS and PC3 tumor tissue. The amount of all macrophages, M1 macrophages and M2 macrophages was analyzed. This was done in addition to evaluating the uptake of nanoparticles by macrophages and tumor cells. Also, the percentage of nanoparticles taken up by macrophages and tumor cells was determined.

Tumors from animal trials 3 and 4 were used for the flow cytometry analysis. Originally, there were ten animals in each of these trials, where five were in the control group (only treated with nanoparticle-stabilized micobubbles), and five in the treated group (treated with nanoparticle-stabilized micobubbles in combination with ultrasound). This is shown in Table 3.1, section 3.3. Although cancer cells were implanted inn all of the animals, not all of them developed a tumor. This resulted in a lower number of tumors in each of the groups. The number of tumors used from each trial are listed in Table 4.3.

Table 4.3: The number of tumors from trial 3 and 4 used in this project. The tumors were analyzed by flow cytometry. The control groups are injected with nanoparticle-stabilized bubbles, while the treated groups are injected with nanoparticle-stabilized micobubbles in combination with ultrasound treatment.

Group	Trial 3 (OHS)	Trial 4 (PC3)
Control	3	2
Treated with US	4	3

4.2.1 Number of viable cells in OHS and PC3 tumors

Each tumor was weighed before a single cell suspension was made from the tumor. The cells in the single cell suspension were then counted to find the number of viable cells in the sample. Table 4.4 show the weight of each of the used tumors, in addition to the number of viable cells per gram tumor.

Table 4.4: The number of viable cells per gram for the tumors in trial 3 and 4. Mechanical disintegration was used to make single cell suspensions from the tumors. The Stomacher time was 3 minutes for OHS tumors and 7 minutes for PC3 tumors.

Experimental group	Weight of the tumor	Number of viable cells
OHS control	0.24g	$24.8x10^6$ viable cells/g
OHS control	0.08g	$19.1x10^6$ viable cells/g
OHS control	0.56g	$44.6x10^6$ viable cells/g
OHS treated	0.21g	$27.4x10^6$ viable cells/g
OHS treated	0.23g	$22.6x10^6$ viable cells/g
OHS treated	0.20g	$28.8x10^6$ viable cells/g
OHS treated	0.09g	$17.2x10^6$ viable cells/g
PC3 control	0.06g	$17.7x10^6$ viable cells/g
PC3 control	0.11g	$20.1x10^6$ viable cells/g
PC3 treated	0.05g	$21.4x10^6$ viable cells/g
PC3 treated	0.19g	$25.3x10^6$ viable cells/g
PC3 treated	0.20g	$23.1x10^6$ viable cells/g

4.2.2 Flow cytometry histograms

Histograms with the fluorescence intensity signal (log) versus the number of cells, were created for all the different fluorescent dyes during flow cytometry. All macrophages (M1 + M2) were stained with DyLight405. In addition to this, M2 macrophages were stained with AlexaFluor488. The nanoparticles contained Nile Red 688 fluorescent dye. The histograms indicate cell populations which are positive for the different fluorescent dyes. Figure 4.5 - Figure 4.8 show representative histograms obtained during flow cytometry of

samples from the different experimental groups: OHS control, OHS treated, PC3 control and PC3 treated. According to the histograms, there was a larger amount of cells positive for all the different fluorescent dyes in OHS tumors compared to PC3 tumors. This indicate a larger amount of macrophages in OHS tumor tissue than in PC3 tumor tissue. In the histograms showing the fluorescent intensity of AlexaFluor488, there were two distinct peaks. This was the case for all experimental groups. For the DyLight405 fluorescent dye, the histograms do not have this distinct peaks, especially not the histograms obtained from PC3 tumors.

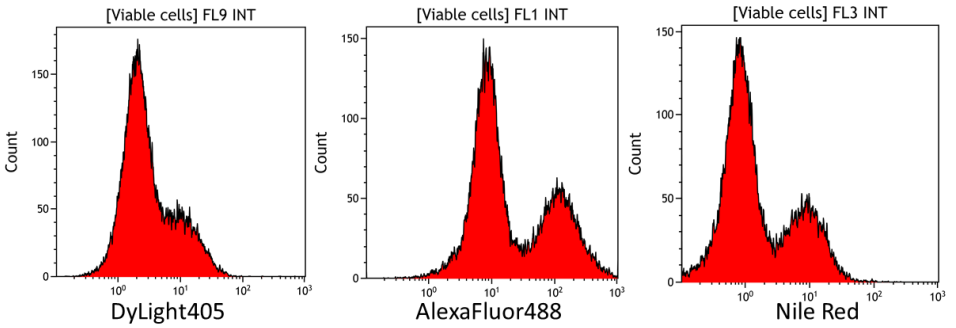

Figure 4.5: Histograms for the OHS control group (injected with nanoparticle-stabilized bubbles), showing the fluorescence intensity signal (log) versus the number of cells. All histograms are gated to only show viable cells. DyLight405 stained all macrophages (M1 + M2), AlexaFluor488 stained only M2 macrophages and Nile Red represent the nanoparticles.

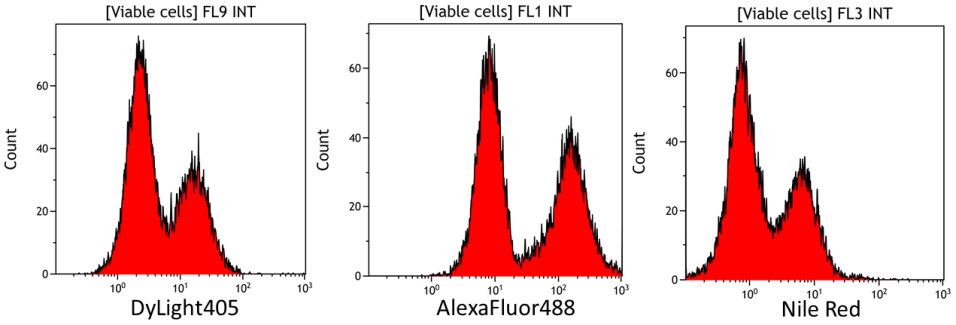

Figure 4.6: Histograms for the OHS treated group (injected with nanoparticle-stabilized bubbles in combination with ultrasound treatment), showing the fluorescence intensity signal (log) versus the number of cells. All histograms are gated to only show viable cells. DyLight405 stained all macrophages (M1 + M2), AlexaFluor488 stained only M2 macrophages and Nile Red represent the nanoparticles.

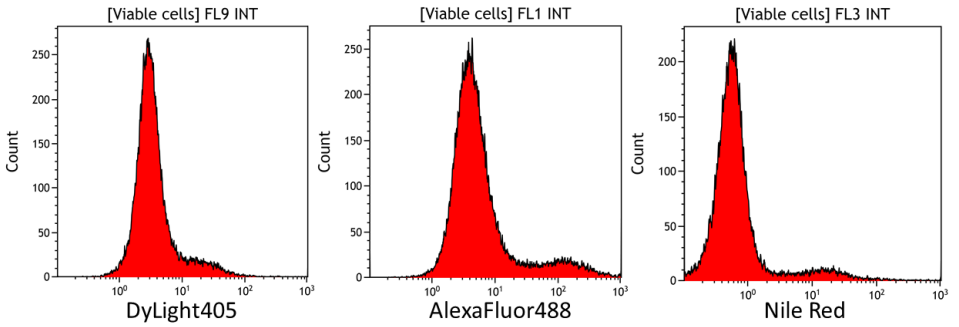

Figure 4.7: Histograms for the PC3 control group (injected with nanoparticle-stabilized bubbles), showing the fluorescence intensity signal (log) versus the number of cells. All histograms are gated to only show viable cells. DyLight405 stained all macrophages (M1 + M2), AlexaFluor488 stained only M2 macrophages and Nile Red represent the nanoparticles.

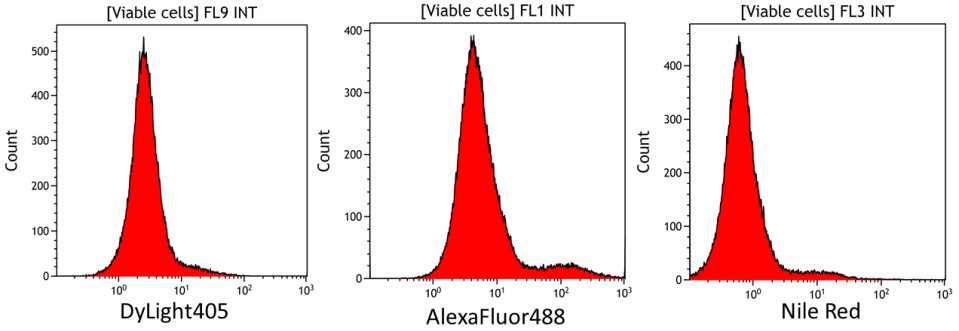

Figure 4.8: Histograms for the PC3 treated group (injected with nanoparticle-stabilized bubbles in combination with ultrasound treatment), showing the fluorescence intensity signal (log) versus the number of cells. All histograms are gated to only show viable cells. DyLight405 stained all macrophages (M1 + M2), AlexaFluor488 stained only M2 macrophages and Nile Red represent the nanoparticles.

4.2.3 Percentage of all macrophages

The mean percentage of all macrophages (M1 + M2) in the four different experimental groups, OHS control, OHS treated, PC3 control and PC3 treated, is presented in Figure 4.9. P-values were calculated from student t-test, but no significant differences in the mean percentage of macrophages between the four different groups were observed.

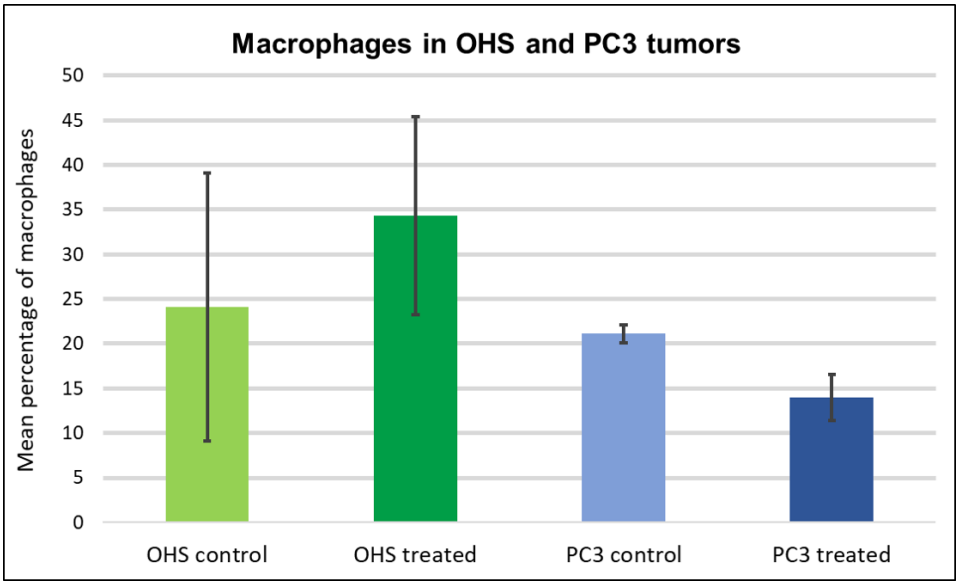

Figure 4.9: Bar plot showing the mean percentage of all macrophages (M1 + M2) in the control group and the group treated with ultrasound, for both OHS and PC3 tumors. The results are based on flow cytometry analysis. The number of tumors varied in the different groups: 3 tumors in OHS control, 4 tumors in OHS treated, 2 tumors in PC3 control and 3 tumors in PC3 treated. The error bars are equal to the standard deviations for each group.

The mean percentage of macrophages in the tumors from the OHS control group was $24.1 \pm 15.0\%$. This was 10.2 percentage point lower compared to the OHS treated group, where the mean percentage of macrophages was $34.3 \pm 11.1\%$. The difference was not significant with a p-value of 0.4. For the PC3 control group, the mean percentage of macrophages was $21.1 \pm 1.0\%$. This value was 7.1 percentage point higher than for the PC3 treated group, where the mean percentage of macrophages was $14.0 \pm 2.6\%$. The p-value was calculated to be 0.06 and the difference was not significant. According to these results, the percentage of macrophages in the different tumor models was not affected by the ultrasound treatment.

The OHS control group had a mean percentage of macrophages that was 3.0 percentage point higher compared to the PC3 control group. From these results, no significant difference in the mean percentage of macrophages was sees between OHS and PC3 tumors. The p-value was 0.8.

4.2.4 Percentage of M1 and M2 macrophages

The mean percentage of M1 and M2 macrophages in the four experimental groups, OHS control, OHS treated, PC3 control and PC3 treated, is presented in Figure 4.10. No significant differences in the mean percentage of M1 macrophages were found between the different groups. Also, the mean percentage of M2 macrophages between the different groups was not defined to be significant. On the other hand, significant differences were found between the mean percentage of M1 and M2 within each of the four groups. P-values calculated from student t-test were used to decide if a difference was significant or not.

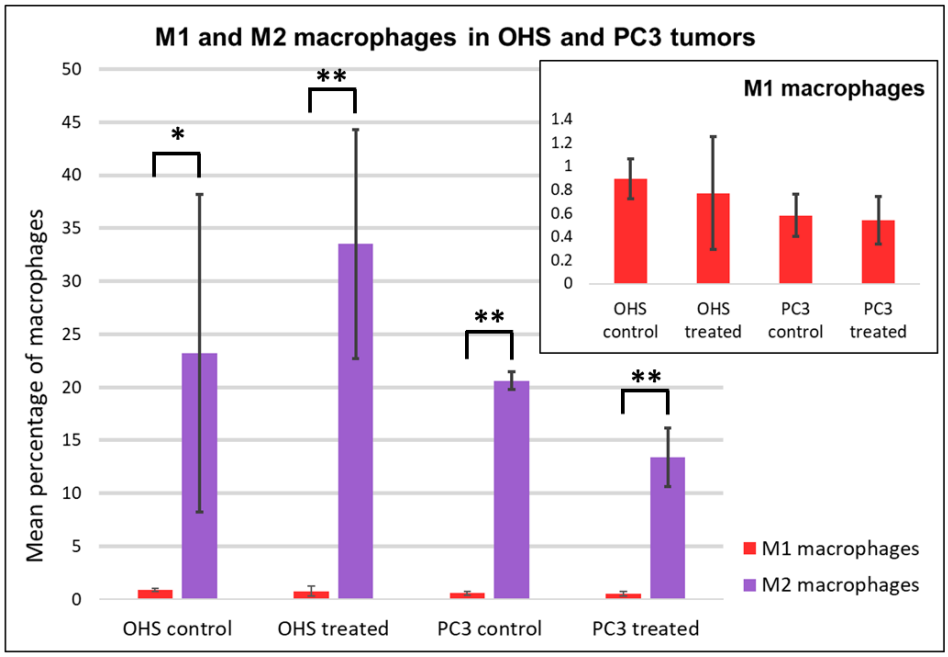

Figure 4.10: Bar plot showing the mean percentage of M1 and M2 macrophages in the control group and the group treated with ultrasound, for both OHS and PC3 tumors. The results are based on flow cytometry analysis. The number of tumors varied in the different groups: 3 tumors in OHS control, 4 tumors in OHS treated, 2 tumors in PC3 control and 3 tumors in PC3 treated. The error bars are equal to the standard deviations for each group. * P-value ≤ 0.05, ** P-value ≤ 0.005.

The mean percentage of M1 macrophages in the tumors from the OHS control groups was $0.9 \pm 0.2\%$. This was 22.3 percentage point lower than the mean percentage of M2 macrophages in the same group. The mean percentage of M2 macrophages in the OHS control group was calculated to be $23.2 \pm 15.0\%$. The difference between the mean percentage of M1 and M2 macrophages for the OHS control group was significant with a p-value of 0.04. For the OHS treated group, the mean percentage of M1 macrophages was $0.8 \pm 0.5\%$ and the mean percentage of M2 macrophages was $33.5 \pm 10.8\%$. The mean percentage of M1 macrophages was 32.7 percentage point lower than the mean percentage

of M2 macrophages. The difference was significant with a p-value <0.005. For the PC3 control group, the mean percentage of M1 macrophages was $0.6\pm0.2\%$. This was 20.0 percentage point lower than the mean percentage of M2 macrophages in the same group, which was $20.6\pm0.8\%$. The p-value was <0.005, and the difference was significant. The mean percentage of M1 macrophages in the PC3 treated group was $0.5\pm0.2\%$, while the mean percentage of M2 macrophages was $13.4\pm2.7\%$. This corresponded to a difference of 12.9 percentage point, which was defined to be significant with a p-value <0.005.

According to these result, there was a much higher amount of M2 macrophages compared to M1 macrophages within each of the four experimental groups.

4.2.5 Uptake of nanoparticles by macrophages

The mean percentage of macrophages (M1 + M2) that contain nanoparticles in the four different experimental groups, OHS control, OHS treated, PC3 control and PC3 treated, is presented in Figure 4.11. P-values from student t-test were used to evaluate for significant differences between the groups. One significant difference was found in the mean percentage of macrophages containing nanoparticles between the OHS control group and the PC3 control group.

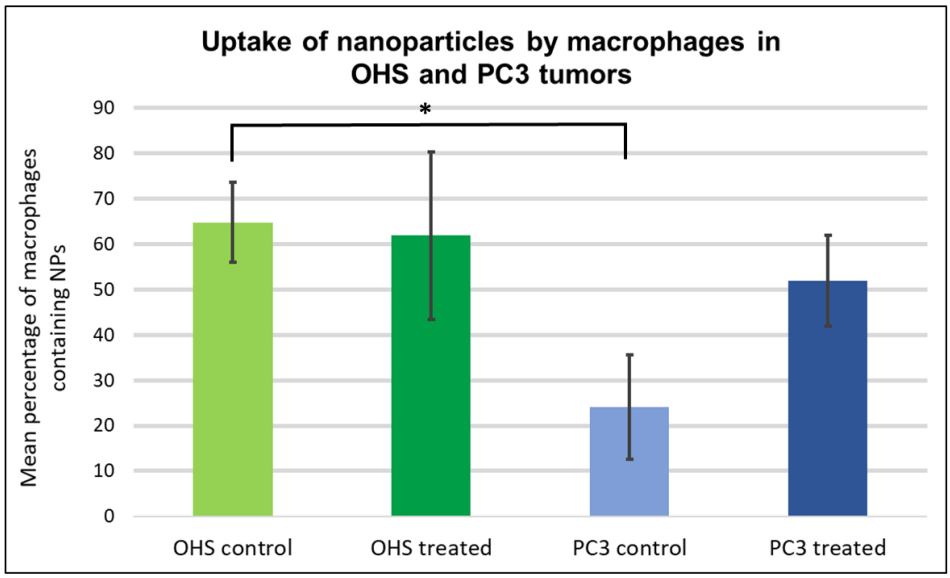

Figure 4.11: Bar plot showing the mean percentage of macrophages (M1 + M2) that contain nanoparticles in the control group and the group treated with ultrasound, for both OHS and PC3 tumors. The results are based on flow cytometry analysis. The number of tumors varied in the different groups: 3 tumors in OHS control, 4 tumors in OHS treated, 2 tumors in PC3 control and 3 tumors in PC3 treated. The error bars are equal to the standard deviations for each of the groups.
* P-value ≤ 0.05.

In the OHS control group, 64.8±8.8% of the macrophages contained nanoparticles. This was 2.9 percentage point higher than the mean percentage of macrophages containing nanoparticles in the OHS treated group, which was 61.9±18.5%. No significant difference in mean percentage of macrophages containing nanoparticles between the OHS control group and the OHS treated group was found. The p-value was calculated to be 0.4. For the PC3 control group, the mean percentage of macrophages containing nanoparticles was 24.1±11.5%. This was 27.8 percentage point lower than the mean percentage of macrophages that had taken up nanoparticles in the PC3 treated group. The difference in the mean percentage of macrophages containing nanoparticles between the PC3 control group and the PC3 treated group was not significant with a p-value of 0.1. These results indicated that ultrasound treatment did not have any effect on the mean percentage of macrophages that engulfed nanoparticles in OHS tumors. For PC3 tumors, the mean percentage of macrophages containing nanoparticles was increased by ultrasound treatment, but this increase was not significant.

The OHS control group had a mean percentage of macrophages containing nanoparticles that was 40.7 percent point higher compared to the PC3 control group. The difference was statistically significant with a p-value of 0.04. According to this, a larger amount of the macrophages in the OHS tumors engulfed nanoparticles compared to the macrophages in the PC3 tumors.

The uptake of nanoparticles by the different types of macrophages, M1 or M2, is presented in Appendix D. Since the mean percentage of M1 macrophages in all of the experimental groups was below 1%, the results based on these data will have several uncertain factors.

4.2.6 Uptake of nanoparticles by OHS and PC3 tumor cells

The mean percentage of tumor cells that contain nanoparticles in the four different experimental groups, OHS control, OHS treated, PC3 control and PC3 treated, is presented in Figure 4.12. P-values were calculated from student t-tests. One significant difference in the mean percentage of tumor cells containing nanoparticles was found between the OHS control group and OHS treated group.

The mean percentage of tumors cells containing nanoparticles in the OHS control group was 1.2±0.5%. This value was 2.1 percentage point lower compared to the OHS control group, where the mean percentage of tumor cells that contained nanoparticles was 3.3±0.8%. This difference was defined as significant with a p-value of 0.02. For the PC3 control group, the mean percentage of tumor cells containing nanoparticles was 1.8±0.2%, while the mean percentage of tumor cells with nanoparticles for the PC3 treated group was 2.4±0.6%. This corresponded to a difference of 0.6 percentage point, which was not significant with a p-value of 0.4. These results indicated that ultrasound treatment increase the mean percentage of tumor cells containing nanoparticles for both OHS and PC3 tumors, but the increase was only significant for OHS tumors.

The mean percentage of tumor cells containing nanoparticles was 0.6 percentage point lower for the OHS control group compared to the PC3 control group. The p-value was 0.3, and the difference was not significant. From these results, there was no difference in the mean percentage of tumor cells containing nanoparticles between OHS and PC3 tumors.

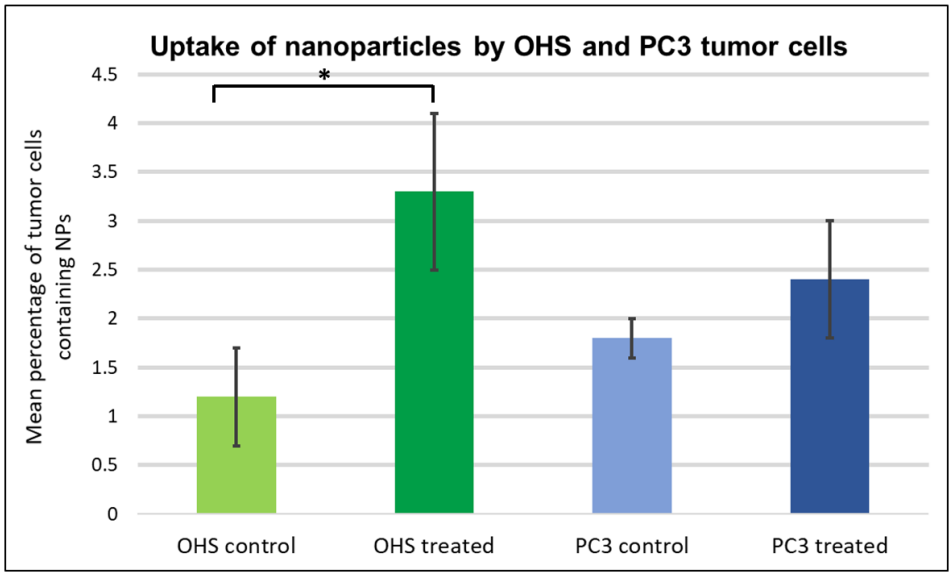

Figure 4.12: Bar plot showing the mean percentage of tumor cells that contain nanoparticles in the control group and the group treated with ultrasound, for both OHS and PC3 tumors. The results are based on flow cytometry analysis. The number of tumors varied in the different groups: 3 tumors in OHS control, 4 tumors in OHS treated, 2 tumors in PC3 control and 3 tumors in PC3 treated. The error bars are equal to the standard deviations for each of the groups. * P-value ≤ 0.05.

4.2.7 The percentage of nanoparticles taken up by macrophages and tumor cells

Nanoparticles taken up by cells will either be inside macrophages or tumor cells. Each single cell can absorb different numbers of nanoparticles. The amount of engulfed nanoparticles located inside macrophages and tumor cells was determined for the four different experimental groups: OHS control, OHS treated, PC3 control and PC3 treated. Figure 4.13 shows the percentage of nanoparticles taken up by macrophages and tumor cells. These results are mean values and based on the fluorescence intensity of Nile Red registered in macrophages and tumor cells. No significant differences in the mean percentage of nanoparticles located inside macrophages and tumor cells were found between the different groups. On the other hand, significant differences were found between the mean percentage of nanoparticles located inside macrophages and tumor cells, within each of the experimental groups.

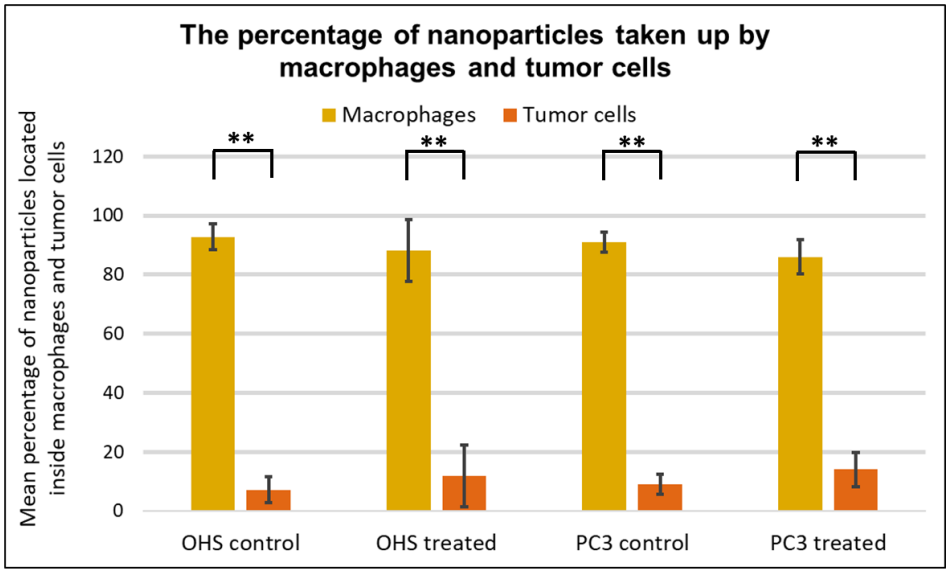

Figure 4.13: Bar plot showing how the amount of nanoparticles taken up by cells are distributed between macrophages and tumor cells. This is shown for the control group and the group treated with ultrasound, in both OHS and PC3 tumors. The results are based on flow cytometry analysis. The number of tumors varied in the different groups: 3 tumors in OHS control, 4 tumors in OHS treated, 2 tumors in PC3 control and 3 tumors in PC3 treated. The error bars are equal to the standard deviations for each of the groups. ** P-value ≤ 0.005.

The mean percentage of nanoparticles located inside macrophages in the tumors from the OHS control group was 92.8±4.4%. This was 85.6 percentage point higher than the mean percentage of nanoparticles located inside tumor cells, which was 7.2±4.4% for the same group. This difference was significant with a p-value < 0.005. For the OHS control group, the mean percentage of nanoparticles taken up by macrophages was 88.1±10.5% and the mean percentage of nanoparticles inside tumor cells was 11.9±10.5%. This corresponded to a significant difference of 76.2 percentage point with a p-value < 0.005. The mean percentage of nanoparticles engulfed by macrophages in the PC3 control tumors was 91.0±3.4%. For the tumor cells in the same group, the mean percentage of nanoparticles was 9.0±3.4%. This difference was 82.0 percentage point and significant with a p-value < 0.005. The mean percentage of nanoparticles located inside macrophages in the tumors from the PC3 treated group was 86.0±5.7%. This was 72.0 percentage point higher compared to the mean percentage of nanoparticles inside tumor cells for the same group, which was 14.0±5.7%. The difference was significant with a p-value < 0.005.

According to these results, most of the nanoparticles were taken up by macrophages instead of tumor cells. This was the case for all of the four experimental groups. For the groups treated with ultrasound, a slight increase was seen in the mean percentage of nanoparticles located inside tumor cells. However, these increases were tiny, which indicate that ultrasound treatment had low effect on the percentage of nanoparticles taken up by macrophages and tumor cells.

4.3 Confocal laser scanning microscopy analysis

Tumor sections from trial 1 and 2 were stained and imaged by the use of a confocal laser scanning microscope (CLSM). The image analysis was performed to evaluate how all macrophages (M1+M2) and nanoparticles were distributed around blood vessels in OHS and PC3 tumor tissue. In addition to this, the uptake of nanoparticles by macrophages at different distances from the blood vessels was studied. Also the total amount of macrophages, nanoparticles and uptake of nanoparticles by macrophages in the images was determined. The results are based on the functional blood vessels since only these were stained with lectin-FITC.

4.3.1 Confocal laser scanning microscope images

The nanoparticles in the tumor sections were imaged before staining of macrophages, while the macrophages were imaged after staining. Some representative CLSM images of the nanoparticles, macrophages and blood vessels for both OHS and PC3 tumor tissue are shown in Figure 4.14 - Figure 4.17. This includes images from the control groups and the groups treated with ultrasound.

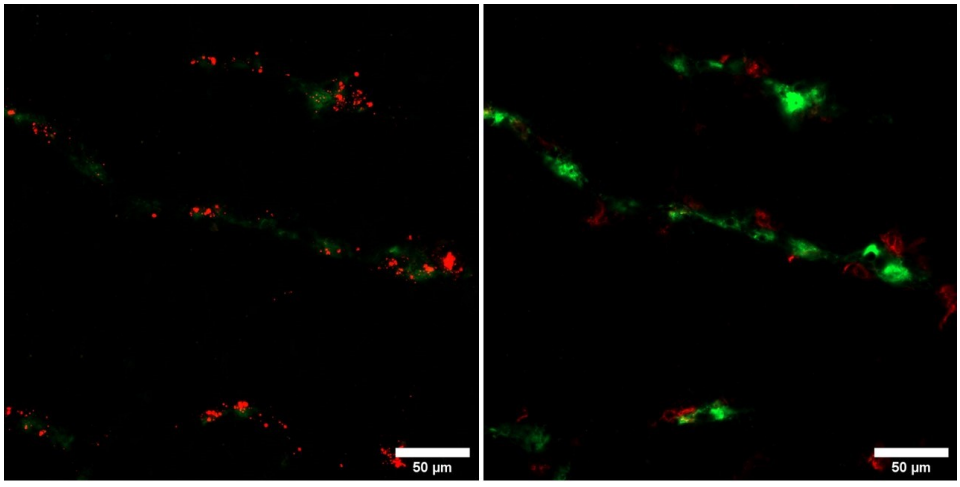

Figure 4.14: Images from the OHS control group. To the left is an image of the nanoparticles (red) and blood vessels (green). The image to the right show the macrophages (red) and blood vessels (green). Both images are captured at the same location on the tumor section. Scale bars are $50\,\mu\mathrm{m}$.

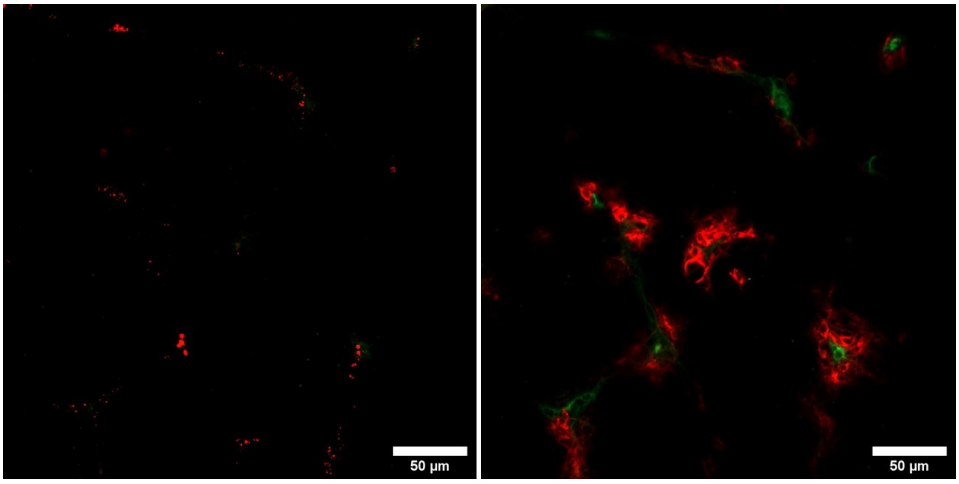

Figure 4.15: Images from the OHS treated group. To the left is an image of the nanoparticles (red) and blood vessels (green). The image to the right show the macrophages (red) and blood vessels (green). Both images are captured at the same location on the tumor section. Scale bars are $50\,\mu\mathrm{m}$.

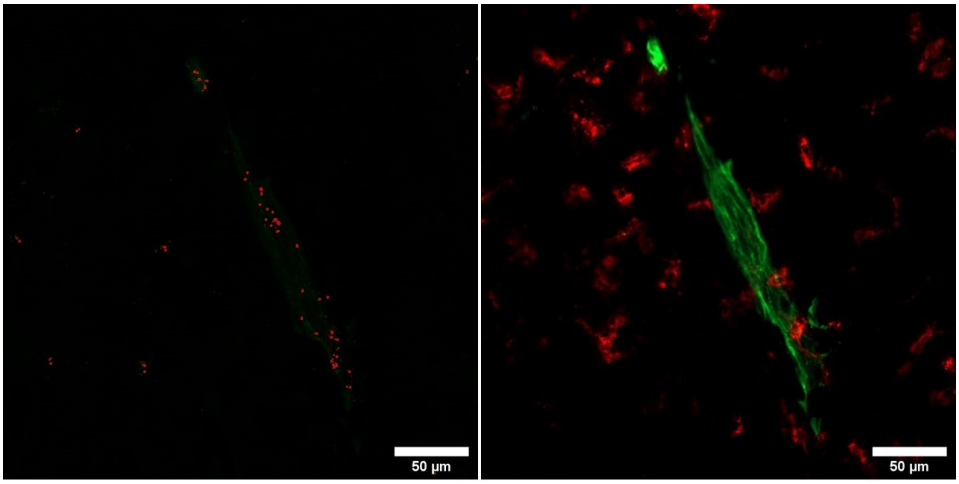

Figure 4.16: Images from the PC3 control group. To the left is an image of the nanoparticles (red) and blood vessels (green). The image to the right show the macrophages (red) and blood vessels (green). Both images are captured at the same location on the tumor section. Scale bars are $50\,\mu\mathrm{m}$.

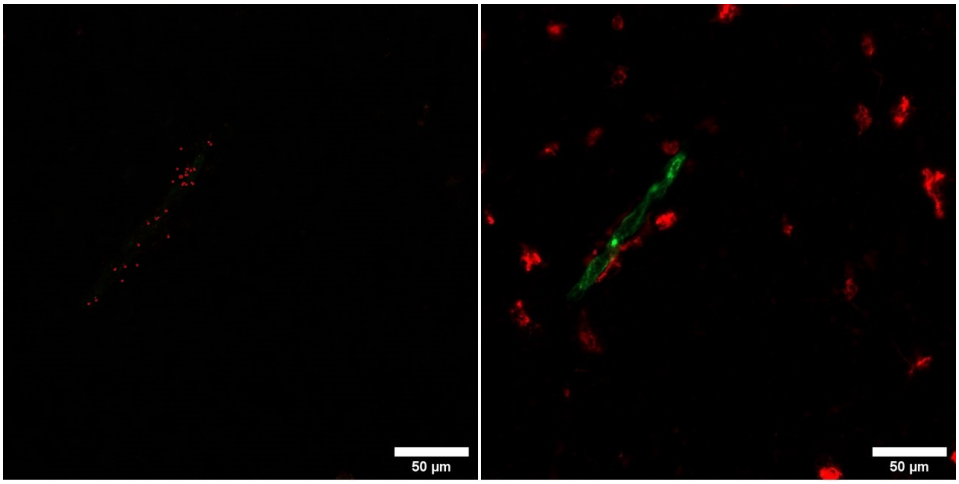

Figure 4.17: Images from the PC3 treated group. To the left is an image of the nanoparticles (red) and blood vessels (green). The image to the right show the macrophages (red) and blood vessels (green). Both images are captured at the same location on the tumor section. Scale bars are $50\,\mu\mathrm{m}$.

4.3.2 Area percentage of all macrophages

The mean area percentage of all macrophages (M1 + M2) in the images from the four different experimental groups, OHS control, OHS treated, PC3 control and PC3 treated, is presented in Figure 4.18. P-values from student t-test were used to determine if there were some significant differences. No significant differences in the mean area percentage of macrophages in the images between the four different groups were observed.

In the images from the OHS control group, the mean area percentage of macrophages was $7.5\pm4.1\%$. This was 1.8 percentage point higher compared to the OHS treated group, where the mean area percentage of macrophages was $5.7\pm3.9\%$. This difference was not significant with a p-value of 0.06. For the PC3 control group, the mean area percentage of macrophages in the images was $5.8\pm3.0\%$. This was 1.1 percentage point higher than for the PC3 treated group, where the mean area percentage of macrophages in the images was $6.9\pm5.0\%$. This difference was not significant with a p-value of 0.3. These results indicated that ultrasound did not affect the mean area percentage of macrophages in OHS and PC3 tumor tissue.

The OHS control group had a mean area percentage of macrophages in the images that was 1.7 percentage point higher than for the PC3 control group. The p-value was 0.06 and the difference was not defined to be significant. According to this, there was no difference in the mean area percentage of macrophages between OHS and PC3 tumor tissue.

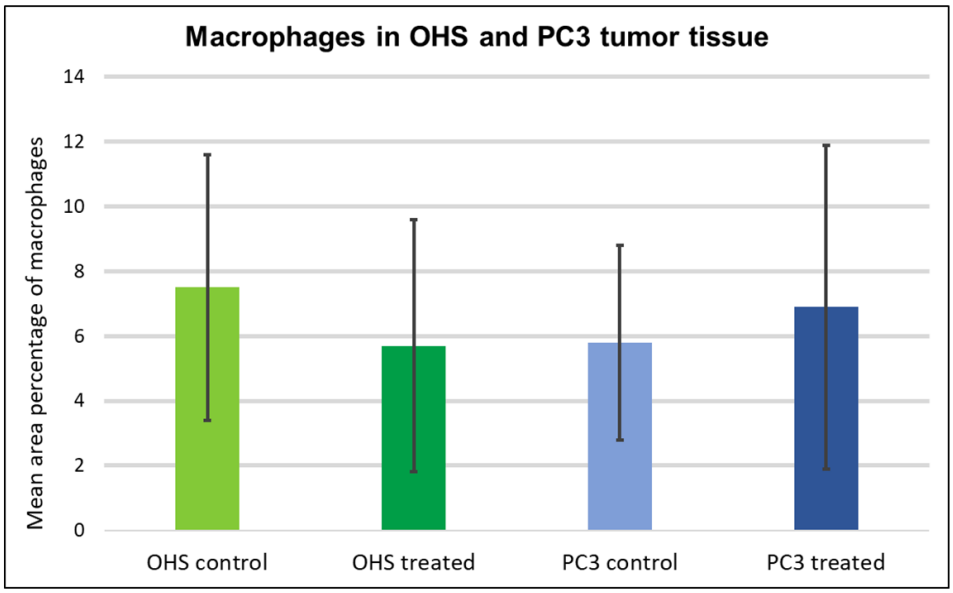

Figure 4.18: Bar plot showing mean area percentage of all macrophages (M1 + M2) in the control group and the group treated with ultrasound, for both OHS and PC3 tumor tissue. The results are based on images of tumor sections captured by the use of a confocal laser scanning microscope. The area percentage of macrophages was measured in all images from each group, and the mean values are presented in this plot. The number of images varied in the different groups: 36 images in OHS control, 48 images in OHS treated, 48 images in PC3 control and 36 images in PC3 treated. The error bars are equal to the standard deviations for each of the groups.

4.3.3 Macrophages around blood vessels in OHS tumor tissue

The distribution of all macrophages (M1 + M2) around blood vessels in OHS tumor tissue, for both the control group and the group treated with ultrasound, is shown in Figure 4.19. The histogram shows the mean percentage of macrophages at different distances from the nearest blood vessel wall. According to the plot, there was a higher mean percentage of macrophages close to the blood vessel walls compared to distances further away. This was seen for macrophages in both the control group and the treated group. There were no significant differences in the mean percentage of macrophages at the different distances between the control group and the group treated with ultrasound.

The macrophages within the distance 0-5 μm was defined to be inside the vasculature. For the OHS control group, the mean percentage of macrophages inside the blood vessels was 21.6$\pm$14.1%, and the mean percentage of macrophages extravasated from the blood vessels and into the tumor tissue was 78.4$\pm$14.1%. For the OHS treated group, the mean percentage of macrophages inside the vasculature was 17.2$\pm$11.2%. The mean percentage of macrophages extravasated from the blood vessels was 82.8$\pm$11.2% for the same group. This was 4.4 percentage point higher compared to the control group, but the difference was not statistically significant with a p-value of 0.1.

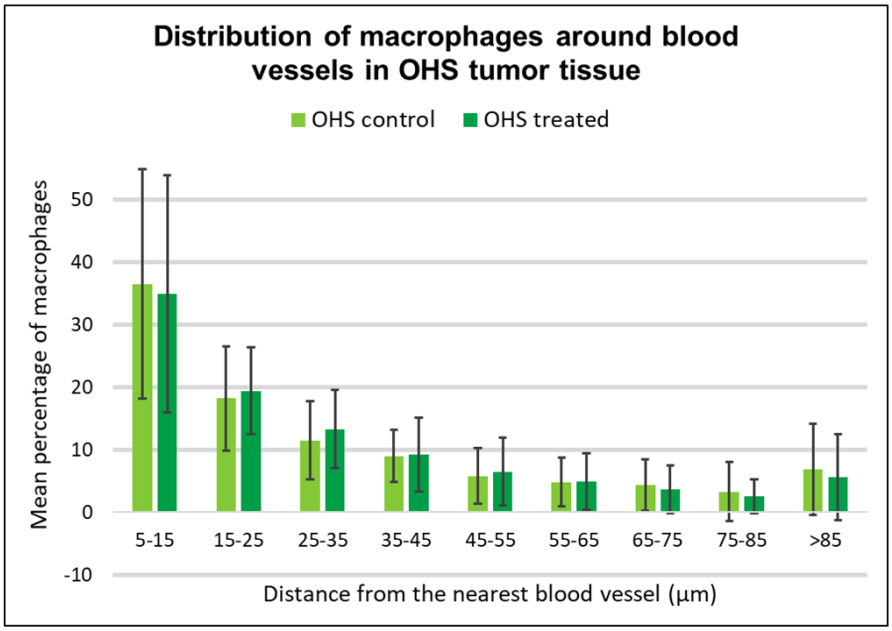

Figure 4.19: Histogram of the mean percentage of all macrophages (M1+M2) at different distances from the nearest blood vessel wall in OHS tumor tissue. The histogram is normalized according to the number of images in the OHS control group (36 images) and OHS treated group (48 images). The error bars are equal to the standard deviations for each of the distance groups. The macrophages within a distance 0-5 µm were defined to be inside the vasculature and they are not included in this plot.

4.3.4 Macrophages around blood vessels in PC3 tumor tissue

The distribution of all macrophages (M1 + M2) around blood vessels was studied for PC3 tumor tissue, for both the control group and the group treated with ultrasound. The results are presented in Figure 4.19. The histogram shows the mean percentage of macrophages at different distances from the nearest blood vessel wall. As shown in the plot, a higher percentage of macrophages were located close to the blood vessel walls compared to distances further away from the blood vessels. This was seen for macrophages in both the control group and the group treated with ultrasound. No significant differences in the mean percentage of macrophages at the different distances between the control group and the treated group were observed.

The macrophages within the distance 0-5 µm was defined to be inside the blood vessels. For the PC3 control group, the mean percentage of macrophages inside the vasculature was 10.4±6.7%, and the mean percentage of macrophages extravasated into the tumor tissue was 89.6±6.7%. The mean percentage of macrophages inside blood vessels for the PC3 treated group was calculated to be 9.2±7.5%, while 90.8±7.5% of the macrophages were extravasated from the blood vessels. There was no statistical difference in the mean percentage of extravasated macrophages between the control group and the group treated with ultrasound. The difference corresponded to 1.2 percentage point and the calculated p-value was 0.6.

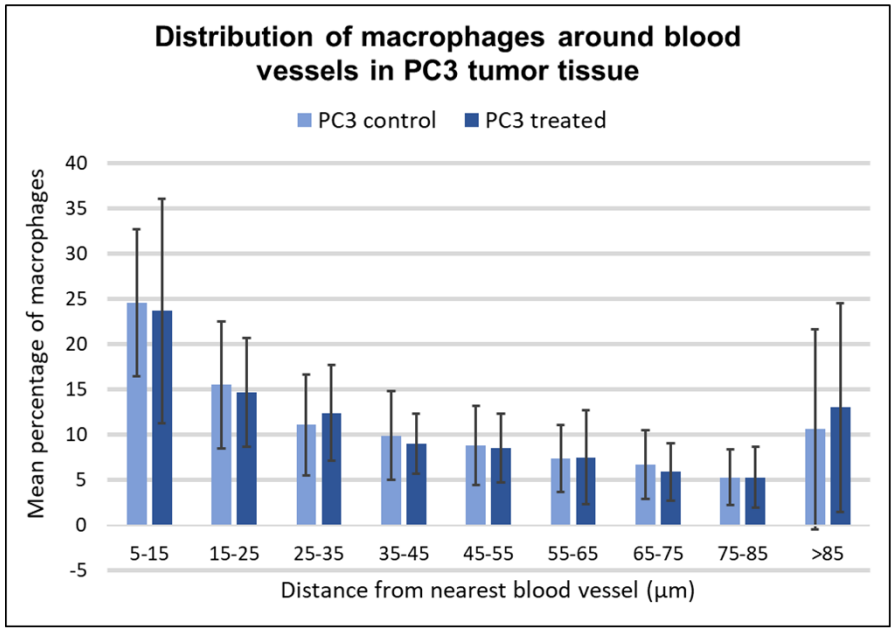

Figure 4.20: Histogram of the mean percentage of all macrophages (M1+M2) at different distances from the nearest blood vessel wall in PC3 tumor tissue. The histogram is normalized according to the number of images in the PC3 control group (48 images) and PC3 treated group (36 images). The error bars are equal to the standard deviations for each of the distance groups. The macrophages within a distance 0-5 µm were defined to be inside the vasculature and they are not included in this plot.

4.3.5 Area percentage of nanoparticles

The mean area percentage of nanoparticles in the images from the four experimental groups, OHS control, OHS treated, PC3 control and PC3 treated, is presented in Figure 4.21. P-values were calculated from student t-tests. Significant differences in the mean area percentage of nanoparticles were found between the control group and the treated group, for both OHS and PC3 tumor tissue.

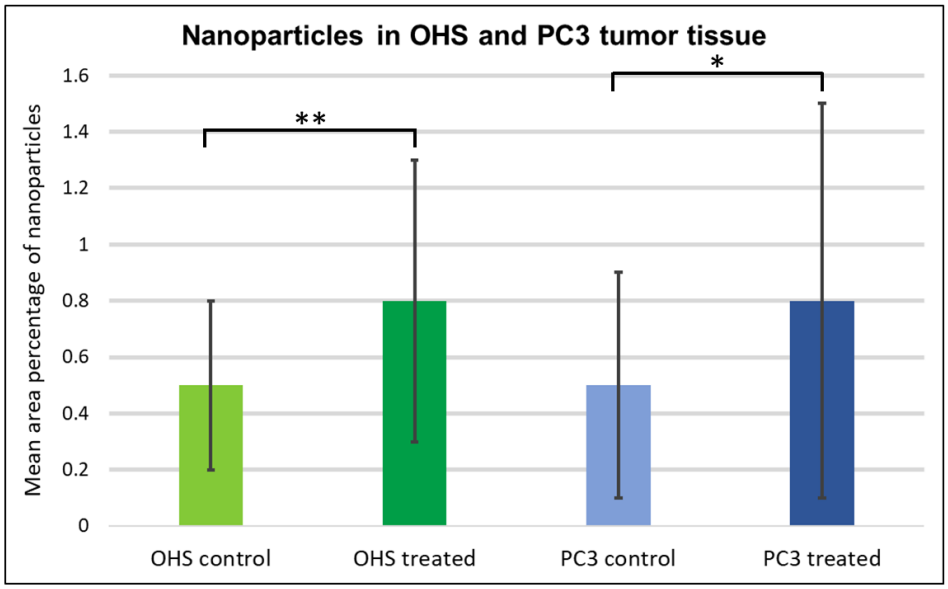

Figure 4.21: Bar plot showing the mean area percentage of nanoparticles in the control group and the group treated with ultrasound, for both OHS and PC3 tumor tissue. The results are based on images of tumor sections captured by the use of a confocal laser scanning microscope. The area percentage of nanoparticles was measured in all images from each group and the mean values are presented in this plot. The number of images varied in the different groups: 36 images in OHS control, 48 images in OHS treated, 48 images in PC3 control and 36 images in PC3 treated. The error bars are equal to the standard deviations for each of the groups. * P-value ≤ 0.05, ** P-value ≤ 0.005.

The mean area percentage of nanoparticles in the images from the OHS control group was $0.5\pm0.3\%$. This was 0.3 percentage point lower than the mean area percentage of nanoparticles in the images from the OHS treated group, which was $0.8\pm0.5\%$. The difference was significant with a p-value <0.005. For the PC3 control group, the mean area percentage of nanoparticles was $0.5\pm0.4\%$. The mean area percentage of nanoparticles for the PC3 treated group was $0.8\pm0.7\%$. For the PC3 control group, the mean area percentage of macrophages was 0.3 percentage point lower compared to the group treated with ultrasound. This difference was significant with a p-value of 0.03. According to these results, the mean area percentage of nanoparticles in the images increases with ultrasound treatment for both OHS and PC3 tumor tissue.

The OHS control group had a mean area percentage of nanoparticles in the images that was the same as calculated for the PC3 control group. From this result, there is no difference in the mean area percentage of nanoparticles between OHS and PC3 tumor tissue.

4.3.6 Nanoparticles around blood vessels in OHS tumor tissue

The distribution of nanoparticles around blood vessels in OHS tumor tissue was evaluated for both the control group and the group treated with ultrasound. The results are shown in Figure 4.22, where the histogram shows the mean percentage of nanoparticles at different distances from the nearest blood vessel wall. The mean area percentage of nanoparticles was largest close to the blood vessels and decreased with increasing distance. This was observed for both the control group and the group treated with ultrasound. No significant differences in the mean percentage of nanoparticles at the different distances was seen between the two experimental groups.

The nanoparticles within a distance 0-5 µm was defined to be inside the vasculature. For the OHS control group, the mean percentage of nanoparticles inside the blood vessels was 42.4±23.2%, while 57.6±23.2 of the nanoparticles were extravasated into the tumor tissue. The mean percentage of nanoparticles inside blood vessels in the OHS treated group was 35.3±21.2%, and the mean percentage of extravasated nanoparticles was 64.7±21.2%. For the group treated with ultrasound, the mean percentage of extravasated nanoparticles was 7.1 percentage point higher compared to the control group. This difference was not significant with a p-value of 0.2.

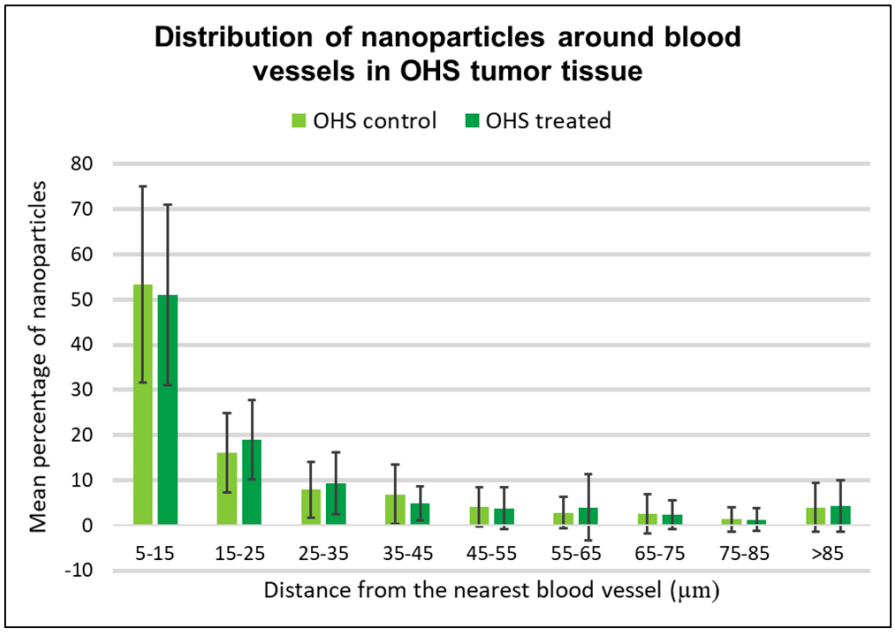

Figure 4.22: Histogram of the mean percentage of nanoparticles at different distances from the nearest blood vessel wall in OHS tumor tissue. The histogram is normalized according to the number of images in the OHS control group (36 images) and OHS treated group (48 images). The error bars are equal to the standard deviations for each of the distance groups. The nanoparticles within a distance 0-5 µm were defined to be inside the vasculature and they are not included in this plot.

4.3.7 Nanoparticles around blood vessels in PC3 tumor tissue

The distribution of nanoparticles around blood vessels in PC3 tumor tissue is presented in Figure 4.23. The histogram shows the mean percentage of nanoparticles at different distances from the nearest blood vessel wall, for both the control group and the group treated with ultrasound. The highest percentage of nanoparticles is located close to the blood vessels. The percentage of nanoparticles decreases further away from the blood vessel walls. This was seen for the nanoparticles in both the control group and the treated group. The difference in mean percentage of nanoparticles at the different distances was not significant between the two experimental groups.

The nanoparticles within a distance 0-5 µm was defined to be inside the blood vessels. For the PC3 control group the mean percentage of nanoparticles localised inside the vasculature was 50.8±27.6%. The mean percentage of nanoparticles extravasated from the blood vessels was 49.2±27.6%. For the group treated with ultrasound, the mean percentage of nanoparticles inside the blood vessels was 42.6±25.1%. On the other hand, the mean percentage of extravasated nanoparticles was 57.4±25.1% for the same group. The mean percentage of nanoparticles extravasated from the blood vessels was 8.2 percentage point higher for the group treated with ultrasound compared to the control group. This difference was not significant with a p-value of 0.2.

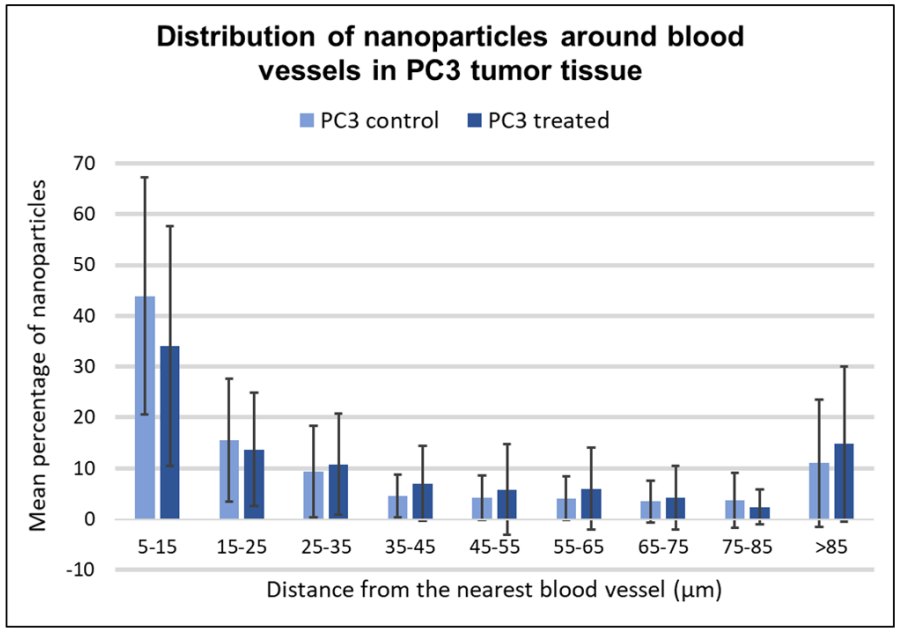

Figure 4.23: Histogram of the mean percentage of nanoparticles at different distances from the nearest blood vessel wall in PC3 tumor tissue. The histogram is normalized according to the number of images in the PC3 control group (48 images) and PC3 treated group (36 images). The error bars are equal to the standard deviations for each of the distance groups. The macrophages within a distance 0-5 µm were defined to be inside the vasculature and they are not included in this plot.

4.3.8 Area percentage of nanoparticles inside macrophages

The mean area percentage of nanoparticles inside macrophages for the four different experimental groups, OHS control, OHS treated, PC3 control and PC3 treated, is presented in Figure 4.24. P-values were calculated from student t-test. One significant difference was found in the mean area percentage of nanoparticles inside macrophages between the OHS control group and PC3 control group.

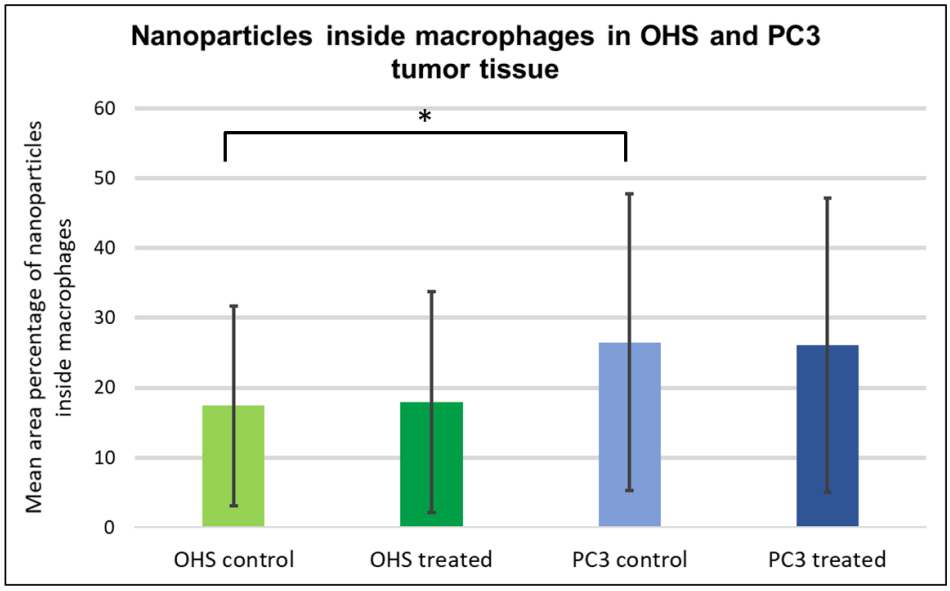

Figure 4.24: Bar plot showing the mean area percentage of nanoparticles inside macrophages in the control group and the group treated with ultrasound, for both OHS and PC3 tumor tissue. The results are based on images of tumor sections captured by the use of a confocal laser scanning microscope. The area percentage of nanoparticles inside macrophages was measured in all images from each group and the mean values are presented in this plot. The number of images varied in the different groups: 36 images in OHS control, 48 images in OHS treated, 48 images in PC3 control and 36 images in PC3 treated. The error bars are equal to the standard deviations for each of the groups.
* P-value ≤ 0.05.

The mean area percentage of nanoparticles located inside macrophages in the OHS control group was 17.4±14.3%. For the OHS treated group, the mean area percentage of nanoparticles inside macrophages was 17.9±15.8%. This corresponded to a difference of 0.5 percentage point and it was not significant with a p-value of 0.9. For the PC3 tumor tissue, the mean area percentage of nanoparticles inside macrophages was 26.5±21.2% for the control group and 26.1±21.1% for the treated group. This was a difference of 0.4 percentage point. The p-value was 0.9 and the difference was not significant. From these results, ultrasound treatment did not affect the mean area percentage of nanoparticles located inside macrophages in OHS and PC3 tumor tissue.

The OHS control group had a mean area percentage of nanoparticles inside macrophages that was 9.1 percentage point lower than for the PC3 control group. This difference was defined to be significant with a p-value of 0.04. According to these results, a larger mean area percentage of nanoparticles was found to be inside macrophages in PC3 tumor tissue compared to OHS tumor tissue.

4.3.9 Nanoparticles inside macrophages around blood vessels in OHS tumor tissue

The uptake of nanoparticles by macrophages around blood vessels was studied for OHS tumor tissue and the results is presented in Figure 4.25. The histogram shows the percentage of nanoparticles inside macrophages at different distances from the nearest blood vessel wall. The number of pixels defined as nanoparticles inside macrophages at a certain distance, was divided by the total number of nanoparticle pixels at the same distance. This fraction was multiplied by one hundred to get the percentage of nanoparticle pixels inside macrophages at different distances.

The plot shows that a higher mean percentage of nanoparticles was taken up by macrophages close to the blood vessels compared to distances further away. For the interval between 5-15 μm, 20.6$\pm$17.0% of the nanoparticles were taken up by macrophages in the control group. This was similar to the mean percentage of nanoparticles inside macrophages for the treated group at the same distance, which was 21.0$\pm$19.1%. For distances $>$85 μm the mean percentage of nanoparticles inside macrophages was 8.1$\pm$18.5% for the control group and 6.5$\pm$18.9% for the group treated with ultrasound. The difference in mean percentage of nanoparticles taken up by macrophages between distance 5-15 μm and distances $>$85 μm was 12.5 percentage point for the control group and 14.5 percentage point for the treated group. Both differences were significant with p-values $<$0.005.

The mean percentage of nanoparticles engulfed by macrophages at the different distance intervals decreases at distances further away from the blood vessels. This was observed for both the control group and the group treated with ultrasound. No significant differences in the mean percentage of nanoparticles inside macrophages at the different distances were observed between the two experimental groups.

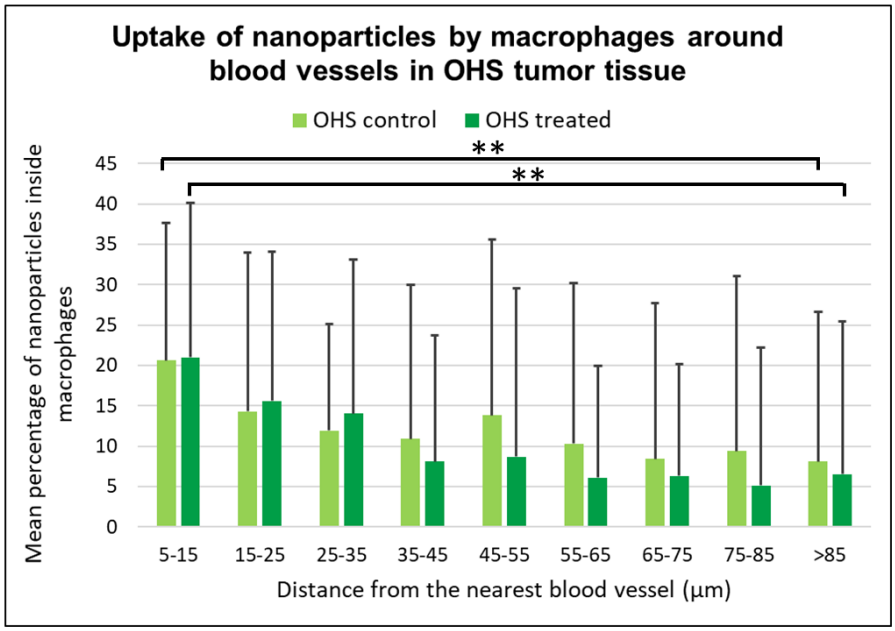

Figure 4.25: Histogram of the mean percentage of nanoparticles inside macrophages at different distances from the nearest blood vessel wall in OHS tumor tissue. The histogram is normalized according to the number of images in the OHS control group (36 images) and OHS treated group (48 images). The error bars are equal to the positive standard deviations for each of the distance groups. The macrophages within a distance 0-5 µm were defined to be inside the vasculature and they are not included in this plot. ** P-value ≤ 0.005.

4.3.10 Nanoparticles inside macrophages around blood vessels in PC3 tumor tissue

The uptake of nanoparticles by macrophages around blood vessels in PC3 tumor tissue, for both the control group and the group treated with ultrasound, is shown in Figure 4.26. The percentage of nanoparticles inside macrophages at different distances from the nearest blood vessel wall, is presented in the histogram. For each distance, the number of pixels defined as nanoparticles inside macrophages was divided by the total number of nanoparticle pixels at the same distance. This fraction was multiplied by one hundred to get the percentage of nanoparticle pixels inside macrophages at different distances.

For the interval between 5-15 µm, the mean percentage of nanoparticles inside macrophages was 28.3±24.4% for the control group and 31.7±26.9% for the group treated with ultrasound. Distances >85 µm had a mean percentage of nanoparticles inside macrophages calculated to be 20.1±33.4% for the control group and 22.2±27.8% for the treated group.

The difference in mean percentage of nanoparticles taken up by macrophages between distance 5-15 µm and distances >85 µm was 7.2 percentage point for the control group. This difference was not significant with a p-value of 0.2. For the group treated with ultrasound, the difference in mean percentage of nanoparticles inside macrophages between 5-15 µm and distances >85 µm was 9.5 percentage point. The p-value was 0.1 and the difference was not significant.

This indicated a slight decrease in the mean percentage of nanoparticles engulfed by macrophages close to the blood vessels compared to increased distances, but the decrease was not significant. The mean percentage of nanoparticles inside macrophages varied a lot, going up and down between different distance intervals, for both the control group and the group treated with ultrasound. No significant differences in the mean percentage of nanoparticles inside macrophages at the different distances were observed between the two experimental groups.

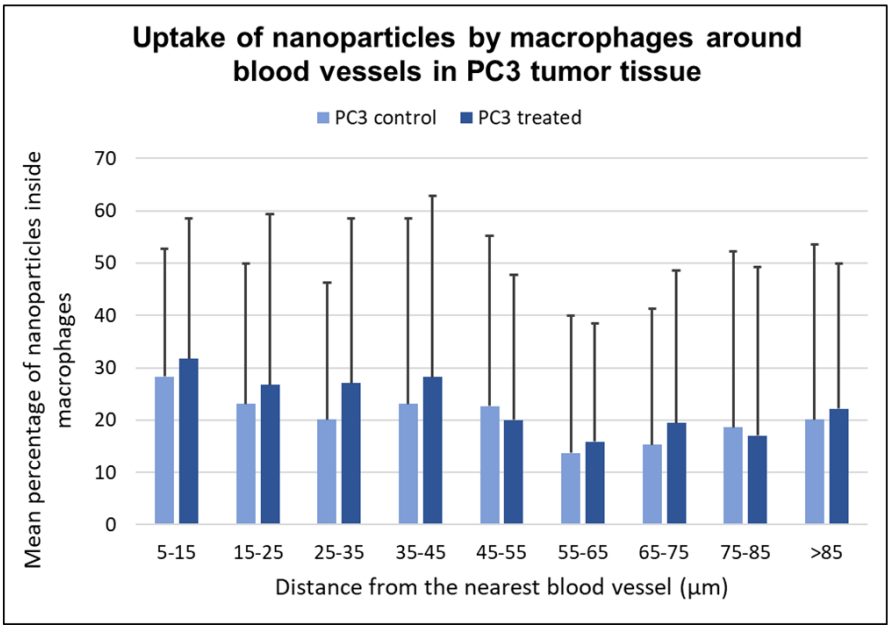

Figure 4.26: Histogram of the mean percentage of nanoparticles inside macrophages at different distances from the nearest blood vessel wall in PC3 tumor tissue. The histogram is normalized according to the number of images in the PC3 control group (48 images) and PC3 treated group (36 images). The error bars are equal to the positive standard deviations for each of the distance groups. The macrophages within a distance 0-5 µm were defined to be inside the vasculature and they are not included in this plot.

4.3.11 Comparison of macrophages and nanoparticles extravasated in OHS and PC3 tumor tissue

Macrophages

A student t-test was used to study wheter or not there was a statistically significant difference in the mean percentage of macrophages extravasated, between the OHS control group and the PC3 control group. The mean percentage of macrophages extravasated from the blood vessels was 78.4±14.1% for the OHS control group and 89.6±6.7% for the PC3 control group. This corresponded to a difference of 11.2 percentage point which was statistically significant with a p-value of <0.005. According to this, a larger amount of macrophages extravasated from the blood vessel in PC3 tumor tissue compared to OHS tumor tissue.

Nanoparticles

No statistically significant difference was found between the mean percentage of nanoparticles extravasated, between the OHS control group and the PC3 control group. The mean percentage of nanoparticles extravasated from the blood vessels was 57.6±23.2% for the OHS control group and 49.2±27.6% for the PC3 control group. The difference was 8.4 percentage point and not significant with a p-value of 0.2.

Chapter 5

Discussion

5.1 Methods

Tumors were analyzed by flow cytometry in order to obtain information regarding the amount of macrophages and their uptake of nanoparticles. Tumor sections were imaged by confocal laser scanning microscopy and were mainly used for distance analysis. These methods and their uncertainties are discussed in the following sections.

5.1.1 Flow cytometry analysis

In the flow cytometry study, fewer tumors than originally intended were used due to poor tumor growth in many of the animals. The low amount of tumors in each of the four experimental groups is an uncertainty factor in the obtained results.

Several of the tumors used to make single cell suspensions had particularly low mass. Even though a tumor had a high number of viable cells per gram, the total amount of viable cells obtained from the tumor was low due to the low mass. For some of the tumors, it was challenging to achieve one million viable cells from the tumor, which was the required number of cells to make one sample. 100 000 cells from each sample were counted, but if this was not achievable for all samples, the flow cytometer would stop counting after 3 minutes. This indicated that the different samples contained a varying number of cells. The tumors with the least mass gave the fewest number of viable cells according to the flow cytometer. A sample that containes a large number of cells provides a more representative result compared to samples with few cells. The varying amount of cells in the samples may affect the results and be a source of uncertainty.

For all samples, it was desirable to separate out the dead cells since they gave a lot of false positive fluorescence. A near IR-dye was used for this purpose. The near-IR dye binds to the surfaces of viable cells, resulting in a weak fluorescent signal from these cells. Dead cells with permeable membranes react with this dye throughout their whole volume, resulting in a high fluorescent signal. Optimally, this should appear as two distinct peaks in the live/dead histogram, but this did not work as intended. For several of the samples, only one distinct peak was observed in the associated histogram. This indicated a weak staining

of all cells. To be able to separate the viable and dead cells, a forward scatter density plot was used. A gate was placed between the two populations, but the placement of the gate was difficult due to the populations' close proximity to each other. A small displacement of the gate results in noticeable changes in the number of cells within each population. If only a few dead cells were included in the population defined as viable cells, false positive fluorescence will be observed, and the obtained results will be affected.

During the flow cytometry, it was observed that AlexaFluor488 stained almost the same, or even a higher, number of cells compared to DyLight405. In the histograms showing the fluorescent intensity of AlexaFluor488 there were two distinct peaks. The peak placed to the right indicated cells positive for AlexaFluor488. For DyLight405, two distinct peaks were not observed in the histograms. This was not as expected since AlexaFluor488 should only stain M2 macrophages, while DyLight405 should stain all macrophages (M1+M2). Hence, a larger amount of cells positive for DyLight405 compared to AlexaFluor488 should be observed. One explanation for this result may be that the primary antibody CD206 also binds to dendritic cells in addition to monocytes and M2 macrophages. On the other hand, the F4/80 antibody mainly binds to macrophages including M1 and M2 macrophages inside tumor tissue. Also monocytes in the blood stream express F4/80 receptors at their surfaces, but to a lesser degree than macrophages inside tissues[62, 63]. Another reason that may have affected the results is that a higher concentration of the CD206 antibody was used compared to the F4/80 antibody. The reason for choosing different concentrations was based on the suggested concentrations from their respective datasheets. Although there were various factors that may have affected the staining of the macrophages, the results indicated that there is a predominance of M2 macrophages in both OHS and PC3 tumor tissue.

In the concentration study of primary antibodies, no positive populations for either AlexaFluor488 or DyLight405 were observed. This was the reason why the primary antibodies were used in concentrations of 20 times the suggested datasheet concentrations. On the other hand, when samples from trial 3 and 4 were run through the flow cytometer, large populations of cells positive for both fluorescent antibodies were seen. This was not as expected. Samples from trial 3 and 4 were stained by the use of the same method, with the same time parameters and steps as used in the concentration study. There is no good explanation for this result, but one thing worth mentioning is that two different batches of antibodies were used in the concentration study and in the main study. New batches of both primary antibodies were used to stain the samples from trial 3 and 4, but they were purchased from the same producer as the batches used in the concentration study. If the concentration study had given the same result as the main study, it might have been more appropriate to choose a lower concentration of primary antibodies to avoid the risk of unspecific bindings.

5.1.2 Confocal laser scanning microscopy analysis

All calculated values from the image analysis had large standard deviations. This was expected since there were large variations in the mean area percentage of both macrophages and nanoparticles in the different images. : In other words, some images contained many macrophages and nanoparticles, whereas others contained very few. The large standard deviations indicate a high degree of uncertainty in these results. This is important to keep in mind during interpretation of the results.

Imaging with CLSM

Imaging of the nanoparticles in the tumor sections were done before staining of the macrophages. As described previously, the use of a mounting medium and cover glass would alter the structure of the tumor section after removal. Therefore, this equipment was not used even though it made it more challenging to capture images of decent quality. The lack of this equipment lead to two major problems. The autofluorescence of the tissue would drown out the fluorescence of the blood vessels and nanoparticles, or the fluorescence signal became difficult to observe due to the signal it self being too weak. This may have caused a calculated result with a lower amount of nanoparticles than it originally contained. The varying fluorescence from the nanoparticles and blood vessels made it difficult to find optimal image setting for all images. However, the same image settings were used on all images to make it possible to compare the images in further analysis. The images captured after staining of the macrophages had a much higher quality due to use of both mounting medium and cover glass.

During imaging, the optical section may affect the visualization of the fluorescent substances in the images. The pinhole size was adjusted to obtain an optical section with a thickness of $3\,\mu\mathrm{m}$. A thin optical section is required to achieve a high horizontal resolution and contrast in the image. Small sizes of the pinhole limit the number of photons that reach the detector. Due to this, it was not possible to detect the fluorescent substances by the use of a smaller optical section than $3\,\mu\mathrm{m}$. If it is desirable to use a small pinhole size, the power of the excitation laser have to be high, in addition to the need of a longer exposure time compared to use of larger pinhole sizes. For an optical section of $3\,\mu\mathrm{m}$, the power of the excitation lasers were already relatively high, and even higher power levels were not desirable to avoid the risk of photobleaching. Other measures were also taken to prevent loss of fluorescence intensity from the sections. The exposure time during imaging was attempted to be as short as possible. In addition to this, the tumor sections were stored in the dark between staining and imaging.

Bleed-through between the different image channels were tested and not observed to be a problem. This was due to large distances between the emission wavelengths for the fluorescent dyes.

The blood vessel channel was used to determine the different locations to be imaged. This will strengthen the results since the images are taken independently from the amount of macrophages and nanoparticles in different areas on the section. For PC3 tumor tissue, the blood vessels were placed in the center of the images. This was done to increase the probability that the imaged macrophages and nanoparticles were extravasated from the imaged blood vessel. This was not possible for OHS tumor tissue, due to the high density

of blood vessels. Macrophages and nanoparticles in these images may be extravasated from blood vessels outside the image. In reality, the macrophages, nanoparticles and blood vessels are distributed in 3D inside the tissue, while the captured images are in 2D. From this, it is possible that the imaged macrophages and nanoparticles may be extravasated from a blood vessel in a plane over or under the image plane.

Each area on the tumor sections was imaged both before and after staining of the macrophages. This was due to the removal of nanoparticles during the staining of macrophages. All areas were given coordinates to be able to image the same area twice. If the images before and after staining were offset by even a few pixels, the amount of nanoparticles defined to be inside macrophages would be affected. For some areas, it was observed small changes in the structures of the tumor sections after staining of the macrophages. This may have affected the results.

Image analysis

There are several factors in the image analysis that may have affected the calculated results. However, since the same method is used to analyze all images, it is possible to compare images from the different experimental groups.

During image analysis, the Moments algorithm was applied on the nanoparticle channel, followed by the Despeckle filter. This was done to remove a lot of noise, but due to the small size of the nanoparticles, it was difficult to distinguish between noise and particles. A mask including the nanoparticles was used in the image analysis. To make sure that all nanoparticles were included, no area limit was set on these masks. Due to the the lack of an area limit, this mask also included noise that had not been filtered out by the Moments algorithm and the Despeckle filter. This may have affected the calculated area percentage of nanoparticles in the images.

The Triangle algorithm and the Despeckle filter were applied on the macrophage channel to reduce the noise in the images. A mask was used to decide the areas in the image defined as macrophages. The mask was adjusted to only include particles larger than $40\,\mu m^2$. This removed the noise, but kept the macrophages within the optical section. Due to the area limit on the mask, the amount of macrophages in the images was not affected in a significant way by the noise.

To assess the distribution of macrophages and nanoparticles around blood vessels, removal of noise from the blood vessel channel was essential. The Otsu algorithm and the Despeckle filter were used for this purpose. This removed the major amount of noise in the images, but some noise was still present. A distance map was created based on the binary image of the blood vessel channel. If there were only a few pixels of noise in this image, this noise was defined as blood vessels. This definitely affected the distance analysis.

5.2 Macrophages and nanoparticles in OHS and PC3 tumor tissue

The percentage of all macrophages, M1 and M2 macrophages, nanoparticles and uptake of nanoparticles by macrophages, were found for OHS and PC3 tumor tissue. The results were obtained by the use of flow cytometry and confocal laser scanning microscopy (CLSM), and they are discussed in the following sections. The control groups were injected with nanoparticle-stabilized bubbles, while the treated groups were injected with nanoparticle-stabilized micobubbles in combination with focused ultrasound treatment locally on the tumor.

5.2.1 All macrophages

No significant difference were found in the mean percentage of macrophages between the OHS control group and PC3 control group when calculating from the flow cytometry analysis. Although no significant differences were seen, the results indicate that there was a slightly higher mean percentage of macrophages in OHS tumors than PC3 tumor tumors. This result is as expected. *E. Sulheim et al.*[9] presents a study were they characterized the vascular fraction in both OHS and PC3 tumor tissue. They found a higher density and fraction of blood vessels in OHS tumor tissue compared to PC3 tumor tissue. Since macrophages arise from circulating monocytes in the blood stream, it is expected to find a higher percentage of macrophages in OHS tumors compared to PC3 tumors.

The percentage of macrophages in tumors have also been quantified as a part of other studies. *Q. Dai et al*[60] and *R. Franklin et al.*[64] have studied the percentage of macrophages by the use of flow cytometry, respectively in SKOV-3 ovary cancer xenografts and PyMT breast cancer xenografts. Both studies observed dominant populations of macrophages within the tumors, which is consistent with the flow cytometry analysis of OHS and PC3 tumor in this thesis.

Recently, *M. Fusser et al.*[65] presented a study where they looked at the use of polymeric nanoparticles in treatment of breast cancer xenografts. The polymeric nanoparticles were the same as used in this thesis. They have characterized the fraction of macrophages in tumors by the use of IVIS spectrum in vivo imaging system. Compared to tumors only treated with saline, the fraction of macrophages inside the tumors was increased for tumors treated with nanoparticles (without drug). This indicates an elevated inflammations in the tumors when they are treated with nanoparticles. Recruitment of more monocytes to the tumors occurs, resulting in a larger fraction of macrophages within the tumor tissue. The tumors characterized in this thesis were all treated with nanoparticles, including the control group. Perhaps the calculated mean percentage of macrophages in OHS and PC3 tumors would have been lower if the tumors were not treated with nanoparticles. However, the characterization method used in *M. Fusser et al.*[65] and this thesis are different, and the measurement were executed at different times after injection.

From the flow cytometry analysis, no significant differences in the mean percentage of macrophages were found between the control group and the group treated with focused ultrasound. For OHS tumor tissue, there was an increase in the mean percentage of macrophages for the treated group compared to the control group. The opposite was

observed for PC3 tumors, where the group treated with ultrasound contained the lowest mean percentage of macrophages, which is an inexplicable result. A low number of tumors in each of the experimental group is used, and this result may be because of local variations from tumor to tumor. There is no published literature where the effect of focused ultrasound on tumor associated macrophages in a nanoparticle-stabilized DDS is studied. On the other hand, studies have been conducted to investigate the delivery of cells by the use of focused ultrasound. *A. Burgess et al.*[66] and *R. Alkins et al.*[67] have presented studies where focused ultrasound and microbubbles are used to disrupt the blood brain barrier. The aim was to obtain an increased delivery, respectively of stem cells and natural killer cells to brain tumors. This was successful according to the results from these studies. *H. Liu et al.*[68] have presented another study where they investigated the infiltration of macrophages during disruption of the blood brain barrier by focused ultrasound and microbubbles. They found that there is an increased infiltration of macrophages during disruption of the blood brain barrier due to an inflammatory response. The infiltration of macrophages were reduced by the use of certain ultrasound parameters. The ultrasound settings used in this thesis does not ensure inertial cavitations, but collapse of the microbubbles was expected. During expansion of the microbubbles, they push on the vessel walls and make them more permeable. Due to this, a larger percentage of macrophages was expected by the use of ultrasound due to an inflammatory response. This was seen for OHS tumors, but not for PC3 tumors.

From the CLSM analysis, the mean area percentage of macrophages in the images were calculated for both OHS and PC3 tumor tissue. The difference between the mean area percentage of macrophages in the OHS control group and the PC3 control group was not significant. In addition to this, no significant differences were found between the control group and the group treated with focused ultrasound. There was a large difference between the amount of macrophages found by flow analysis and by CLSM analysis. A much higher percentage of macrophages were found in both OHS and PC3 tumor models by the use of flow cytometry compared to CLSM. The main reason for this may be that flow cytometry analysis is based on cells from the entire tumor, while CLSM analysis is only based on 2D images from some selected locations inside the tumors.

Although the two analysis methods did not give the same percentage of macrophages, they both indicated that there were no significant differences in the percentage of macroph–ages by the use of ultrasound. This also corresponds to the results from the specialization project carried out by the author during the autumn 2018[10]. Based on this, it was concluded that focused ultrasound does not affect the mean percentage of macrophages in OHS and PC3 tumor tissue.

5.2.2 M1 and M2 macrophages

According to the flow cytometry analysis, no significant differences were found in the mean percentage of M1 and M2 macrophages between OHS and PC3 tumors. On the other hand, significant differences were found between the mean percentage of M1 and M2 macrophages within one experimental group. M2 macrophages were the major type of macrophages in both OHS and PC3 tumors.

Q. Xiao et al.[69] study the polarization of macrophages from M1 to M2 in OHS mice xenografts. They observed that the polarization of the macrophages occurs within the tumor tissue. 1 week after implantation of cancer cells, M1 macrophages were the main type of macrophages within the tumor tissue. 3 weeks after implantation this was altered and M2 macrophages were the major type of macrophages within the tumor tissue. The fraction of M1 and M2 macrophages were also analyzed after 10 weeks and the obtained result was similar to week 3. They concluded that polarization of macrophages from M1 to M2 mainly occurs during the first 3 weeks after implantation. These results are consistent with results obtained in this thesis, where M2 macrophages were found to be the major type of macrophages within OHS tumors.

M. Lundhold et al.[70] presented a study where they examined M1 and M2 macrophages in prostate cancer. They found that the majority of macrophages were M2 macrophages in PC3 tumor tissue, which is consistent with the results obtain in this thesis.

Several studies [70], [71] and [72] present how M1 and M2 macrophages correlate to good or poor prognosis in prostate cancer. All studies concluded that a large amount of M2 macrophages are related to poor prognosis and survival rate. According to *Q. Zhou et al.*[73], a large fraction of M2 macrophages promotes metastasis from OHS tumors and this is correlated to poor survival rate for the patients. The main reason for the poor prognosis is that M2 macrophages promote angiogenesis and tumor growth by production of different cytokines and vascular growth factors[16].

Due to the high fraction of M2 macrophages within OHS and PC3 tumors, in addition to the poor prognosis related to this type of macrophages, M2 macrophages can potentially be used in cancer therapy. A way to inhibit tumor growth is polarization of M2 macrophages to M1 macrophages. *S. Zanganeh et al.*[74] presented a study where they used iron oxide nanoparticles to inhibit tumor growth in early breast and lung cancer. This was done by inducing polarization of M2 macrophages into M1 macrophages within the tumor tissue.

5.2.3 Nanoparticles

The mean area percentage of nanoparticles in OHS and PC3 tumor tissue were calculated from the CLSM images. No difference in the percentage of nanoparticles were observed between the two tumor models. This result is not as expected. *E. Sulheim et al.*[9] found that OHS tumor tissue were better perfused and contained a higher density of blood vessels compared to PC3 tumor tissue. Due to this, a higher accumulation of nanoparticles within OHS tumor tissue was expected. A larger fraction of blood vessels will be able to carry more nanoparticles that may extravasate from the blood vessels and be distributed within the tissue.

A higher inflow time of microbubbles in OHS tumor tissue compared to PC3 tumor tissue was also reported by *E. Sulheim et al.*[9]. They argued that this was related to the fact that the microbubbles were relatively large in size, which caused an retention of the microbubbles inside the vasculature. This occurs due to a chaotic vasculature with several dead ends inside OHS tumor tissue. The result was a limited flow through the blood vessels. The higher inflow time of blood vessels normally results in a larger accumulation of nanoparticles within OHS tumor tissue compared to PC3 tumor tissue. As mention earlier, this was not consistent with the result in this thesis.

From the image analysis, significant differences were found in the mean area percentage of nanoparticles between the control group and the group treated with ultrasound. This was observed for both OHS and PC3 tumor tissue. Catharina de Lange Davies' research group has previously reported studies [6, 75] where an increased accumulation of nanoparticles inside tumor tissues was observed after treatment with nanoparticle-stabilized microbubbles and focused ultrasound. *S. Snipstad et al.*[6] study the effect of nanoparticle-stabilized microbubbles and focused ultrasound in breast cancer xenografts, while *S. Eggen et al.*[75] looked at this in prostate cancer xenografts. Both found an increased accumulation of nanoparticles within the tumor tissue by the use of focused ultrasound, which is consistent with the obtained results in this master thesis. Several other studies [76–80] have also published results where the use of nanoparticles and microbubbles in combination with focused ultrasound enhanced the delivery of nanoparticles to the tumor tissue.

Optimal ultrasound settings are essential to achieve a desired accumulation of nanoparticles within tumor tissue. *H. Han et al.*[76] reported that high intensity focused ultrasound was more efficient at accumulating nanoparticles within the tumor tissue compared to the use of lower intensities. *S. Snipstad et al.*[6] and *S. Eggen et al.*[75] documented that a high MI results in higher accumulation of nanoparticles within the tumors. A high value of the MI increases the probability of inertial cavitations and collapse of the microbubbles. According to the their results, destruction of the microbubbles are favorable compared to stable cavitations at lower MI. Stable cavitations cause microstreaming and an increased permeability of the vasculature when microbubbles expand and push on the walls of the vessel. During collapse of the microbubbles, shock waves and jet streams increase the permeability of the blood vessels even more. The nanoparticles are shot into the tumor tissue at this point[6, 43]. The ultrasound settings used in this thesis does not ensure inertial cavitations, but collapse of the microbubbles was expected.

5.2.4 Uptake of nanoparticles by macrophages

The mean percentage of macrophages containing nanoparticles were examined for both OHS and PC3 tumors by flow cytometry. At the time of writing, there were no published literature that describe the uptake of nanoparticles by macrophages in a drug delivery system based on nanoparticle-stabilized microbubbles and focused ultrasound.

A larger mean percentage of macrophages that engulfed nanoparticles was observed in OHS control tumors than in PC3 control tumors. This difference was significant and the results are hard to explain. As mention previously, *E. Sulheim et al.*[9] reported a higher density of blood vessels in OHS tumor tissue compared to PC3 tumor tissue. This may lead to an increased accumulation of nanoparticles within the tumor due to a larger fraction of blood vessels that carry nanoparticles. When a large amount of nanoparticles are presented inside the tumor tissue, it may be reasonable that a high percentage of the macrophages engulf the available nanoparticles. However, it is important to keep in mind that the high vascular fraction in OHS tumor tissue also may lead to a large amount of macrophages within the tumor. For PC3 tumors, the opposite is expected. This refers to a lower percentage of macrophages within the tumor tissue, in addition to a lesser amount of nanoparticles. Deduced from this, it is challenging to explain why a larger percentage of the macrophages within OHS tumor tissue contain nanoparticles compared to the

macrophages in PC3 tumor tissue. Nonetheless, this may indicate that the macrophages inside the two tumor microenvironments behave differently.

No significant differences were found in the mean percentage of macrophages containing nanoparticles between the control group and the group treated with ultrasound, but some tendencies were observed. For OHS tumors, there was a slight decrease in the mean percentage of macrophages in the treated group compared to the control group. For PC3 tumors, an increase was observed for the group treated with ultrasound compared to the control group. When the tumors were treated with ultrasound, an increase in the amount of macrophages containing nanoparticles was expected. According to *S. Snipstad et al.*[6] and *S. Eggen et al.*[75], there will be an increased accumulation of nanoparticles within tumor tissue by the use of nanoparticle-stabilized microbubbles in combination with focused ultrasound on the tumor. It makes sense that a higher percentage of the macrophages engulf nanoparticles when there are more nanoparticles available in the tumor tissue. For PC3 tumors, the result was as expected. A higher mean percentage of the macrophages contained nanoparticles in the group treated with ultrasound compared to the control group. For OHS tumors the outcome was opposite, where a slight decrease was seen for the treated group compared to the control group. One reason for this may be that the amount of macrophages containing nanoparticles are already high for the OHS control group. Due to this, ultrasound treatment will not increase the percentage of macrophages that have taken up nanoparticles even further. For the PC3 tumors, the proportion of macrophages containing nanoparticles was low in the control group. The uptake of nanoparticles by macrophages is further discussed in section 5.2.6.

5.2.5 Uptake of nanoparticles by tumor cells

From flow cytometry analysis, a slight increase in the mean percentage of tumor cells containing nanoparticles was seen for PC3 control tumors compared to OHS control tumors. However, this difference was not significant. As previously described, *E. Sulheim et al.*[9] stated a higher density of blood vessels in OHS tumor tissue than in PC3 tumor tissue. This may lead to a higher accumulation of nanoparticles within OHS tumor tissue due to a high inflow of blood throughout the tumor. Based on this argument, it would be expected to find a higher percentage of tumor cells that contain nanoparticles within OHS tumors compared to PC3 tumors. This is not consistent with the obtained result in this thesis.

The focused ultrasound treatment increase the the mean percentage of tumor cells containing nanoparticles for both OHS and PC3 tumors, but the increase was only significant for OHS tumors. An increase in the percentage of tumor cells with nanoparticles is predicted when the tumors are treated with ultrasound. *S. Snipstad et al.*[6] and *S. Eggen et al.*[75] reported an increased accumulation of nanoparticles within tumor tissue by the use of nanoparticle-stabilized microbubbles in combination with focused ultrasound on the tumor. When there is a large amount of nanoparticles available within the tumor tissue, it is reasonable to expect that a higher percentage of the tumor cells will take up nanoparticles. Comparatively, tumor tissue containing fewer nanoparticles will likely have a lower percentage of tumor cells taking up nanoparticles. This support the theory that ultrasound treatment increase the uptake of nanoparticles by tumor cells. Others [81, 82] have previously reported an enhanced intracellular drug uptake by tumor cells when micelles were used in combination with ultrasound. *J. Hauser et al.*[83] presented a study where they an-

alyzed the effect of therapautic ultrasound on the endocytotic activity of human fibroblast. They concluded that ultrasound treatment enhanced the endocytotic activity. These studies may indicate that ultrasound does not only increases the amount of nanoparticles within the tissue, but the treatment also stimulates cellular uptake. The uptake of nanoparticles by tumor cells is further discussed in section 5.2.6.

5.2.6 The percentage of nanoparticles taken up by macrophages and tumor cells

The mean percentage of nanoparticles taken up by macrophages and tumor cells were analyzed by flow cytometry. For both OHS and PC3 tumors, the majority of the nanoparticles inside the tumors was taken up by macrophages instead of tumor cells. This indicates that tumor associated macrophages work as a large barrier that prevents nanoparticles from being taken up by cancer cells.

Macrophages are phagocytic cells [7], and due to this it is reasonable that these cells engulf a large amount of nanoparticles. However, the observed amount of engulfed nanoparticles was higher than expected. *Q. Dai et al.*[60] presented a study where they quantified the delivery of ligand-coated nanoparticles to solid tumors. They found a larger amount of nanoparticles inside macrophages than inside tumor cells, which is the same was observed in this thesis. From the study, they concluded that the majority of the intratumoral nanoparticles were either trapped in the ECM or engulfed by macrophages.

J. Hoppstädter et al.[84] study the uptake of silica nanoparticles in M1 and M2 macrophages. They found an increased uptake of nanoparticles by M2 polarized macrophages compared to by M1 macrophages. In this thesis, M2 macrophages were the majority type of macrophages inside both OHS and PC3 tumor tissue. One reason for the large uptake of nanoparticles by macrophages observed in this thesis may be because most of the macrophages were of the M2 type. Since the M2 macrophages are related to both poor prognosis and engulf large amount of nanoparticles, they have a great potential in future cancer therapies.

Most of today's cancer therapy focus on killing malignant tumor cells, but these cells can become resistant to chemotherapeutic agent. The high phacocytic activity of M2 macrophages can be utilized to target and kill these cells with the aim of inhibit tumor growth. *M. Cieslewicz et al*[85] published a study where they delivered proapoptotic peptides to M2 macrophages in colon cancer by targeting the macrophages. The proapoptotic peptide selectively reduced the M2 macrophages and this led to inhibition of the tumor growth. *M. Fusser et al.*[86] presented a study which includes investigation of macrophages within breast cancer xenografts. They found that the amount of M2 macrophages within the tumor tissue was significantly reduced in tumors treated with nanoparticles containing cytotoxic drugs, compared to tumors only treated with nanoparticles. They suggested that this result was due to uptake of nanoparticles by M2 macrophages. This led to the macrophages being killed by the cytotoxic drug encapsulated inside the nanoparticles.

No significant differences in the mean percentage of nanoparticles inside macrophages and tumor cells were found between the control group and treated group. The majority of nanoparticles inside the tumors was still taken up by macrophages even though the tumors

were treated with focused ultrasound. However, the mean percentage of nanoparticles inside macrophages was slightly decreased for the groups treated with ultrasound, and the mean percentage of nanoparticles within tumor cells was slightly increased. This was observed for both OHS and PC3 tumors. This may indicate that a higher percentage of the nanoparticles accumulate in tumor cells by the use of focused ultrasound compared to no ultrasound, but these differences were not significant. As previously discussed in section 5.2.5, differences were found in the mean percentage of tumor cells containing nanoparticles between the control group and the treated group. This difference were significant for OHS tumors.

The images capture through the use of CLSM were also analyzed to find the mean area percentage of nanoparticles located inside macrophages. These results show a smaller percentage of nanoparticles inside macrophages compared to the results obtained by flow cytometry. The reason for this is that nanoparticles located outside the macrophages in the images, may be in the ECM in addition to being inside tumor cells. Nanoparticles located in the ECM are not included in the flow cytometry analysis since this analysis is based on counting of single cells. However, the image analysis showed that a substantial percentage of the nanoparticles were located inside the macrophages. Nevertheless, there was a higher percentage of nanoparticles located outside the macrophages. Based on the results from the flow cytometry analysis, there will be a lower percentage of nanoparticles within tumor cells compared to macrophages. This indicates that a large amount of the nanoparticles are trapped in the extracellular matrix. This is consistent with *Q. Dai et al.*[60] which concluded that most of the intratumolar nanoparticles were either trapped in the ECM or taken up by macrophages.

5.3 Distance analysis of macrophages and nanoparticles in OHS and PC3 tumor tissue

The distribution of macrophages and nanoparticles, in addition to the uptake of nanoparticles by macrophages at different distances around blood vessels, were studied for OHS and PC3 tumor tissue. The results are discussed in the following sections.

5.3.1 Distribution of macrophages around blood vessels

For both OHS and PC3 tumor tissue, there was a higher mean percentage of macrophages close to the blood vessel walls compared to distances further away. There were no significant differences between the two group that indicate any effect of the ultrasound treatment. A higher concentration of macrophages close to the blood vessels is as expected since the macrophages arise from monocytes in the blood stream[8, 12]. *Q. Dai et al.*[60] have studied how macrophages were distributed around blood vessels inside SKOV-3 xenografts. They also found the highest density of macrophages close to the blood vessels, which is consistent with the results in this thesis and the theory.

For OHS tumor tissue, the mean percentage of macrophages decreased faster with increased distance away from the blood vessels than for PC3 tumor tissue. This indicated that a larger amount of the macrophages was located close to the blood vessels in OHS

tumor tissue. For PC3 tumor tissue, the macrophages penetrated further into the tumor tissue. The limited penetration of macrophages in OHS tumor tissue compared to PC3 tumor tissue may be explained by the tumor microenvironment. *E. Sulheim et al.*[9] characterized the microenvironment in both of these tumor models. They found a higher cell density and a higher density of blood vessels inside OHS tumor tissue than in PC3 tumor tissue. Both of these factors may limit the penetration. When there is a dense network of blood vessels, the available distance a macrophage can penetrate from a blood vessel is limited by half of the distance to the nearest blood vessel. From this, a high density of blood vessels limits the penetration length for the macrophages. The observed distribution of macrophages around blood vessels is the same as the result in the specialization project by the author[10].

A larger amount of macrophages extravasated from the blood vessel was observed in PC3 tumor tissue compared to OHS tumor tissue. This difference was significant, but the result was not as predicted. Due to the high density of blood vessels in OHS tumor tissue [9], it would be expected to observe a larger amount of macrophages extravasated in this tumor model compared to in PC3 tumor tissue. From the image analysis, a larger mean area percentage of macrophages were seen in OHS tumor tissue compared to PC3 tumor tissue. This does not correspond to the fact that fewer macrophages extravasate in OHS tissues than PC3 tissues. The reason why these results are contradictory is that the macrophages located inside the vasculature are included in calculation of the mean area percentage of macrophages. However, the percentage of macrophages was higher inside OHS tumors compared to PC3 tumors from the flow cytometry analysis.

For both OHS tumor tissue and PC3 tumor tissue, a slightly increased mean percentage of macrophages were extravasated in the group treated with ultrasound compared to the control group. This difference was not significant. Based on previously discussion in section 5.2.1, it was concluded that the percentage of macrophages within the tissue were not affected by the ultrasound treatment. Hence, no more macrophages should be extravasated in the group treated with ultrasound.

5.3.2 Distribution of nanoparticles around blood vessels

The percentage of nanoparticles was highest close to the blood vessel walls compared to distances further away from the blood vessels, for both OHS and PC3 tumor tissue. This is as expected since the nanoparticles extravasate from the blood stream into the tumor tissue.

For OHS tumor tissue, the mean percentage of nanoparticles was higher when close to the blood vessels compared to that in PC3 tumor tissue. In addition to this, the mean percentage of nanoparticles decreased faster with increased distance for OHS tumor tissue compared to PC3 tumor tissue. This means that the nanoparticles within PC3 tumor tissue penetrated longer distances than the nanoparticles within OHS tumor tissue. As for the macrophages, the penetration length is limited by half the distance to the nearest blood vessel. Due to the high density of blood vessels in OHS tumor tissue [9], it is reasonable that nanoparticles within these tumors are located closer to the blood vessels than in PC3 tumors. The penetration of nanoparticles in OHS tumors may also be limited by the high cellular density within the tissue [9]. As discussed in section 5.2.6, a high amount of the nanoparticles were trapped in the extracellular matrix. *Q. Dai et al.*[60] stated the ECM

was a barrier for penetration of nanoparticles through tumor tissue. *P. Netti et al.*[30] presented a study where they found that a high collagen content inside the extra cellular matrix was related to high penetration resistance for therapeutic agents. *E. Sulheim et al.*[9] also study the collagen content in several tumor models. They found no correlation between the uptake of nanoparticles and collagen density in any of the models. Based on these studies, the extra cellular matrix limits the penetration of nanoparticles through the tumor tissue. However, it is not certain that collagen is the main barrier for penetration inside the extracellular matrix.

A higher percentage of nanoparticles was located close to the blood vessels for the control groups compared to the groups treated with ultrasound. This indicated that a larger amount of the nanoparticles penetrated longer distances into the tumor tissue for the group treated with ultrasound compared to the control group. The results were not significant, but was seen in both OHS and PC3 tumor tissue. One of the main goals by the use of focused ultrasound of the tumor is to improve the penetration of nanoparticles through the extra cellular matrix, resulting in improved accumulation and distribution of nanoparticles within the tumor tissue.

No significant difference was seen in the mean percentage of extravasated nanoparticles between OHS tumor tissue and PC3 tumor tissue. However, a tendency indicate that a larger percentage of nanoparticles extravasated in OHS tumors. This result is as expected. The high density of blood vessels in OHS tumor tissue [9] have potential to carry more nanoparticles than the blood vessels in PC3 tumor tissue. Due to this, a higher amount of extravasated nanoparticles is expected in OHS tumors. From the image analysis, there were no difference in the mean area percentage of nanoparticles between the two tumor models. It should be mentioned that these results were unexpected and do not distinguish between nanoparticles inside and outside the blood vessels.

The ultrasound treatment showed an increased extravasation of nanoparticles in both OHS and PC3 tumor tissue. The differences between the control group and the treated group were not significant. These results are expected and consistent with the calculated mean area percentage of nanoparticles from the images. The mean area percentage of nanoparticles in the images were significantly increased by the use of focused ultrasound. When a larger amount of nanoparticles extarvasate from the blood vessels, it is reasonable that a larger area percentage of the images is defined as nanoparticles. These results are consistent with the studies presented by *S. Snipstad et al.*[6] and *S. Eggen et al.*[75]. As mentioned previously, both these studies found an increased accumulation of nanoparticles within the tumor tissue, by the use of nanoparticle-stabilized microbubbles in combination with focused ultrasound on the tumor.

5.3.3 Uptake of nanoparticles by macrophages around blood vessels

For OHS tumor tissue, there was a significant decrease in the mean percentage of nanoparticles inside macrophages between distance 5-15 μm and distances >85 μm. A higher mean percentage of nanoparticles was taken up by macrophages close to the blood vessel walls compared to distances further away from the blood vessels. Significant differences in the mean percentage of nanoparticles inside macrophages between distance 5-15 μm and distances >85 μm were not found in PC3 tumor tissue. There was a slightly decrease in the mean percentage of nanoparticles taken up by macrophages close to the blood vessels com-

pared to increased distances, but the decrease was not significant. The mean percentage of nanoparticles inside macrophages varied up and down between the different distance intervals. For both OHS and PC3 tumor tissue, a large mean percentage of macrophages and nanoparticles was observed close to the blood vessel walls. The mean percentage of both macrophages and nanoparticles decreased by increased distance from the blood vessels. This decrease was more rapid in OHS tumor tissue compared to PC3 tumor tissue, especially for the nanoparticles. This may be a reason why a significant decrease in the mean percentage of nanoparticles inside macrophages, between distance 5-15 µm and distances >85 µm, was observed for OHS tumor tissue and not for PC3 tumor tissue.

Q. Dai et al.[60] studied macrophages around blood vessels to see how they limit the penetration of nanoparticles through the tumor tissue. They observed that a high percentage of macrophages close to the blood vessels leads to a large uptake of nanoparticles in this area. In this thesis, there was a high percentage of both macrophages and nanoparticles located close to the blood vessels. In addition to this, a high percentage of the nanoparticles was located inside macrophages at these distances. Based on this, a large amount of the intratumoral nanoparticles were taken up by macrophages close to the blood vessels.

For both OHS and PC3 tumor tissue, the results indicate that not all nanoparticles are taken up by macrophages. Some of them escape the macrophages and penetrates through the extracellular matrix. The results are based on nanoparticles located inside macrophages at different distances. The nanoparticles may have been taken up by macrophages at a certain distance. Another option is that they are taken up at an earlier distance and carried through the ECM inside a penetrating macrophage.

5.4 Further research

The results from this thesis are of great interest and need to be investigated further. A larger quantity of tumors should be used to achieve more representative results for the different tumor models. Uptake of nanoparticles by macrophages of other DDSs would also be interesting to study.

Additionally, studying whether or not there are any differences in uptake of nanoparticles by M1 and M2 macrophages in different DDSs may be useful. This was attempted in this thesis, but the small amount of tumors and cells defined as M1 macrophages made the results highly uncertain. Results from the study presented by *M. Fusset et al.*[65] indicated that there may be a difference in the uptake of nanoparticles between the two different types of macrophages inside tumor tissue.

Further optimization of the method used in this thesis is necessary before supplementary analysis can be done. The near-IR dye that was used to separate the dead cells from the viable ones, functioned poorly. Due to this, a greater concentration of this dye, or simply the use of a better performing fluorescent dye, is necessary. Large variations in fluorescence signals were observed from the concentration study to the main experiments. Therefore, a new concentration study is recommended in order to find better performing concentrations for the primary antibodies.

Chapter 6

Conclusion

From flow cytometry analysis, large populations of macrophages were found within both OHS tumor tissue and PC3 tumor tissue. The amount of M2 macrophages was completely dominating compared to the amount of M1 macrophages in both tumor models.

Focused ultrasound used in combination with nanoparticle-stabilized microbubbles does not affect the percentage of macrophages within neither OHS tumor tissue nor PC3 tumor tissue. On the other hand, the ultrasound treatment results in a significantly increased accumulation of nanoparticles within both OHS tumor tissue and PC3 tumor tissue. From this, an increased percentage of tumor cells containing nanoparticles were also observed by the use of ultrasound, but the increase was only significant for tumor cells in OHS tumor tissue.

A significantly higher percentage of the macrophages within OHS tumor tissue contained nanoparticles compared to in PC3 tumor tissue. Ultrasound treatment increased the percentage of macrophages containing nanoparticles for PC3 tumor tissue, but the increase was not significant.

For both OHS tumor tissue and PC3 tumor tissue, the majority of the nanoparticles were engulfed by macrophages. The macrophages function as barriers for the nanoparticles, and thus limit the delivery of nanoparticles to tumor cells. The majority of the nanoparticles were taken up by macrophages even though the tumors were treated with focused ultrasound. A large amount of the nanoparticles were also trapped in the extracellular matrix.

Distance analysis of tumor sections showed that the percentage of macrophages and nanoparticles were at its highest close to the blood vessel walls, and decreased with increasing distance from the blood vessels. In OHS tumor tissue, the decrease was more rapid than in PC3 tumor tissue. A greater amount of the intratumoral nanoparticles were taken up by macrophages close to the blood vessels in OHS tumor tissue compared to that of PC3 tumor tissue.

Bibliography

[1] *Global Cancer Obervatory*. `https://gco.iarc.fr/`. (Visited on 12/02/2019).

[2] Karen A Kurdziel et al. "Human dosimetry and preliminary tumor distribution of 18F-fluoropaclitaxel in healthy volunteers and newly diagnosed breast cancer patients using PET/CT". In: *Journal of nuclear medicine: official publication, Society of Nuclear Medicine* 52.9 (2011), p. 1339.

[3] Hans-Peter Gerber, Peter D Senter, and Iqbal S Grewal. "Antibody drug-conjugates targeting the tumor vasculature: current and future developments". In: *MAbs*. Vol. 1. 3. Taylor & Francis. 2009, pp. 247–253.

[4] Margaret A. Knowles and Peter J. Selby. *Introduction to the Cellular and Molecular Biology of Cancer*. 4th Edition. New York, USA: Oxford University Press; 2005.

[5] Ýrr Mørch et al. "Nanoparticle-stabilized microbubbles for multimodal imaging and drug delivery". In: *Contrast media & molecular imaging* 10.5 (2015), pp. 356–366.

[6] Sofie Snipstad et al. "Ultrasound improves the delivery and therapeutic effect of nanoparticle-stabilized microbubbles in breast cancer xenografts". In: *Ultrasound in medicine & biology* 43.11 (2017), pp. 2651–2669.

[7] Peter J Murray and Thomas A Wynn. "Protective and pathogenic functions of macrophage subsets". In: *Nature reviews immunology* 11.11 (2011), p. 723.

[8] W Hu et al. "Tumor-associated macrophages in cancers". In: *Clinical and Translational Oncology* 18.3 (2016), pp. 251–258.

[9] Einar Sulheim et al. "Multi-modal characterization of vasculature and nanoparticle accumulation in five tumor xenograft models". In: *Journal of Controlled Release* 279 (2018), pp. 292–305.

[10] Marianne Elise Lia. *Characterization of macrophages in tumor tissue*. Specialization project, autumn 2018, NTNU.

[11] Hiroshi Maeda et al. "Tumor vascular permeability and the EPR effect in macromolecular therapeutics: a review". In: *Journal of controlled release* 65.1-2 (2000), pp. 271–284.

[12] P Allavena and A Mantovani. "Immunology in the clinic review series; focus on cancer: tumour-associated macrophages: undisputed stars of the inflammatory tumour microenvironment". In: *Clinical & Experimental Immunology* 167.2 (2012), pp. 195–205.

[13] Debra H Josephs, Heather J Bax, and Sophia N Karagiannis. “Tumour-associated macrophage polarisation and re-education with immunotherapy”. In: *Front Biosci (Elite Ed)* 7 (2015), pp. 293–308.

[14] Meri R Räihä and Pauli A Puolakkainen. “Tumor-associated macrophages (TAMs) as biomarkers for gastric cancer: A review”. In: *Chronic diseases and translational medicine* 4.3 (2018), pp. 156–163.

[15] Karin Binnemars-Postma, Gert Storm, and Jai Prakash. “Nanomedicine strategies to target tumor-associated macrophages”. In: *International journal of molecular sciences* 18.5 (2017), p. 979.

[16] Nadine Jetten et al. “Anti-inflammatory M2, but not pro-inflammatory M1 macrophages promote angiogenesis in vivo”. In: *Angiogenesis* 17.1 (2014), pp. 109–118.

[17] Kyong Yeun Jung et al. “Cancers with higher density of tumor-associated macrophages were associated with poor survival rates”. In: *Journal of pathology and translational medicine* 49.4 (2015), p. 318.

[18] Moniek Heusinkveld and Sjoerd H van der Burg. “Identification and manipulation of tumor associated macrophages in human cancers”. In: *Journal of translational medicine* 9.1 (2011), p. 216.

[19] Tianmeng Sun et al. “Engineered nanoparticles for drug delivery in cancer therapy”. In: *Angewandte Chemie International Edition* 53.46 (2014), pp. 12320–12364.

[20] David F Williams. “On the mechanisms of biocompatibility”. In: *Biomaterials* 29.20 (2008), pp. 2941–2953.

[21] Twan Lammers et al. “Drug targeting to tumors: principles, pitfalls and (pre-) clinical progress”. In: *Journal of controlled release* 161.2 (2012), pp. 175–187.

[22] Rakesh K Jain and Triantafyllos Stylianopoulos. “Delivering nanomedicine to solid tumors”. In: *Nature reviews Clinical oncology* 7.11 (2010), p. 653.

[23] Donald E Owens III and Nicholas A Peppas. “Opsonization, biodistribution, and pharmacokinetics of polymeric nanoparticles”. In: *International journal of pharmaceutics* 307.1 (2006), pp. 93–102.

[24] Susumu Nagayama et al. “Time-dependent changes in opsonin amount associated on nanoparticles alter their hepatic uptake characteristics”. In: *International journal of pharmaceutics* 342.1-2 (2007), pp. 215–221.

[25] Hidenori Otsuka, Yukio Nagasaki, and Kazunori Kataoka. “PEGylated nanoparticles for biological and pharmaceutical applications”. In: *Advanced drug delivery reviews* 64 (2012), pp. 246–255.

[26] B Hobson and J Denekamp. “Endothelial proliferation in tumours and normal tissues: continuous labelling studies”. In: *British journal of cancer* 49.4 (1984), p. 405.

[27] Y Boucher et al. “Interstitial fluid pressure in intracranial tumours in patients and in rodents”. In: *British journal of cancer* 75.6 (1997), p. 829.

[28] Christian Frantz, Kathleen M Stewart, and Valerie M Weaver. “The extracellular matrix at a glance”. In: *J Cell Sci* 123.24 (2010), pp. 4195–4200.

[29] Paul C Hiemenz and Raj Rajagopalan. *Principles of Colloid and Surface Chemistry, revised and expanded*. 3th Edition. CRC press; 1997.

[30] Paolo A Netti et al. “Role of extracellular matrix assembly in interstitial transport in solid tumors”. In: *Cancer research* 60.9 (2000), pp. 2497–2503.

[31] Laurence H Hurley. “DNA and its associated processes as targets for cancer therapy”. In: *Nature Reviews Cancer* 2.3 (2002), p. 188.

[32] Gaurav Sahay, Daria Y Alakhova, and Alexander V Kabanov. “Endocytosis of nanomedicines”. In: *Journal of controlled release* 145.3 (2010), pp. 182–195.

[33] Lewis J. Kleinsmith Jeff Hardin Gregory Bertoni. *Becker’s World of the Cell, Technology Update*. 8th Edition. 2016.

[34] John H Chidlow Jr and William C Sessa. “Caveolae, caveolins, and cavins: complex control of cellular signalling and inflammation”. In: *Cardiovascular research* 86.2 (2010), pp. 219–225.

[35] Lucas Pelkmans and Ari Helenius. “Endocytosis via caveolae”. In: *Traffic* 3.5 (2002), pp. 311–320.

[36] David J. Martin, Irving T.P. Wells, and Christopher R. Goodwin. “Physics of ultrasound”. In: *Anaesthesia and Intensive Care Medicine* 16.3 (2015), pp. 132–135.

[37] PJ White, GT Clement, and K Hynynen. “Longitudinal and shear mode ultrasound propagation in human skull bone”. In: *Ultrasound in medicine & biology* 32.7 (2006), pp. 1085–1096.

[38] Ghaleb A Husseini, William G Pitt, and Ana M Martins. “Ultrasonically triggered drug delivery: breaking the barrier”. In: *Colloids and Surfaces B: Biointerfaces* 123 (2014), pp. 364–386.

[39] William D O’ Brien Jr. “Ultrasound-biophysics mechanisms”. In: *Progress in biophysics and molecular biology* 93.1-3 (2007), pp. 212–255.

[40] Richard B Ashman and Jae Young Rho. “Elastic modulus of trabecular bone material”. In: *Journal of biomechanics* 21.3 (1988), pp. 177–181.

[41] Peter R Hoskins, Kevin Martin, and Abigail Thrush. *Diagnostic ultrasound: physics and equipment*. Cambridge University Press, 2010.

[42] Victor Frenkel. “Ultrasound mediated delivery of drugs and genes to solid tumors”. In: *Advanced drug delivery reviews* 60.10 (2008), pp. 1193–1208.

[43] Sofie Snipstad et al. “Sonopermeation to improve drug delivery to tumors: from fundamental understanding to clinical translation”. In: *Expert opinion on drug delivery* just-accepted (2018).

[44] William G Pitt, Ghaleb A Husseini, and Bryant J Staples. “Ultrasonic drug delivery–a general review”. In: *Expert opinion on drug delivery* 1.1 (2004), pp. 37–56.

[45] Ulrich Kubitscheck. *Fluorescence microscopy: From Principles to Biological Applications*. 2th Edition. Weinheim, Germany: Wiley-VCH; 2017.

[46] G. Ya. Wiederschain. *The Molecular Probes handbook. A guide to Fluorescent Probes and Labeling Technologies*. Editors: I. Johnson and M. Spence. 11th Edition. Moscow. Thermo Fisher Scientific; 2010.

[47] Igor B. Buchwalow and Werner Bocker. *Immunohistochemistry: Basics and Methods*. Berlin, Heidelberg: Springer; 2010.

[48] Michael Brown and Carl Wittwer. "Flow cytometry: principles and clinical applications in hematology". In: *Clinical chemistry* 46.8 (2000), pp. 1221–1229.

[49] Richard R Jahan-Tigh et al. "Flow cytometry". In: *The Journal of investigative dermatology* 132.10 (2012), e1.

[50] Dongeun Huh et al. "Microfluidics for flow cytometric analysis of cells and particles". In: *Physiological measurement* 26.3 (2005), R73.

[51] Douglas B. Murphy and Michael W. Davidson. *Fundamentals of Light Microscopy and Electronic Imaging,* Hoboken, NJ, USA: John Wiley and Sons, Inc; 2012.

[52] Paras N Prasad. *Introduction to biophotonics*. Hoboken, N.J: Wiley-Interscience; 2003.

[53] Martin J Booth. "Adaptive optics in microscopy". In: *Philosophical Transactions of the Royal Society A: Mathematical, Physical and Engineering Sciences* 365.1861 (2007), pp. 2829–2843.

[54] Unni Cecilie Nygaard. *Binding av antistoffer til enkeltceller i tumor målt med flocytometri*. Prosjektarbeid, juni 1996, NTNU.

[55] *Bio-Rad*. `https://www.bio-rad-antibodies.com/monoclonal/mouse-f4-80-antibody-cl-a3-1-mca497.html?f=purified`. (Visited on 09/02/2019).

[56] *Thermo Fisher Scientific*. `https://www.thermofisher.com/antibody/product/CD206-Antibody-Polyclonal/PA5-46994`. (Visited on 09/02/2019).

[57] *Dianova*. `https://www.dianova.com/en/antibodies/secondary-antibodies/`. (Visited on 09/02/2019).

[58] *Thermo Fisher Scientific Live/Dead staining kit*. `https://www.thermofisher.com/no/en/home/references/protocols/cell-and-tissue-analysis/protocols/live-dead-fixable-dead-cell-stains.html`. (Visited on 09/02/2019).

[59] *Kaluza Analysis Software*. `https://www.beckman.com/flow-cytometry/software/kaluza`. (Visited on 01/04/2019).

[60] Qin Dai et al. "Quantifying the ligand-coated nanoparticle delivery to cancer cells in solid tumors". In: *ACS nano* 12.8 (2018), pp. 8423–8435.

[61] Johannes Schindelin et al. "Fiji: an open-source platform for biological-image analysis". In: *Nature methods* 9.7 (2012), p. 676.

[62] BD BioSciences. "Human and mouse CD marker handbook". In: *Becton, Dickinson and Company., San Jose, CA* 95131 (2010).

[63] S Gordon et al. "Antigen markers of macrophage differentiation in murine tissues". In: *Macrophage biology and activation*. Springer, 1992, pp. 1–37.

[64] Ruth A Franklin et al. "The cellular and molecular origin of tumor-associated macrophages". In: *Science* 344.6186 (2014), pp. 921–925.

[65] Markus Fusser et al. “Cabazitaxel-loaded Poly (2-ethylbutyl cyanoacrylate) nanoparticles improve treatment efficacy in a patient derived breast cancer xenograft”. In: *Journal of Controlled Release* (2018).

[66] Alison Burgess et al. “Targeted delivery of neural stem cells to the brain using MRI-guided focused ultrasound to disrupt the blood-brain barrier”. In: *PloS one* 6.11 (2011), e27877.

[67] Ryan Alkins et al. “Focused ultrasound delivers targeted immune cells to metastatic brain tumors”. In: *Cancer research* 73.6 (2013), pp. 1892–1899.

[68] Hao-Li Liu et al. “In vivo assessment of macrophage CNS infiltration during disruption of the blood–brain barrier with focused ultrasound: a magnetic resonance imaging study”. In: *Journal of Cerebral Blood Flow & Metabolism* 30.1 (2010), pp. 177–186.

[69] Qiang Xiao et al. “Inhibition of macrophage polarization prohibits growth of human osteosarcoma”. In: *Tumor Biology* 35.8 (2014), pp. 7611–7616.

[70] Marie Lundholm et al. “Secreted factors from colorectal and prostate cancer cells skew the immune response in opposite directions”. In: *Scientific reports* 5 (2015), p. 15651.

[71] M Lanciotti et al. “The role of M1 and M2 macrophages in prostate cancer in relation to extracapsular tumor extension and biochemical recurrence after radical prostatectomy”. In: *BioMed research international* 2014 (2014).

[72] Ann Erlandsson et al. “M2 macrophages and regulatory T cells in lethal prostate cancer”. In: *The Prostate* (2018).

[73] Qian Zhou et al. “All-trans retinoic acid prevents osteosarcoma metastasis by inhibiting M2 polarization of tumor-associated macrophages”. In: *Cancer immunology research* 5.7 (2017), pp. 547–559.

[74] Saeid Zanganeh et al. “Iron oxide nanoparticles inhibit tumour growth by inducing pro-inflammatory macrophage polarization in tumour tissues”. In: *Nature nanotechnology* 11.11 (2016), p. 986.

[75] Siv Eggen et al. “Ultrasound-enhanced drug delivery in prostate cancer xenografts by nanoparticles stabilizing microbubbles”. In: *Journal of controlled release* 187 (2014), pp. 39–49.

[76] Hyounkoo Han et al. “Effect of high intensity focused ultrasound (HIFU) in conjunction with a nanomedicines-microbubble complex for enhanced drug delivery”. In: *Journal of Controlled Release* 266 (2017), pp. 75–86.

[77] Caitlin W Burke et al. “Ultrasound-activated agents comprised of 5FU-bearing nanoparticles bonded to microbubbles inhibit solid tumor growth and improve survival”. In: *Molecular Therapy* 22.2 (2014), pp. 321–328.

[78] Benjamin Theek et al. “Sonoporation enhances liposome accumulation and penetration in tumors with low EPR”. In: *Journal of controlled release* 231 (2016), pp. 77–85.

[79] Lingxi Xing et al. “Ultrasound-mediated microbubble destruction (UMMD) facilitates the delivery of CA19-9 targeted and paclitaxel loaded mPEG-PLGA-PLL nanoparticles in pancreatic cancer”. In: *Theranostics* 6.10 (2016), p. 1573.

[80] Chung-Yin Lin et al. “Quantitative and qualitative investigation into the impact of focused ultrasound with microbubbles on the triggered release of nanoparticles from vasculature in mouse tumors”. In: *Journal of Controlled Release* 146.3 (2010), pp. 291–298.

[81] NY Rapoport et al. “Ultrasound-triggered drug targeting of tumors in vitro and in vivo”. In: *Ultrasonics* 42.1-9 (2004), pp. 943–950.

[82] Natalya Rapoport et al. “Intracellular uptake and trafficking of Pluronic micelles in drug-sensitive and MDR cells: Effect on the intracellular drug localization”. In: *Journal of pharmaceutical sciences* 91.1 (2002), pp. 157–170.

[83] Joerg Hauser et al. “Ultrasound enhanced endocytotic activity of human fibroblasts”. In: *Ultrasound in medicine & biology* 35.12 (2009), pp. 2084–2092.

[84] Jessica Hoppstädter et al. “M2 polarization enhances silica nanoparticle uptake by macrophages”. In: *Frontiers in pharmacology* 6 (2015), p. 55.

[85] Maryelise Cieslewicz et al. “Targeted delivery of proapoptotic peptides to tumor-associated macrophages improves survival”. In: *Proceedings of the National Academy of Sciences* 110.40 (2013), pp. 15919–15924.

[86] Markus Fusser et al. “Cabazitaxel-loaded Poly (2-ethylbutyl cyanoacrylate) nanoparticles improve treatment efficacy in a patient derived breast cancer xenograft”. In: *Journal of Controlled Release* 293 (2019), pp. 183–192.

Appendix A - Non-specific binding of secondary antibodies

OHS and PC3 samples were stained with only secondary antibodies and live/dead dyes to determine if there was any non-specific binding of these antibodies. Both DyLight405 and AlexaFluor488 were used in a concentration of $0.5\,\mu g/10^6$ cells. These samples were compared to samples only stained with live/dead dyes. Overlay histograms with fluorescence intensity versus the number of cells, for samples stained with secondary antibodies and samples only stained with live/dead dyes, are shown in Figure 6.1 and Figure 6.2.

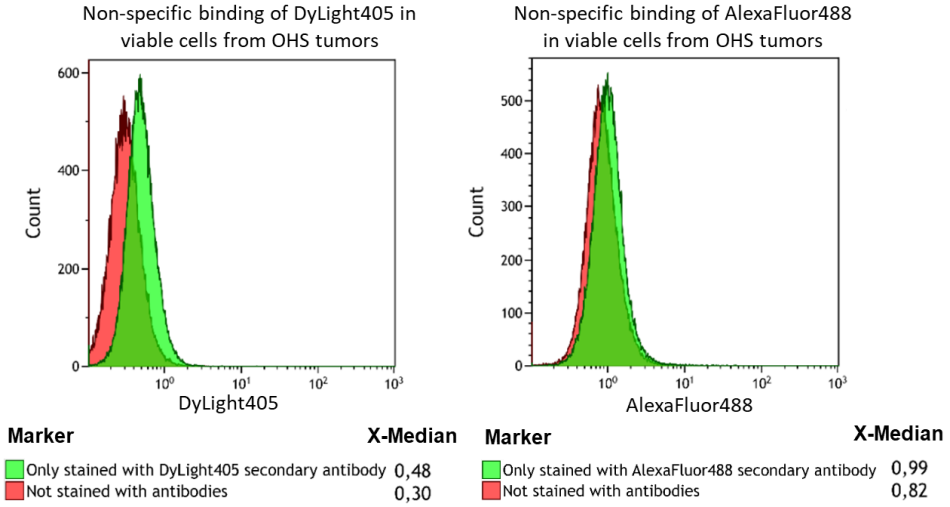

Figure 6.1: Two overlay plot showing histograms from staining of OHS single cell suspension with only secondary antibodies. The overlay plot to the left shows the fluorescence intensity of DyLight405 versus the number of cells. DyLight405 was used in a concentration of $0.5\,\mu g/10^6$ cells. The overlay plot to the right shows the fluorescence intensity of AlexaFluor488 versus the number of cells. AlexaFluor488 was used in a concentration of $0.5\,\mu g/10^6$ cells. Samples that were not stained with antibodies are also included. The x-medians for the fluorescence intensity signals from the different samples are presented for both of the overlay plots.

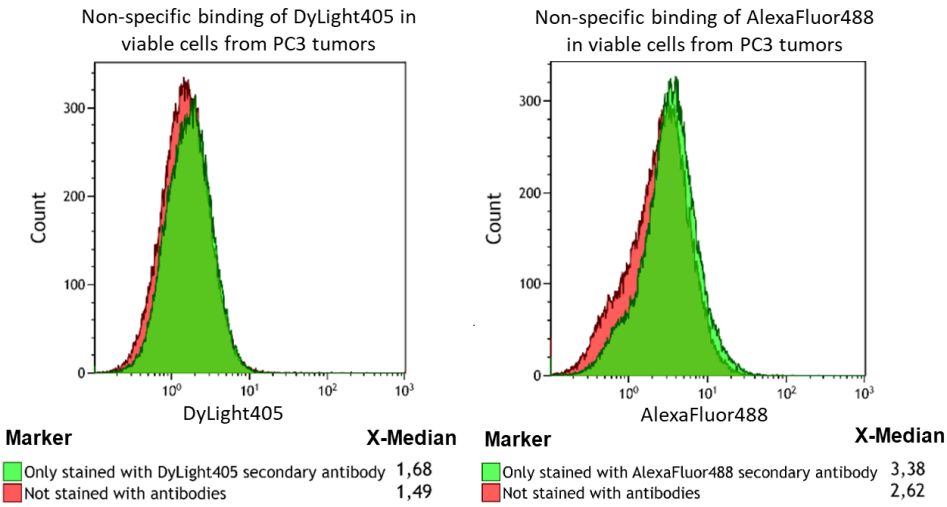

Figure 6.2: Two overlay plot showing histograms from staining of PC3 single cell suspension with only secondary antibodies. The overlay plot to the left shows the fluorescence intensity of DyLight405 versus the number of cells. DyLight405 was used in a concentration of $0.5\,\mu g/10^6$ cells. The overlay plot to the right shows the fluorescence intensity of AlexaFluor488 versus the number of cells. AlexaFluor488 was used in a concentration of $0.5\,\mu g/10^6$ cells. Samples that were not stained with antibodies are also included. The x-medians for the fluorescence intensity signals from the different samples are presented for both of the overlay plots.

There was a small difference in x-medians between the samples stained with antibodies and the samples only stained with live/dead dyes. This show tendencies to slightly non-specific binding of secondary antibodies for both OHS and PC3 cells.

Appendix B - Compensation flow cytometer

A protocol in the flow cytometer software was made to compensate for non-specific binding of antibodies and for spillover of fluorescence between the different detectors. This compensation file is shown in Figure 6.3. The detectors listed horizontally in the table leaked fluorescence into the detectors listed vertically. The compensation for this spillover of fluorescence is shown as numbers in the table.

Spillover (%)

	FL1	FL2	FL3	FL4	FL5	FL8	FL9	FL10
FL1		0,00	15,00	0,00	0,00	0,00	2,40	0,00
FL2	0,00		0,00	0,00	0,00	0,00	0,00	0,00
FL3	2,40	0,00		0,00	0,00	0,00	3,00	0,00
FL4	0,00	0,00	0,00		0,00	0,00	0,00	0,00
FL5	0,00	0,00	0,00	0,00		0,00	0,00	0,00
FL8	7,00	0,00	12,00	0,00	0,00		0,00	0,00
FL9	0,00	0,00	0,00	0,00	0,00	0,00		0,00
FL10	0,00	0,00	0,00	0,00	0,00	0,00	0,00	

FL1 = AlexaFluor488 (M2 macrophages)
FL3 = Nile Red (nanoparticles)
FL8 = Live/dead
FL9 = DyLight405 (M1 + M2 macrophages)

Figure 6.3: Compensation file used to compensate for non-specific binding of antibodies and for spillover of fluorescence between the different detectors. This compensation was used for the samples in trial 3 and 4.

Appendix C - Macros/scripts used for image analysis

To make the image analysis efficient different macros/scripts were written. These programs were applied to all images and the results were one text file for each image. Figure 6.4 show the script used to analyse the amount of macrophages at different distances around blood vessels. Figure 6.5 show the script used to analyse the amount of nanoparticles inside macrophages at different distances around blood vessels. Figure 6.6 show the script used to analyse the amount of nanoparticles outside macrophages at different distances around the blood vessels.

Macrophages at different distances around blood vessels

```
image = "image of macrophages"

run("Set Scale...", "distance=1024 known=319.5 pixel=1 unit=um global");
run("Split Channels");

selectWindow(image + " (red)");
setAutoThreshold("Triangle dark");
setOption("BlackBackground", true);
run("Convert to Mask");

run("Despeckle");

run("Analyze Particles...", "size=40-Infinity display clear summarize add");

selectWindow(image + " (green)");
setAutoThreshold("Otsu dark");
setOption("BlackBackground", true);
run("Convert to Mask");
run("Despeckle");
run("Invert");
run("Options...", "iterations=1 count=1 black edm=32-bit do=Nothing");
run("Distance Map");

roiManager("Select", 0);
roiManager("Select", newArray());
roiManager("Show None");
roiManager("Show All");
roiManager("Combine");
setBackgroundColor(0, 0, 0);
run("Clear Outside");


run("Histogram", "bins=32 x_min=0 x_max=512 y_max=Auto");
```

Figure 6.4: The script used to analyse the amount of macrophages at different distances around the nearest blood vessel. All steps in FIJI are included.

Nanoparticles inside macrophages at different distances around blood vessels

```
image1 = "image of nanoparticles"
image2 = "image of macrophages"

selectWindow(image1);
selectWindow(image2);

run("Set Scale...", "distance=1024 known=319.5 pixel=1 unit=um global");

selectWindow(image2);
run("Split Channels");
selectWindow(image2 + " (red)");
setAutoThreshold("Triangle dark");
setOption("BlackBackground", true);
run("Convert to Mask");
run("Analyze Particles...", "size=40-Infinity display clear summarize add");

selectWindow(image1);
run("Split Channels");
selectWindow(image1 + " (red)");
setAutoThreshold("Moments dark");
setOption("BlackBackground", true);
run("Convert to Mask");

roiManager("Select", 0);
roiManager("Select", newArray());
roiManager("Show None");
roiManager("Show All");
roiManager("Combine");
setBackgroundColor(0, 0, 0);
run("Clear Outside");

selectWindow(image1 + " (red)");
roiManager("Show All");
roiManager("Show None");
roiManager("Deselect");
run("Analyze Particles...", "size=0-Infinity display clear summarize add");

selectWindow(image2 + " (green)");
setAutoThreshold("Otsu dark");
setOption("BlackBackground", true);
run("Convert to Mask");
run("Invert");
run("Options...", "iterations=1 count=1 black edm=32-bit do=Nothing");
run("Distance Map");

roiManager("Select", 0);
roiManager("Select", newArray());
roiManager("Show None");
roiManager("Show All");
roiManager("Combine");
setBackgroundColor(0, 0, 0);
run("Clear Outside");


run("Histogram", "bins=32 x_min=0 x_max=512 y_max=Auto");
```

Figure 6.5: The script used to analyse the amount of nanoparticles inside macrophages at different distances around the nearest blood vessel. All steps in FIJI are included.

Nanoparticles outside macrophages at different distances around blood vessels

```
image1 = "image of nanoparticles"
image2 = "image of macrophages"

selectWindow(image1);
selectWindow(image2);

run("Set Scale...", "distance=1024 known=319.5 pixel=1 unit=um global");

selectWindow(image2);
run("Split Channels");
selectWindow(image2 + " (red)");
setAutoThreshold("Triangle dark");
setOption("BlackBackground", true);
run("Convert to Mask");
run("Analyze Particles...", "size=40-Infinity display clear summarize add");

selectWindow(image1);
run("Split Channels");
selectWindow(image1 + " (red)");
setAutoThreshold("Moments dark");
setOption("BlackBackground", true);
run("Convert to Mask");

roiManager("Select", 0);
roiManager("Select", newArray());
roiManager("Show None");
roiManager("Show All");
roiManager("Combine");
setBackgroundColor(0, 0, 0);
run("Clear");

selectWindow(image1 + " (red)");
roiManager("Show All");
roiManager("Show None");
roiManager("Deselect");
run("Analyze Particles...", "size=0-Infinity display clear summarize add");

selectWindow(image2 + " (green)");
setAutoThreshold("Otsu dark");
setOption("BlackBackground", true);
run("Convert to Mask");
run("Invert");
run("Options...", "iterations=1 count=1 black edm=32-bit do=Nothing");
run("Distance Map");

roiManager("Select", 0);
roiManager("Select", newArray());
roiManager("Show None");
roiManager("Show All");
roiManager("Combine");
setBackgroundColor(0, 0, 0);
run("Clear Outside");


run("Histogram", "bins=32 x_min=0 x_max=512 y_max=Auto");
```

Figure 6.6: The script used to analyse the amount of nanoparticles outside macrophages at different distances around the nearest blood vessel. All steps in FIJI are included.

Appendix D - Uptake of nanoparticles by M1 and M2 macrophages

The uptake of nanoparticles by M1 and M2 macrophages is presented in Figure 6.7. One significant difference was found in the uptake of nanoparticles between M1 and M2 macrophages for the OHS control group. For this group, 33.1±10.0% of the M1 macrophages contained nanoparticles and 66.5±9.8% of the M2 macrophages contained nanoparticles. This corresponded to a difference of 33.4 percentage point, which was significant with a p-value of 0.03. Since the mean percentage of M1 macrophages in all experimental groups was below 1%, the results based on these data will have several uncertain factors.

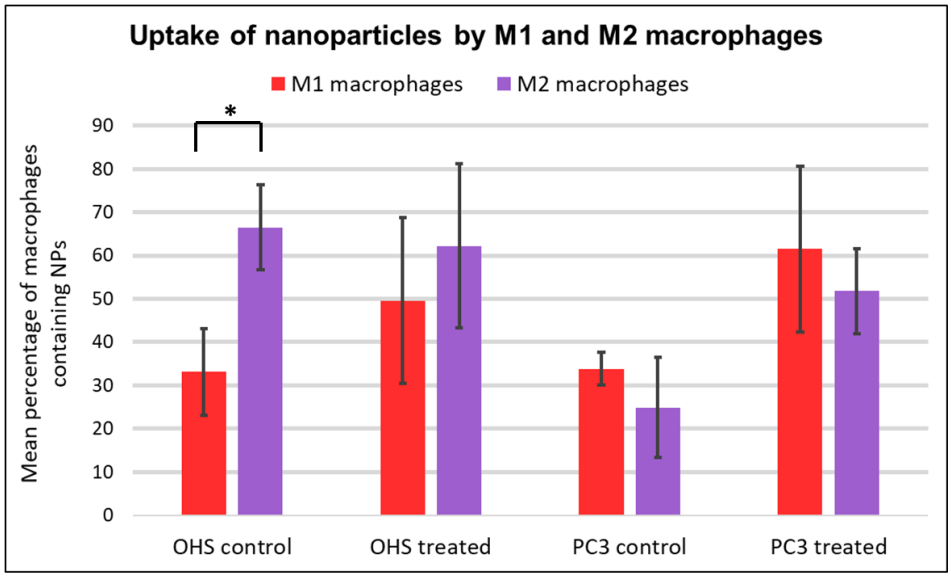

Figure 6.7: Bar plot showing the mean percentage of M1 and M2 macrophages that contain nanoparticles in the control group and the group treated with ultrasound, for both OHS and PC3 tumors. The results are based on flow cytometry analysis. The number of tumors varies in the different groups: 3 tumors in OHS control, 4 tumors in OHS treated, 2 tumors in PC3 control and 3 tumors in PC3 treated. The error bars are equal the standard deviations for each of the groups.
* P-value ≤ 0.05.